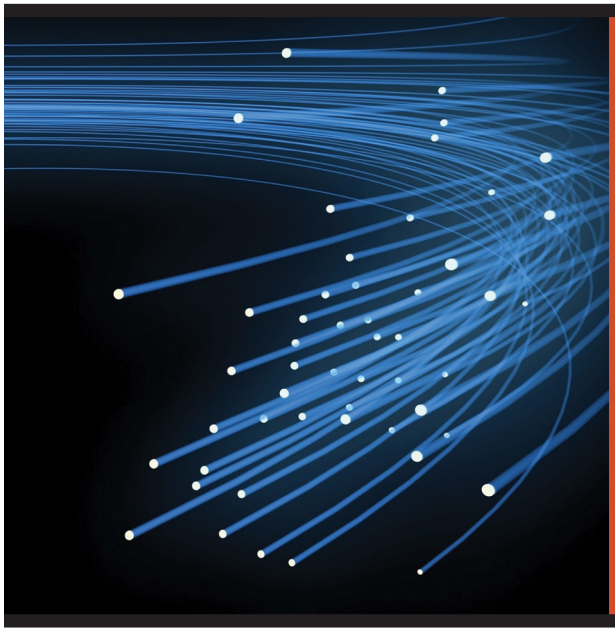

Data transmission techniques for short-range optical fiber and wireless communication links

Tien-Thang Pham

Ph. D. Thesis

December 2012

DTU Fotonik
Department of Photonics Engineering

Data transmission techniques for short-range optical fiber and wireless communication links

Tien-Thang Pham

Supervisors:

Professor Idelfonso Tafur Monroy and

Assistant Professor Jesper Bevensee Jensen

Delivery date: 10th December 2012

DTU Fotonik
Department of Photonics Engineering
Technical University of Denmark
Building 343
2800 Kgs. Lyngby
DENMARK

DTU Fotonik
Institut for Fotonik

Abstract

The research work described in this thesis is devoted to experimental investigation of techniques for cost-effective high-speed optical communications supporting both wired and wireless services. The main contributions of this thesis have expanded the state-of-the-art in two main areas: high-speed optical/wireless integration and advanced modulation formats for intensity modulation with direct detection (IM/DD) optical systems.

Regarding optical/wireless integration, this thesis focuses on integration of broadband ultra-wide band (UWB) and 60-GHz band wireless systems into optical fiber access networks to distribute wireless services in personal area networks (PANs). Photonic technologies to generate and distribute gigabit UWB and 60-GHz-band signals are proposed and demonstrated. Two novel methods are proposed and demonstrated to optically generate Federal Communications Commission (FCC)-compliant gigabit UWB signals and integrate them into baseband wavelength division multiplexing-passive optical networks (WDM-PONs). Performance of UWB signals and other wired/wireless signals in different scenarios including heterogeneous wired and wireless access networks, converged communication and sensing networks are experimentally assessed. For 60-GHz radio-over-fiber (RoF) systems, possibilities to simplify the system architecture and to use multimode fiber (MMF) together with single-mode fiber (SMF) to transport gigabit data at 60-GHz band are experimentally investigated. Additionally, the quality of video services distributed in a simplified 60-GHz RoF system is both experimentally and theoretically studied by analyzing the trade-off between the distortion introduced by the video coding and distortion introduced by the optical/wireless transmission channel.

Next to optical/wireless integration, this thesis explores techniques for delivery of high speed baseband signals in IM/DD optical links. To improve spectral efficiency (SE), a novel approach is introduced to implement advanced modulation formats, using subcarrier frequencies below the baud

rate including half and quarter the baudrate. Compared to conventional single subcarrier modulation, quarter-cycle and half-cycle quadrature amplitude modulation (QAM) achieve a improvement of the SE by 37.5% and 25%, respectively. The feasibility of half-cycle QAM signals for IM/DD optical links is demonstrated by transmission of a 10-Gbps half-cycle 4-QAM signal over 20-km SMF and a 9-Gbps 4-QAM signal over 1 km MMF both using VCSELs and simple electrical transceiver structures. The proposed approach results in the 3 dB improvement of chromatic dispersion tolerance and 1.5 dB improvement of modal dispersion tolerance at the bit-error-ratio (BER) of 10^{-5} compared to similar OOK systems operating at the same bitrate.

In conclusion, techniques proposed in this thesis demonstrate the feasibility of employing photonic technologies for the generation and distribution of gigabit wireless signals. They also demonstrate seamless integrability of wired and wireless signals into a unified optical fiber platform. Additionally, half-cycle QAM modulation has prospects to increase SE and bit rates in high-speed short-range optical communication systems.

Resumé

Forskningsarbejdet beskrevet i denne afhandling beskriver omfattende eksperimentelle undersøgelser af metoder til kost-effektive høj hastigheds optiske og trådløse kommunikationssystemer. Hovedbidragene i afhandlingen har udvidet state-of-the-art indenfor to områder: Høj-hastigheds optisk/trådløs integration, og avancerede modulationsformater til intensitets modulation og direkte detektion (IM/DD).

Vedrørende optisk/trådløs integration, fokuserer afhandlingen på integration af bredbånds ultrawide-band (UWB) og 60-GHz trådløse systemer med optiske access netværk for at distribuere trådløse tjenester til personlige netværk (PAN). Fotoniske teknologier til generation og distribution af gigabit ultrawide-band (UWB) og 60-GHz signaler er foreslået og demonstreret. To nye metoder til optisk generation af UWB signaler, der overholder Federal Communications Commission (FCC) krav, samt integrationen af disse i passive optiske netværk (PON), er foreslået og demonstreret. Ydelsen af UWB og andre typer trådløse og kablede signaler er undersøgt eksperimentelt i forskellige arkitekturer, bl.a. heterogene fiber og trådløse netværk samt kombineret kommunikation og sensor-netværk. For 60-GHz radio-over-fiber (RoF) systemer er muligheden for at opnå en simplificering gennem en kombination af multimode fiber (MMF) og singlemode fiber (SMF) til gigabit data over 60-GHz forbindelser eksperimentelt undersøgt. Derudover er kvaliteten af videosignaler distribueret over et simplificeret 60-GHz system undersøgt eksperimentelt og teoretisk ved at analysere forholdet mellem forvrængning introduceret af videokodning og forvrængning introduceret i transmissionskanalen.

Udover optisk/trådløs integration, udforsker denne afhandling teknikker til høj-hastigheds baseband signaler i IM/DD forbindelser. For at forbedre den spektrale effektivitet, er en ny metode for avancerede modulationsformater introduceret. Denne baserer sig på anvendelsen af bærebølgefrekvenser, der er mindre end signalets symbolrate, eksempelvis halvdelen

og en fjerdedel af symbolraten. Kvadratur amplitude modulation (QAM) ved en fjerdedel hhv. halvdelen af signalets symbolrate giver således en 37.5% hhv. en 25% forbedring i spektral effektivitet.

Anvendeligheden af føromtalte halv-cyklus QAM er blevet demonstreret ved at transmittere et 10-Gbps 4-QAM signal over 20 km SMF og et 9-Gbps signal over 1 km MMF. Begge systemer anvender direkte modulerede vertikal kavitet overflade emitterende lasere (VCSELs) og simple elektriske sender/modtager implementeringer. I forhold til tilsvarende konventionelle binært amplitudemodulerede signaler opnåedes en 3-dB forbedring af tolerancen overfor kromatisk dispersino og en 1,5-dB forbedring at tolerancen overfor inter-modal dispersion; begge ved en bit-fejl sansynlighed på 10^{-5}.

Det kan konkluderes at de i denne afhandling foreslåede teknikker demonstrerer anvendeligheden af optiske teknologier til distribution af gigabit trådløse signaler. Endvidere demonstreres integrérbarheden af af trådløse og optiske signaler i en fælles platform. Derudover er de mulige forbedringer i spektral effektivitet og dispersionstolerance ved anvendelse af halvcyklus QAM modulation demonstreret.

Acknowledgements

I owe my gratitude to many great people who have contributed to this thesis and made the time working on my Ph.D. an unforgettable experience.

First and foremost, my gratitude is to my main supervisor, Idelfonso Tafur Monroy for accepting me as his student, for his guidance, feedback, encouragement and directing my research. Idelfonso taught me a great deal about the value of adapting to changes and taking risks. He has been a steady influence and a valuable source of motivation throughout my Ph.D. career.

I am grateful to my co-advisor, Jesper Bevensee Jensen for his discussions, advice and patient help, that helped me sort out the technical details of my work.

Lars Dittmann was helpful in the early stages of my Ph.D. study. Thank Lars for accepting my change. I sincerely thank Xianbin Yu for being with me for a long part of my Ph.D. study. My work has greatly benefited from his support and guidance.

For this thesis, I would like to thank my Ph.D. committee members: Prof. Il-Sug Chung, Prof. Didier Erasme and Prof. Antonio Texeira for their time, insightful comments and interesting discussion questions.

The former and current members of the Metro-Access group have contributed immensely to both my personal and professional life at DTU: Tim, Kamau, Neil, Darko, J.J., Antonio, Roberto, Valeria, Maisara, Xiaodang, Miguel, Xema, Silvia, Alexander, Robert, Xu, Bomin and guest researchers. The group has been a source of friendships as well as good advice and great collaboration. I want to express my deep appreciation for all you guys. I also want to thank other colleagues at DTU Fotonik, especially in Network Technology and Service Platform group which I am apart of.

It was a great chance for me to spend 8 months of my Ph.D. study in California. I have learned a lot from both American university and company. I thank Professor Connie Chang-Hasnain at U.C. Berkeley for

accepting me as a visiting researcher of her group and giving many valuable advices for my simulations. Many thanks also to The-Linh Nguyen, for giving me the connection with Finisar for internship. I must also express my gratitude to Chris Cole and his group members for inspirational discussions and guidance. I am very happy to be a member of his group again.

I acknowledge the financial, academic and technical/non-technical support of DTU Fotonik and its staffs during my Ph.D study. I also acknowledge Oticon fonden, Otto Mønsteds fond for travel support to conferences, Danish Agency for Science, Technology and Innovation (DASTI) for financial support I received for my external stay at U.C. Berkeley.

I am profoundly indebted to my friends in Vietnam, Denmark, America and elsewhere for their encouragement and support for my little family in the last 3 years.

Finally, I am grateful to my family. Thank my parents, my parents-in-law and my sisters for their infinite support throughout everything. I would like to dedicate this thesis to the memories of my brother-in-law who passed away when I was doing Ph.D. I would like to thank my wife, Hue and my little boy, Hai Dang (lighthouse - fyrtårn) for their love, patience and encouragement. Particularly, thank Hue for her support when I have needed it the most and Dang for a perfect source of distraction.

Denmark, 10 September 2012

Tien-Thang Pham.

Summary of Original Work

This thesis is based on the following original publications:

[**PAPER 1**] **T. T. Pham**, X. Yu, T.B. Gibbon, L. Dittmann and I.Tafur Monroy, "WDM-PON-compatible system for simultaneous distribution of gigabit baseband and wireless ultrawideband services with flexible bandwidth allocation," *IEEE Photonics Journal*, vol. 3, no. 1, pp. 13—19, 2011.

[**PAPER 2**] **T. T. Pham**, X. Yu, L. Dittmann and I. Tafur Monroy, "Integration of optically generated impulse radio UWB signals into baseband WDM-PON," *IEEE Photonics Technology Letters*, vol. 23, no. 8, pp. 474–476, 2012.

[**PAPER 3**] **T. T. Pham**, N. G. Gonzalez, X. Yu, D. Zibar, L. Dittmann and I. Tafur Monroy, "Robust BPSK impulse radio UWB-over-fiber systems using optical phase modulation," in *Proc. Optical Fiber Communication Conference and Exposition*, *OFC/NFOEC*, paper OTuF6, Los Angeles, CA, 2011.

[**PAPER 4**] N. G. Gonzalez, A. Caballero, R. Borkowski, V. Arlunno, **T. T. Pham**, R. Rodes, X. Zhang, M. B. Othman, K. Prince, X. Yu, J. Jensen, D. Zibar, I. Tafur Monroy, "Reconfigurable digital coherent receiver for metro-access networks supporting mixed modulation formats and bit-rates," in *Proc. Optical Fiber Communication Conference and Exposition*, *OFC/NFOEC*, paper OMW7, Los Angeles, CA, 2011.

[**PAPER 5**] **T. T. Pham**, T. Braidwood Gibbon and I. Tafur Monroy, "VCSEL-based gigabit IR-UWB link for converged communication and sensing applications in optical metro-access networks," *Optics Communications*, vol. 285, no. 14, pp. 5068–5072, 2012.

[**PAPER 6**] **T. T. Pham**, A. Lebedev, M. Beltran, X. Yu, R. Llorente, I. Tafur Monroy, "Combined single-mode/multimode fiber link supporting simplified in-building 60-GHz gigabit wireless access," *Optical Fiber Technology*, vol. 18, no. 4, pp. 226–229, 2012.

[**PAPER 7**] A. Lebedev, **T. T. Pham**, M. Beltrán, X. Yu, A. Ukhanova, R. Llorente, I. Tafur Monroy, S. Forchhammer, "Optimization of high-definition video coding and hybrid fiber," *Optics Express*, vol. 19, no. 26, pp. B895–B904, 2011.

[**PAPER 8**] **T. T. Pham**, R. Rodes, J. Bevensee Jensen, C. J. Chang-Hasnain, and I. Tafur Monroy, "Half-cycle QAM modulation for VCSEL-based optical fiber links," in *Proc. of European Conference and Exhibition on Optical Communication (ECOC 2012)*, Amsterdam, Netherland, 2012.

[**PAPER 9**] **T. T. Pham**, R. Rodes, J. Bevensee Jensen, C. J. Chang-Hasnain, and I. Tafur Monroy, "Sub-cycle QAM modulation for VCSEL-based optical fiber links," *OSA Optics Express*, accepted for publication, 2012.

[**PAPER 10**] **T. T. Pham**, R. Rodes, J. Estaran, J. Bevensee Jensen and I. Tafur Monroy, "Half-cycle modulation for VCSEL based 6-Gbaud 4-QAM transmission over 1 km multimode fiber link," *IET Electronics Letters*, vol. 48, no. 17, pp. 1074–1076, 2012.

[**PAPER 11**] J. Estaran, R. Rodes, **T. T. Pham**, M. Ortsiefer, C. Neumeyr, J. Rosskopf and I.'Tafur Monroy "Quad 14Gbps L-band VCSEL-based system for WDM migration of 4-lanes 56 Gbps Optical Data Links," *OSA Optics Express*, accepted for publication, 2012.

Other scientific reports associated with the project:

[PAPER 12] T. B. Gibbon, **T. T. Pham**, C. Neumeyr, E. Ronneberg, M. Ortsiefer, I. Tafur Monroy, "VCSEL-based gigabit impulse radio UWB for converged wireless sensor and communication in-building networks," in *Proc. of European Conference and Exhibition on Optical Communication (ECOC 2010)*, Torino, Italy, 2010.

[PAPER 13] G. Kardaras, **T. T. Pham**, J. Soler, L. Dittmann, "Analysis of control and management plane for hybrid fiber radio architectures," in *Proc. IEEE International Conference on Communication Technology (ICCT)*, Nanjing, China, 2010.

[PAPER 14] R. Rodes, **T. T. Pham**, J. B. Jensen, T. B. Gibbon, I.Tafur Monroy, "Energy-efficient VCSEL-based multiGigabit IR-UWB over fiber with airlink transmission system," in *Proc. Annual Meeting of the IEEE Photonics Society*, Denver, CO pp. 222–223, 2010.

[PAPER 15] T. B. Gibbon, K. Prince, **T. T. Pham**, A. Tatarczak, I. Tafur Monroy, "VCSEL Transmission at 10 Gb/s for 20 km single mode fiber WDM-PON without dispersion compensation or injection locking," *Optical Fiber Technology* vol. 17, no. 1, pp: 41–45, 2011.

[PAPER 16] V. Arlunno, N. G. Gonzalez, A. Caballero, R. Borkowski, **T. T. Pham**, R. Rodes, X. Zhang, M. B. Othman, K. Prince, X. Yu, J. Jensen, D. Zibar, I.Tafur Monroy, "Reconfigurable digital coherent receiver for hybrid optical fiber/wireless metro-access networks," presented at *2nd Annual Workshop on Photonic Technologies for Access and Biophotonics*, Stanford, CA, 2011.

[PAPER 17] A. J. Caballero, **T. T. Pham**, J. B. Jensen, I. Tafur Monroy, "Carrierless N-dimensional modulation format for multiple service differentiation in optical in-home networks," in *Proc. of IEEE Photonics Conference*, Arlington, Virginia, 2011.

[PAPER 18] R. Rodes, M. Wieckowski, **T. T. Pham**, J. B. Jensen, I. Tafur Monroy, "VCSEL-dased DWDM PON with 4 bits/s/Hz spectral effi-

ciency using carrierless amplitude phase modulation," in *Proc. of European Conference and Exhibition on Optical Communication (ECOC 2011)*, Geneva, 2011.

[PAPER 19] R. Rodes, M. Wieckowski, **T. T. Pham**, J. B. Jensen, J. Turkiewicz, J. Siuzdak, I. Tafur Monroy, "Carrierless amplitude phase modulation of VCSEL with 4 bit/s/Hz spectral efficiency for use in WDM-PON," *OSA Optics Express*, vol. 19, no. 27, pp. 26551–26556, 2011.

[PAPER 20] M. B. Othman, **T. T. Pham**, X. Zhang, L.Deng, J. B. Jensen and I. Tafur Monroy1, "Comparison of carrierless amplitude-phase (CAP) and discrete multitone (DMT) modulation," submitted to *OFC/NFOEC*, 2013.

[PAPER 21] **T. T. Pham**, A. Lebedev, M. Beltran, X. Yu, R. Llorente, I. Tafur Monroy, "SMF/MMF based in-building gigabit wireless access systems using simplified 60-GHz transceivers," in *Proc. of European Conference and Exhibition on Optical Communication (ECOC 2011)*, Geneva, 2011.

[PAPER 22] R. Rodes, **T. T. Pham**, J. B. Jensen, I. Tafur Monroy, "Radio frequency over glass integrated into FTTx by using 1,3 um VCSELs: experimental performance assessment," in *Proc. of IEEE Photonics Conference (IPC 2011)*, Arlington, Virginia, 2011.

[PAPER 23] V. S. C. Teichmann, A. N. Barreto, **T. T. Pham**, R. Rodes, I. Tafur Monroy, and D. A. A. Mello, "CSC-FDE for MMF short reach optical interconnects using directly modulated 850 nm VCSELs," *OSA Optics Express*, vol. 20, no. 23, pp. 25369–25377, 2012.

[PAPER 24] J. Estaran, R. Rodes, **T. T. Pham**, M. Ortsiefer, C. Neumeyr, J. Rosskopf and I.'Tafur Monroy "Quad 14Gbps L-band VCSEL-based system for WDM migration of 4-lanes 56 Gbps Optical Data Links," in *Proc. of European Conference and Exhibition on Optical Communication (ECOC 2012)*, Amsterdam, Netherland, 2012.

[PAPER 25] M. Iglesias, R. Rodes, **T. T. Pham**, I. Tafur Monroy, "Real time algorithm temperature compensation in tunable laser / VCSEL based WDM-PON system," in *Proc. ICUMT*, Russia, 2012.

[PAPER 26] X. Yu, T. Braidwood Gibbon, R. Rodes, **T. T. Pham**, I. Tafur Monroy, "System wide implementation of photonically generated impulse radio ultra-wideband for gigabit fiber-wireless access," *OSA/IEEE Journal of Lightwave Technology*, accepted for publication, 2012.

Contents

Chapter 1

Introduction

This chapter provides an introduction to the topics of this thesis. An overview of the covered topics is presented in sections 1.3-1.5, analysis of related state-of-the-art is given in sections 1.6. The main contributions of this Ph.D. thesis that extend the state-of-the-art are described in section 1.7.

1.1 Outline of the thesis

This thesis is structured in 3 chapters as follows: Chapter 1 introduces the context of the main research papers included in this thesis. It provides a short overview of the evolution of both optical fiber access networks and wireless networks with emphasis on wireless personal area networks (WPANs). Integration of wireless and baseband signals into a passive optical network (PON), an important step towards a converged broadband access network is particularly highlighted. Introduction to attenuation and fiber dispersion, the main considered impairments in optical short-range and access networks, are presented. It is followed by the introduction to optical modulation techniques and their effects on the signal performance. Finally, an overview of advanced modulation formats for optical fiber access systems using intensity modulation with direct ditection (IM/DD) is given.

Chapter 2 describes the main contributions of each publication included in this thesis. To conclude, Chapter 3 summarizes the main achievements of this Ph.D. thesis and provides an outlook to the prospects of integrated wireless-fiber networks and advanced modulation formats for PONs and short-range optical networks. All original peer-reviewed publications composing this Ph.D. thesis are appended.

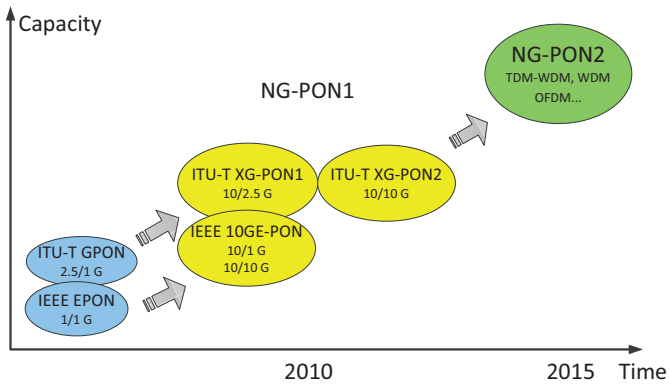

Figure 1.1: PON standardization roadmap [7]. EPON: ethernet passive optical network, GPON: gigabit passive optical network, 10GE-PON: 10 Gbps ethernet passive optical network, XG-PON: 10-gigabit-capable passive optical network, NG-PON1: The first next-generation passive optical network, NG-PON2: The second next-generation passive optical network.

1.2 Broadband access networks

Over the last decades, the demand from both residential and business customers worldwide for bandwidth has evolved from simple e-mail exchanges and limited business file transfers to increasing broadband access supporting data-intensive applications such as high-definition television (HDTV), video-on-demand (VoD), online gaming, voice-over-IP (VoIP) and high-speed Internet. Many of those applications require data rates faster than hundreds of Mbps. For instance, uncompressed HDTV 1080i requires a transfer rate of 1.485 Gbps while HDTV 1080p requires 2.97 Gbps. Consequently, it is predicted that for fixed network, Internet-generated broadband traffic will increase approximately 50 percent year over year on fixed networks and 200 percent on mobile networks [1]. Such growing demand has put severe pressure on the communication network infrastructures to provide broadband access supporting diverse services at a low cost. This also has resulted in an remarkable evolution of both wired and wireless access networks over the past years.

1.2.1 Broadband optical fiber access networks

Passive optical networks PONs are widely considered to be the most promising cost-effective and high-performance solution for broadband access networks [2–5]. The standardization roadmap for PONs is presented in Fig.

1.1. Fiber-to-the-home (FTTH) is being deployed in large scale in Asia, United States and also in Europe to replace coaxial cable based access systems. Two main FTTH-PON standards currently deployed are Ethernet passive optical network (EPON) (IEEE 802.3ah, 2004) and gigabit passive optical network (GPON) (ITU-T G.984). Both solutions cover distances of up to 20 km, use point-to-multipoint topology and time-division multiplexing (TDM) technology with variable split-ratio – commonly, from 32 to 64 users. There is no active equipment required in the field.

Although TDM-PONs provide higher bandwidth than traditional copper-based access networks, they are not transparent to different signal formats and data rates. In case the network is upgraded to support higher data rates or different transmission protocols, it requires replacing the electronics in both the optical network unit (ONU) and the optical line termination (OLT). Additionally, next-generation optical access networks are expected to be capable of providing much higher bandwidth up to Gbps per user and beyond to promote the growth of the ongoing evolution in services and applications and also protect legacy investments [3]. The application of wavelength division multiplexing (WDM) technology straight forwardly offers a new dimension to increase the bandwidth for the upgrade of PON to next-generation access solutions. In a WDM-PON, ONUs have light sources operating at different wavelengths coexisting in the same fiber. WDM-PON offers several advantages that enable operators to consolidate converged networks and to provide high speed access for business, mobile backhaul and FTTH [4–6] as follows:

- Higher bandwidth: with dedicated wavelength and bandwidth for each ONU, each ONU can have its own maximum downstream and upstream bandwidth without sharing with other ONUs. The need for ranging or collision avoidance scheme for upstream path is eliminated
- Flexible bandwidth and format: data rate or even modulation format on each wavelength channel can be different
- Higher security: WDM-PON is a virtual point-to-point configuration. Signal from an ONU is not shared with any other ONUs
- Fast network reconfiguration due to the flexibility in wavelength allocation
- Higher upgrade-ability and scalability because of the dedicated link and dedicated wavelength. The change of one channel does not effect the operation of others.

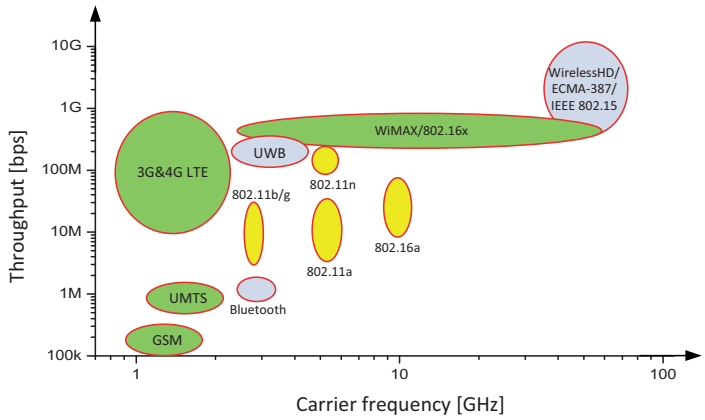

Figure 1.2: Throughput and allocated frequency of some wireless services. UWB: ultra-wide band, GSM: Global System for Mobile Communications, LTE: Long Term Evolution, UMTS: Universal Mobile Telecommunications System, WiMAX: Worldwide Interoperability for Microwave Access.

The main disadvantage of WDM-PONs at present is the high cost of equipment related to the remote node and ONUs. At the remote node, typically, an arrayed waveguide grating (AWG) is used as an wavelength multiplexer/demultiplexer to combine and separate different wavelengths of channels. Although they have been improved a lot during the last years, especially thermal stability issues [8], their cost is still higher than power splitters of TDM-PONs. Regarding the ONUs, how to transmit at an specific wavelength without requiring a high-cost tunable laser is important. Wavelength dependence makes network upgrades and maintenance difficult as they require manual reconfiguration of the equipment in the end-user side. Several approaches have been proposed to overcome this challenge such as using spectrum sliced broaband lightsource, injection-locked Fabry-Pérot laser, reflective semiconductor optical amplifier (RSOA) or tunable laser [6].

Recently, WDM-PON has been deployed for field trials in some countries for example in Korea by Korea Telecom, in Japan by KDDI, in Norway by LG-Nortel. However, there is no large scale worldwide commercial deployment yet.

1.2.2 Broadband short-range wireless networks

Regarding wireless access, since the first transatlantic wireless experiment in 1901 [9], various wireless communication technologies have been developed that make end-users benefit from their convenience, flexibility, and mobil-

ity. Examples of some current wireless standards for those networks are illustrated in Fig. 1.2. Those standards have become popular for different application scenarios, for example, Global System for Mobile Communications (GSM) and Long Term Evolution (LTE) for wireless wide area network (WWAN), WiFi (IEEE 802.11) for wireless local area network (WLAN), Bluetooth and ZigBee for wireless personal area network (WPAN). During the last years, with the fast growth of the usage of personal wireless devices, the demand for broadband wireless communication has been increasing exponentially up to Gpbs to support multimedia applications, especially video applications [10]. Broadband spectrum is required to support such high data throughput. Unfortunately, wireless technologies operate in low frequency bands such as the license-free industrial, scientific and medical (ISM) radio bands, which are rather crowded and no longer capable of supporting such high bandwidth requirements due to limited available bandwidth. For instance, there are only 70 MHz in the 2.4-GHz band and 500 MHz in the 5-GHz band for WiFi. An approach to fulfill the bandwidth demand is to increase spectral efficiency (SE) over a given bandwidth. SE larger than 1 bit/s/Hz can be achieved by using complex modulation formats, such as phase shift keying (PSK), quadrature amplitude modulation (QAM) or orthogonal frequency-division multiplexing (OFDM). Bandwidth for each mobile user is also can be improved by deploying smaller cell sizes (micro- or pico-cells) to reduce the numbers of mobile users operating and sharing the bandwidth in each cell. Another possibility to achieve high capacity wireless links is to move towards higher RF frequencies, where higher bandwidth is available.

In order to deal with the congestion in current frequency bands, promote flexibility in spectrum sharing as well as allow the development of broadband wireless communications, two new frequency bands have been introduced:

a) ultra-wide band (UWB): UWB communication was approved by the Federal Communications Commission (FCC) in 2002 [11], and has since drawn considerable interest for different applications such as high-speed communication, sensing, radar-imaging technology and localization [12]. UWB communication is an underlay approach. It is allowed below 1 GHz or between 3.1 to 10.6 GHz at sufficiently low power level when operating at larger than 500-MHz signal bandwidth. The maximum allowed equivalent isotropically radiated power (EIRP) is severely restricted to lower than -41.3 dBm/Mhz, which is below the noise level of other existing wireless communication standards in that frequency band. Fig. 1.3 illustrates the allowed transmitted EIRP of UWB signals and the co-operation of UWB

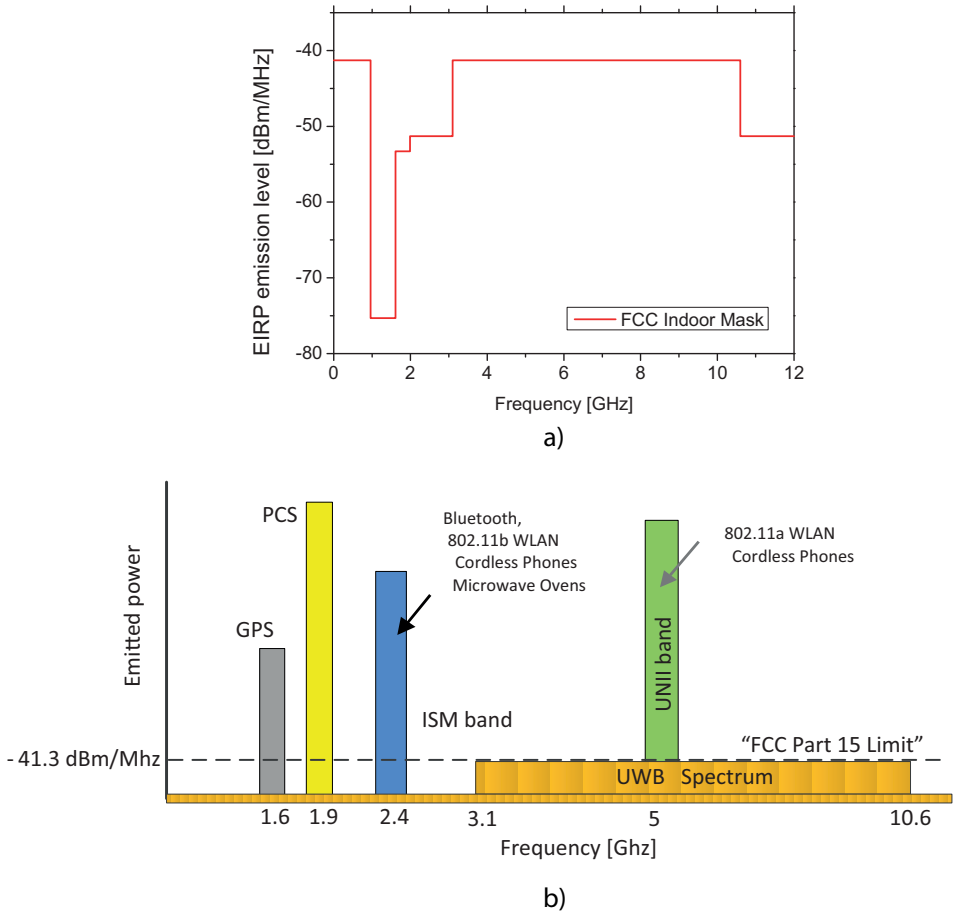

Figure 1.3: a) FCC mask for UWB emission power and b) coexistence of UWB and other wireless standards. GPS: Global Positioning System, PCS: personal communications service, ISM: industrial, scientific and medical radio bands.

communication with other wireless systems.

a) millimeter-wave (mmW) band: mmW band is a range of electromagnetic waves with frequencies between 30 GHz and 300 GHz, or the wavelength of one to ten millimeter. Compared to lower frequency bands, the mmW band can offer a massive amount of spectral space to support high-speed applications [13, 14]. In particular, the 60-GHz band has gained much attention and been viewed as the most promising carrier in next-generation WPAN [15]. 60-GHz frequencies are well absorbed by oxygen (Fig. 1.4 [16]) and several construction materials [17]. Additionally, free-

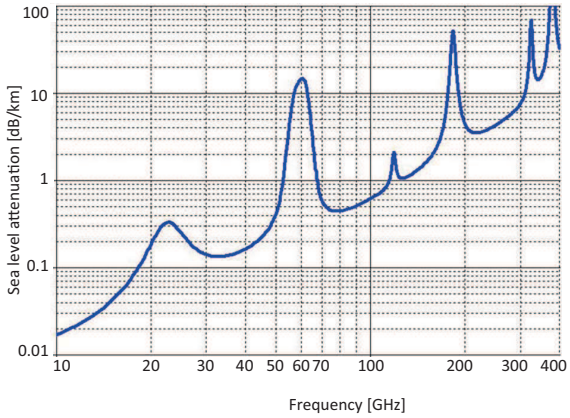

Figure 1.4: Atmospheric and molecular absorption [16].

space loss at the 60-GHz band is also very high (68 dB/m compared with 46.5 dB/m at 5 GHz) that limits long distance interference and makes the 60-GHz band suitable to build small-cell networks. Regulatory agencies in several countries has allocated the 60-GHz band with up to 7-GHz bandwidth for unlicensed use: 57-64 GHz band in Canada, Korea and United States, 59-66 GHz band in Europe and Japan. Transmitted power up to 40 dBm EIRP is allowed. The wide bandwidth and high allowable transmitted power enable multi-Gbps wireless transmission over typical in-home and in-building networks up to 10 m. 60-GHz band communication has been standardized for WPAN by several working groups such as Ecma International, WirelessHD and IEEE 802.15.3c [18–20]. This has resulted in growing interest in using this resource for new consumer applications requiring very high data-rate wireless transmission and some products has been commercialized, for example TruLink 60-GHz WirelessHD Kit by C2G [21].

1.2.3 Radio-over-fiber and integration with baseband WDM-PONs for future converged access networks

Improving capacity of wireless links by utilizing high-frequency carriers or reducing the coverage of each base station (BS) operating at low-frequency carriers both results in the necessity for the deployment of small-cell wireless networks. Larger numbers of BSs are required to provide the wireless service to a certain geographic area and more extensive feeder networks are needed to service those BSs. Low capital expenditure (CAPEX) and operating expense (OPEX) for feeder networks and BSs is a key to success in

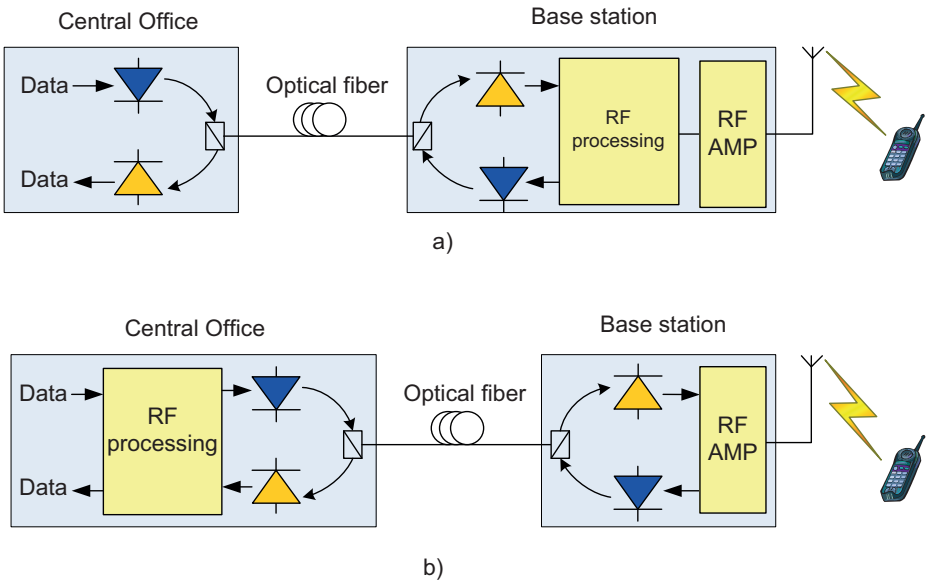

Figure 1.5: a) A conventional wireless system and b) basic structure of a radio-over-fiber system..

the market. That aim has led to the development of system architectures where functions such as signal routing/processing, handover and frequency allocation are carried out at a central station (CS), rather than at the BSs and optical fiber is utilized for low-cost wireless signal transport platform. Such network architecture is called radio-over-fiber (RoF).

The basic structures of a conventional wireless system and a RoF system are shown in Fig 1.5. In that system, data is transmitted between the CS and BSs by using an optical fiber or coaxial cable. At the BSs, RF processing is required to convert the digital signal to the wireless signal and vice-versa by RF modulation/demodulation and mixing.

On the other hand, the RoF network typically comprises a CS, where all signal generation, switching, routing, frequency management and RF to optical up-conversion functions are performed, and an optical fiber network, which interconnects a large number of BSs for wireless signal distribution. BSs are functionally simplified and compact and probably have no RF signal processing function. Their main functions are to convert optical signals to wireless ones and vice versa and to amplify and distribute the wireless signals to wireless terminals.

The integration of wireless signals in the form of RoF into optical fiber

access networks helps to form a converged access network. Three architectures of PON-wireless integration have been proposed mainly for EPON and Worldwide Interoperability for Microwave Access (WiMAX) [22]. Among them, microwave-over-fiber architecture is the one transporting baseband signal and RF signal simultaneously from OLT/CS to ONU/BS. The integration of RF signal into baseband WDM-PON can be done by using frequency-division multiplexing (FDM) and/or WDM.

In FDM configuration, the baseband signal for wired services is located at baseband, for example, up to 1.25 GHz for EPON and GPON. The wireless data is modulated on a wireless carrier frequency at a higher frequency band. These two signals are then frequency-multiplexed and modulated onto a common optical carrier. This configuration also allows multiple wireless signals to be accommodated in the link if they occupy different frequency bands. At the receiver side, after photodetection, baseband and wireless signals can be separated using proper filters. This procedure is done for both uplink and downlink. Only one pair of optical transceivers are required for a bidirectional link. Each remote node is made up of an ONU unit that is responsible for the data communication of the baseband passive optical network (PON), and a BS that is responsible for relaying a wirelss signal from and to it. Corresponding to the remote nodes, the central node consists of two types of major modules, including an OLT for the baseband signal and a CS for the wireless signal. The FDM configurations utilize high fiber spectrum because both wired and wireless data are transmitted on a single wavelength.

If the baseband signal and wireless signal are wavelength-multiplexed, each signal is modulated on a different wavelength of a WDM-PON. This architecture requires a pair of transceivers operating at different wavelength for each signal. However, there is no need to separate the baseband signal and wireless signal by using electrical means. Fig. 1.6 illustrates an architecture of next-generation convergence access networks using FDM/WDM configuration and supporting both broadband wired and wireless services.

With the concept of FDM and WDM, a variety of independent wired/wireless standards can be integrated in single platform of a converged access network. Such a network will help to deliver a consistent, high-quality and seamless mobile broadband experience to end-users together with broadband wired services. Additionally, for wireless signals, it efficiently addresses different requirements of individual BSs, bandwidth on-demand provisioning across cells, simple remote radio heads and avoids interference with the baseband spectrum. For network operators, the converged access networks

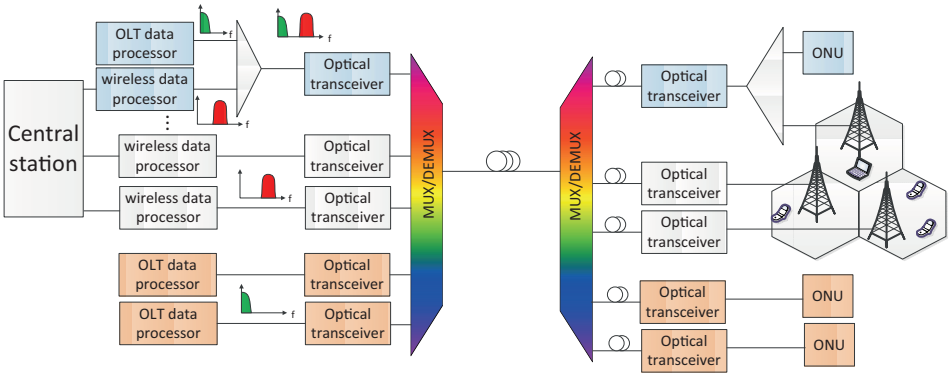

Figure 1.6: Integrated WDM-PON network supporting wired and wireless services.

lower the operating costs, and meet the capital costs objectives of future upgrades. It also facilitates greater sharing of common network infrastructure between multiple network operators.

1.3 Fiber impairments in short-range and PON links

Both wired and wireless signals distributed by optical fibers suffer from fiber impairments which cause degradation of the original signals. The fiber impairments can be divided into two classes: linear impairments and nonlinear impairments [29]. When the launched level power into the fiber is moderate, in the milliwatt range, optical communication systems experience linear effects: attenuation and fiber dispersion. Fiber dispersion includes chromatic dispersion, polarization-mode dispersion (PMD) and modal dispersion. Increasing the launched power can lead to nonlinear effects in the fiber. Nonlinear effects in optical fibers originate from the intensity dependence of the refractive index and stimulated inelastic scattering including self-phase modulation, cross-phase modulation, four-wave mixing, stimulated Raman scattering, and stimulated Brillouin scattering.

Generally, PONs and short-range optical networks have a low launched level power and short transmission distance. Therefore, nonlinear effects may be neglected. Besides attenuation, fiber dispersion is the most important linear impairment that limits the performance of signals.

1.3.1 Attenuation

The propagation of a pulse inside the optical fiber produces power loss leading to the decrease of output optical power. The relationship between the average input power P_{in} and average output power P_{out} of the fiber with the length L is:

$$P_{out} = P_{in}.e^{-\alpha L} \tag{1.1}$$

where α is the attenuation coefficient, commonly measured in dB/km. Fig. 1.7 shows the loss spectrum $\alpha(\lambda)$ of a single-mode fiber (SMF) [29].

1.3.2 Chromatic dispersion in single-mode fiber

The theoretical model of optical propagation in a SMF can be described by nonlinear Schrödinger equation [29], which is given by

$$\frac{\partial A}{\partial z} + \beta_1 \frac{\partial A}{\partial t} + \frac{i\beta_2}{2}\frac{\partial^2 A}{\partial t^2} - \frac{\beta_3}{6}\frac{\partial^3 A}{\partial t^3} + \frac{\alpha\,(z)}{2}A = i\gamma|A|^2 A \tag{1.2}$$

where $A = A(z;t)$ is the optical field, $\alpha(z)$ is the fiber attenuation parameter and γ is the Kerr nonlinear coefficient. β_n is the n-order frequency

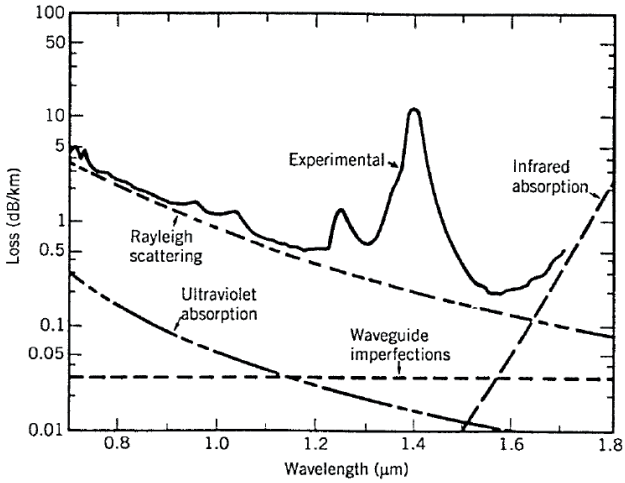

Figure 1.7: Loss spectrum of a single-mode fiber [29].

dependent chromatic dispersion parameters. These coefficients represent different impairments of fiber transmission links. β_n are the derivatives of the mode propagation constant $\beta(\omega)$ in a Taylor series around the carrier frequency ω_0 as follows:

$$\beta(\omega) = \beta_0 + (\omega - \omega_0)\beta_1 + \frac{1}{2}(\omega - \omega_0)^2\beta_2 + \frac{1}{6}(\omega - \omega_0)^3\beta_3 + ... \qquad (1.3)$$

where $\beta_0 \equiv \beta_{\omega 0}$ and β_n is

$$\beta_n = \left(\frac{d^n\beta}{d\omega^n}\right)\omega = \omega_0 \qquad (1.4)$$

In Eq. 1.2, β_1 term corresponds to a constant delay experienced by the pulse as it propagates through the fiber, the second order term β_2 corresponds to dispersion coefficient, which is well known as group-velocity dispersion (GVD). β_1 does not affect the signal quality and shape. Third-order dispersive effects are often negligible in practice. If we also neglect the loss ($\alpha = 0$) and the nonlinear term (in case of low optical power), the pulse propagation equation can be given by:

$$\frac{\partial A}{\partial z} + \frac{i\beta_2}{2}\frac{\partial^2 A}{\partial t^2} = 0 \qquad (1.5)$$

Due to the GVD effect, different frequency components of an optical pulse propagate in the fiber with different velocities that make the pulse

spread. This effect is known as chromatic dispersion. Pulse broadening is proportional to the length of the fiber and generates inter-symbol interference (ISI) in time domain at the output of the fiber. If $\Delta\lambda$ is the spectral width of the pulse, the extent of pulse broadening for a fiber of length L is governed by

$$\Delta T = \frac{d}{d\lambda}\left(\frac{L}{v_g}\right)\Delta\lambda = DL\Delta\lambda \tag{1.6}$$

where

$$v_g = \left(\frac{d\beta}{d\omega}\right)^{-1} \tag{1.7}$$

$$D = \frac{d}{d\lambda}\left(\frac{1}{v_g}\right) = -\frac{2\pi c}{\lambda^2}\beta_2 \tag{1.8}$$

v_g is the group velocity. D is called the dispersion parameter and is expressed in units of $ps/(km-nm)$. The time-domain fiber impulse response can be expressed as:

$$f_{SMF}(t) = \sqrt{\frac{c}{j2D\lambda^2 L}}\exp\left(\frac{j\pi c}{2D\lambda^2 L}t^2\right) \tag{1.9}$$

1.3.3 Modal dispersion in multimode fiber

In a multimode fiber (MMF), there are chromatic dispersion and modal dispersion. Usually, modal dispersion strongly dominates chromatic dispersion. Many different modes are excited and propagate through the fiber with different propagation delays which cause modal dispersion. Generally, MMF is characterized by group velocity differences among propagating modes. Propagating modes are classified into mode group which composes of modes with the same propagation constant. When propagating along the fiber, mode group mixing between mode group occurs. Each output mode is contributed by all input mode groups. Therefore, the impulse response of a MMF is determined by not only modal group delays but also mode group mixing and it is strongly depends on the power distribution of modes induced by launching conditions. The fiber impulse response $f_{MMF}(t)$ of a MMF can be modeled as [30]:

$$f_{MMF}(t) = \sum_{j=1}^{M}\sum_{i=1}^{M}\omega_i.d_{ij}.\delta(t-\tau_{ij}) \tag{1.10}$$

where M is the number of mode groups, w_i is the power distributions of input mode groups and d_{ij} is the power mixing coefficient from input mode group i to output mode group j.

1.4 Modulation/demodulation techniques for short-range and PON networks

1.4.1 Intensity modulation with direct detection

In optical communication, intensity modulation (IM) using a directly modulated laser (DML) with direct detection (DD) is the simplest and most cost-effective method to convert from electrical to optical signals and vice versa. The two processes take place in a laser and a photodiode (PD), respectively. As the transmitted electrical data is superimposed to the laser bias current, the variation of the current driving the laser directly modulates the output power of the laser. At the PD, intensity of optical wave is converted to electrical current based on square-law detection of the PD.

IM also can be done using external modulators. A laser emits continuous wave (CW) light and the modulation is done afterwards by an external optical modulator. There are two external modulators which is commonly used today in optical communication systems: electro-absorption modulator (EAM) and Mach-Zehnder modulator (MZM). External modulators offer much higher modulation bandwidth (up to 60 GHz) than DMLs. The independence between light generation and modulation also can provide better signal quality. EAM is small and can be integrated with the laser on the same substrate. For instance, an electro-absorption modulated laser (EML) is monolithically integrated consisting of a CW distributed feedback laser (DFB) laser followed by an EAM. A MZM-based IQ modulator can be used to generated advanced modulation formats such as quadrature phase shift keying (QPSK). However, as an additional device is required, external modulation results in a more expensive system. The applications of different modulation methods and optical modulators is presented in Fig. 1.8 [31]. For short-range and access networks, due to strict requirement for the cost of the whole system, intensity modulation using a DML such as DFB or vertical-cavity surface-emitting laser (VCSEL) is preferred.

1.4.2 Frequency chirping of directly modulated lasers

For optical links using DMLs, direct intensity modulation leads to variation of carrier density in the laser active region, which affects the refractive index and in turn the frequency of a generated optical field. The frequency chirping of the laser in interaction with chromatic dispersion causes distortions of the signal when it travels along the optical fiber. In the optical

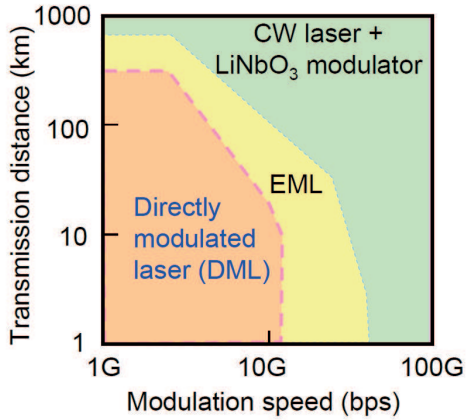

Figure 1.8: Transmitters for optical fiber communication [31].

systems using a standard SMF in 1.5-μm window for long transmission distance, frequency chirp limits the bitrate-distance product that a link can support. The chirp of single-frequency laser is described in the following equation [32, 33]:

$$\Delta v\left(t\right)=\frac{\alpha}{4\pi}\left(\frac{1}{P\left(t\right)}\frac{dP\left(t\right)}{dt}+\kappa P\left(t\right)\right) \tag{1.11}$$

where $\Delta\nu\left(t\right)$ is the instantaneous frequency deviation and $P_L\left(t\right)$ is the instantaneous optical power. α (linewidth enhancement factor) and the κ (adiabatic chirp coefficient) parameter are constants. κ is related to the non-linear gain and depends on the geometry of the device. The first term, proportional to derivative of the output power, describes transient chirp relating to the time derivative of the changing instantaneous optical power with rising and falling pulse edges. The second term, directly proportional to the power, describes adiabatic chirp relating to the instantaneous optical power itself. The optical field of the laser output:

$$E_L\left(t\right)=\sqrt{P_L\left(t\right)}e^{j\phi_L(t)} \tag{1.12}$$

where $P_L\left(t\right)$ is the laser output power and $\phi_L\left(t\right)$ is the integral of a laser frequency deviation.

$$\phi_L\left(t\right)=2\pi\int_0^t\Delta\nu\left(t\right)d\left(t\right) \tag{1.13}$$

The output optical field after fiber transmission can be obtained by taking convolution of the input field with the fiber impulse response in equation 1.9. The output power after fiber transmission:

$$P_O(t) = |E_L(t) * f_{SMF}(t)|^2 \tag{1.14}$$

Fig. 1.9 illustrates the simulated output waveform and frequency chirping of a 1.5-μm VCSEL. The simulation is based on the well-known rate equation for single-mode lasers [34]. Some important physical parameters of VCSELs are listed in Table 1.1. The evolution of the simulated waveforms of 10 Gbps data from a VCSEL and a chirp-free transmitter after fiber transmission are depicted by eye-diagrams in Fig. 1.10 and Fig. 1.11. In general, longer fiber transmission causes signal waveforms to be more distorted. In case of VCSEL based links, the combination of frequency chirping and chromatic dispersion causes the eye-diagrams closure and larger jitter. In **PAPER 15**, our simulation results shows that for 1.5-μm VCSEL based links, transmission dispersion penalty, presented relative to the back-to-back VCSEL performance, is approximately 11 dB after 20-km SMF for 10-Gbps OOK data.

Table 1.1: List of VCSEL parameters used in the simulation

Parameter	**Unit**	**Value**
Confinement factor		0.04
Cavity volume	cm^3	1.80E-12
Wavelength	cm	1.55E-04
Gain compression factor	cm^3	1.5E-17
Transparency carrier density		1.80E+18
Gain coefficient		1800
Spontaneous emission rate into one optical mode	cm^{-3}/s	2.1E+23
Spontaneous emission factor		1.69E-4
Group velocity	cm/s	7.15E9
Linewidth enhancement factor		5

1.5 High spectral efficiency modulation formats for short-range optical systems

With the continuously growing demand for bandwidth, network operators and equipment manufacturers have to turn to high-capacity optical transmission systems. Over the last years, advanced modulation formats have emerged as a promising alternative to conventional on-off keying (OOK) for fiber-optic communication systems. Recently, fully coherent four-bit-per-symbol dual-polarization (DP)-QPSK modulation format has been recommended for 100-Gbps system design [35]. Several demonstrations of higher SE such as optical 16-QAM, optical OFDM have been reported. An intensive review of technological options for advanced modulation formats for serial optical transmission of 100 Gbps and beyond can be found in [36]. Generation of high SE optical modulation formats generally requires complicated optical transceivers. For example, a version of an optical QPSK modulator consists of 2 MZMs, which further have a $\pi/2$ phase difference between them. Additionally, a coherent receiver with digital signal processing (DSP) is required for data detection and demodulation. The cost associated with the implementation of the transceivers may negate the benefits of high SE modulation formats. Such complex systems are envisioned for transport networks. On the other hand, for short-range and PON networks, IM/DD is still preferred because of cost constraints. Therefore, to achieve high SE IM/DD links, high SE electrical modulation formats need to be generated before directly modulating a light source. There are three main possibilities for high SE modulation formats for IM/DD links: pulse amplitude modulation (PAM), subcarrier multiplexing (SCM) and carrierless amplitude phase modulation (CAP).

1.5.1 Baseband pulse amplitude modulation

The basic idea of using PAM for communication is to transmit a sequence of pulses in some pre-specified shape $p(t)$, with the sequence of pulse amplitudes carrying the information. The associated baseband signal at the transmitter is given by [37]:

$$s_{PAM}(t) = \sum_{n} a(n)\, p(t - nT) \tag{1.15}$$

where the numbers $a(n)$ are the pulse amplitudes, and T is the pulse repetition interval or the inter-symbol spacing, so $1/T$ is the symbol rate.

1.5.2 Subcarrier multiplexed QAM modulation

Recently, a popular application of SCM technology in fiber optic systems is analog cable television (CATV) distribution. Compared to PAM, a single-dimension modulation technique, QAM is a two-dimensional signaling method which uses both in-phase and quadrature components to improve SE. In principle, QAM use cosine and sine wave functions as the two basis functions for two dimensions [37]:

$$\phi_1(t) = \sqrt{\frac{2}{\mathrm{E}_g}} g(t) \cos(2\pi f_c t) \tag{1.16}$$

$$\phi_2(t) = -\sqrt{\frac{2}{\mathrm{E}_g}} g(t) \sin(2\pi f_c t) \tag{1.17}$$

The corresponding waveform of M-QAM signals:

$$\begin{aligned} s_{QAM}(t) &= A_{mI}\sqrt{\frac{E_g}{2}}\phi_1(t) + A_{mQ}\sqrt{\frac{E_g}{2}}\phi_2(t), \mathrm{m} = 1, 2, ..., \mathrm{M} \\ &= A_{mI} g(t) \cos(2\pi f_c t) - A_{mQ} g(t) \sin(2\pi f_c t) \end{aligned} \tag{1.18}$$

where E_g is the energy of the signal with the lowest amplitude and $g(t)$ is a pulse shape. A_{mI} and A_{mQ} denote the set of M possible amplitudes for I and Q channels. The general structure of a QAM transceiver is illustrated in Fig. 1.12. The norms of two basis functions calculated in a symbol duration $[0, T]$:

$$\begin{aligned} \langle \phi_1(t), \phi_1(t) \rangle &= \int_0^T \left(\sqrt{\frac{2}{\mathrm{E}_g}} g(t) \cos(2\pi f_c t + \varphi) \right)^2 \\ &= \int_0^T \frac{2}{\mathrm{E}_g} g^2(t) \cos^2(2\pi f_c t + \varphi) \end{aligned} \tag{1.19}$$

$$\begin{aligned} \langle \phi_2(t), \phi_2(t) \rangle &= \int_0^T \left(\sqrt{\frac{2}{\mathrm{E}_g}} g(t) \sin(2\pi f_c t + \varphi) \right)^2 \\ &= \int_0^T \frac{2}{\mathrm{E}_g} g^2(t) \sin^2(2\pi f_c t + \varphi) \end{aligned} \tag{1.20}$$

The inner product of two basis functions in a symbol duration $[0, T]$:

$$\begin{aligned}\langle \phi_1(t), \phi_2(t) \rangle &= \int_0^T \sqrt{\frac{2}{\mathrm{E}_g}} g(t) \cos(2\pi f_c t + \varphi) \sqrt{\frac{2}{\mathrm{E}_g}} g(t) \sin(2\pi f_c t + \varphi) \\ &= \int_0^T \frac{2}{\mathrm{E}_g} g^2(t) \sin 2(2\pi f_c t + \varphi) \end{aligned} \quad (1.21)$$

To generate proper QAM signals, the subcarrier frequency must be chosen so that two basis functions are orthogonal. In other words, the inner product is equal to zero or the integral of $\sin 4\pi f_c t$ is equal to zero in a symbol duration.

FDM extends the concept of single subcarrier modulation by using multiple subcarriers within the same single channel. The total data rate to be sent in the channel is divided between the subcarriers. Different modulation formats can be used for different subcarriers. OFDM is a special case of FDM where the subcarrier frequencies are chosen so that they are orthogonal to each other. It means that cross-talk between the sub-channels is eliminated and inter-carrier guard bands are not required. In practice, OFDM systems are implemented in digital domain using a combination of fast Fourier Transform (FFT) and inverse fast Fourier Transform (IFFT) [38]. The baseband version of OFDM is discrete multi-tone (DMT). Contrary to OFDM, the output signal of DMT modulator after IFFT is real-valued. The imaginary part has a constant value, independent of the modulated data. That part is known at reception and is not transmitted. Therefore, no in-phase and quadrature modulation onto a RF carrier is required. However, DMT requires twice the sampling frequency of OFDM.

1.5.3 Carrierless phase amplitude modulation

Another modulation format which supports multi-dimension and multi-level modulation is CAP format which employs orthogonal waveforms. The basic idea of the CAP system is to use different signals as signature waveforms to modulate different data streams. Instead of using sine and cosine signals, these waveforms are obtained from filters with orthogonal impulse responses [39]. At the transmitter, the signature waveforms are generated by orthogonal shaping filters. At the receiver, the individual data streams are reconstructed by matched filtering. The matched filter used in the receiver

has an impulse response which is the time domain inversion of the impulse response of the transmitter filter. In principle, CAP is similar to quadrature amplitude modulation (QAM) in the sense that both CAP and QAM supports modulation in more than one dimension. Contrary to QAM, however, CAP does not require the generation of sinusoidal carriers at the transmitter and the receiver and it can support more than two dimensions. Fig. 1.13 illustrates the general structure of a multi-dimensional CAP transceiver.

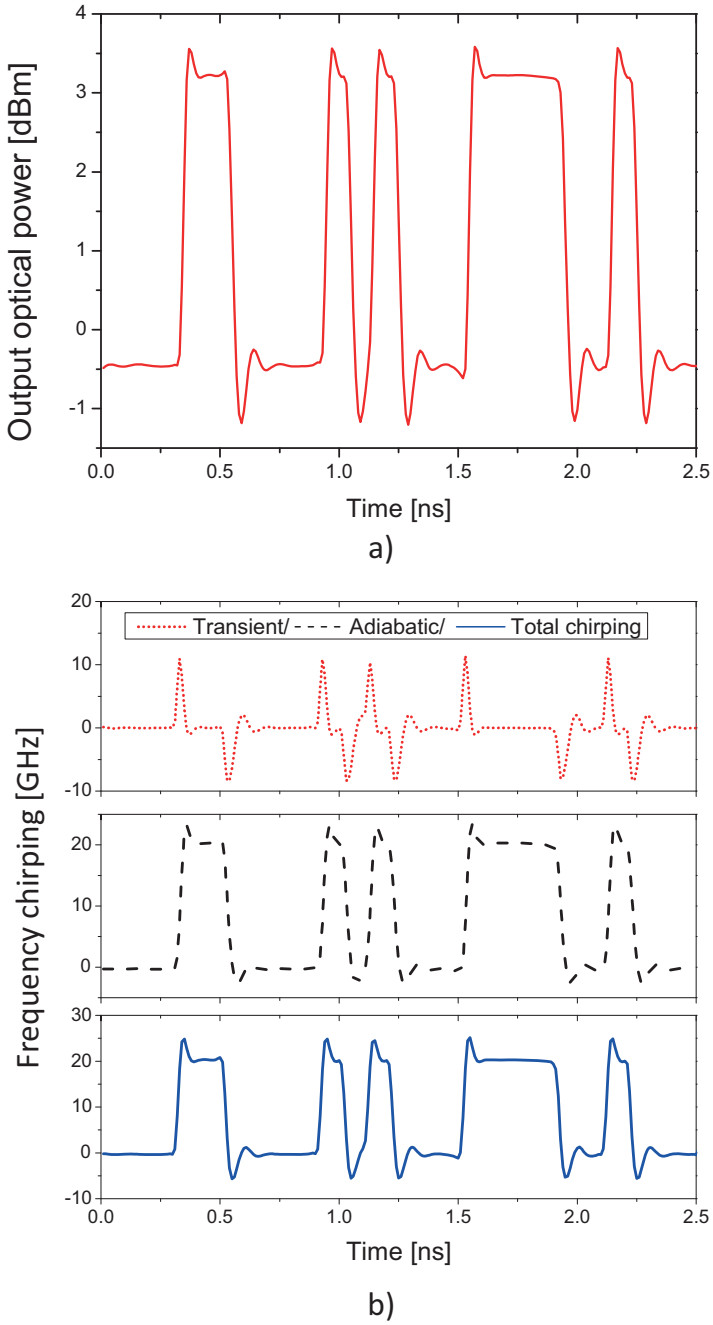

Figure 1.9: Simulated output of VCSEL a) Output power and b) frequency chirping.

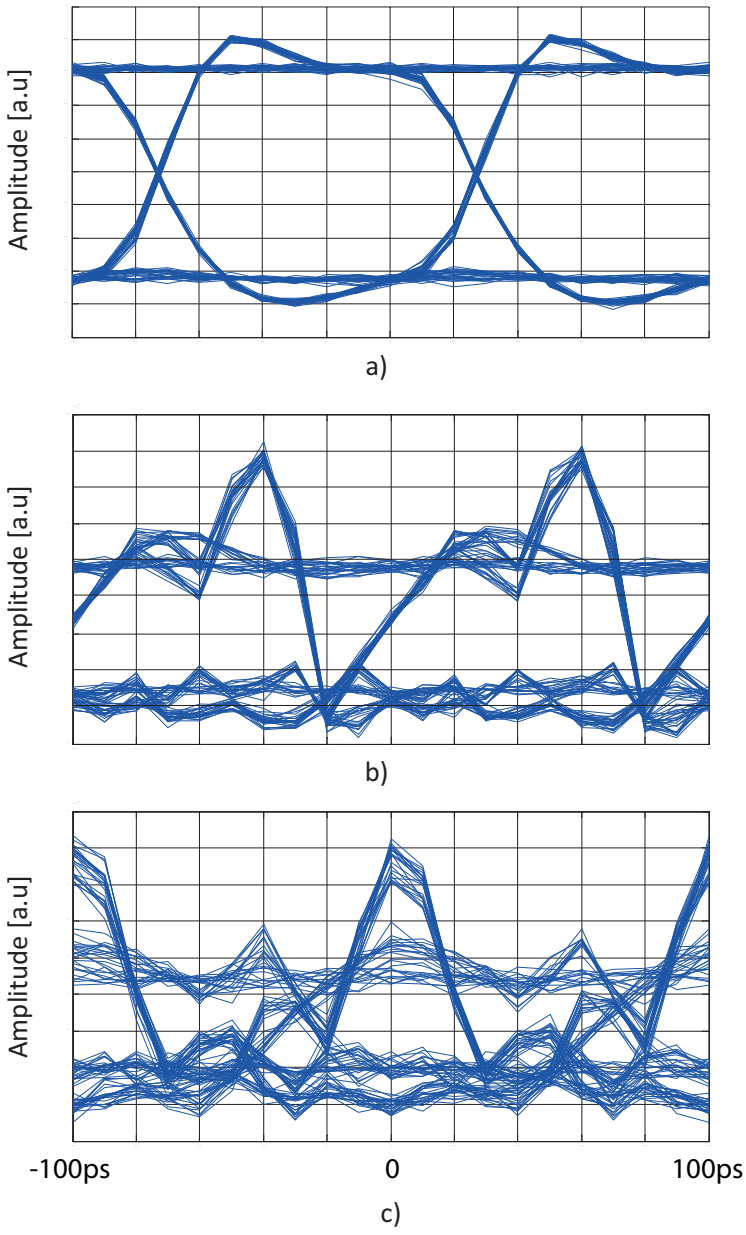

Figure 1.10: Evolution of simulated optical waveform after fiber transmission: a) VCSEL output, b) after 10-km SMF, c) after 20-km SMF.

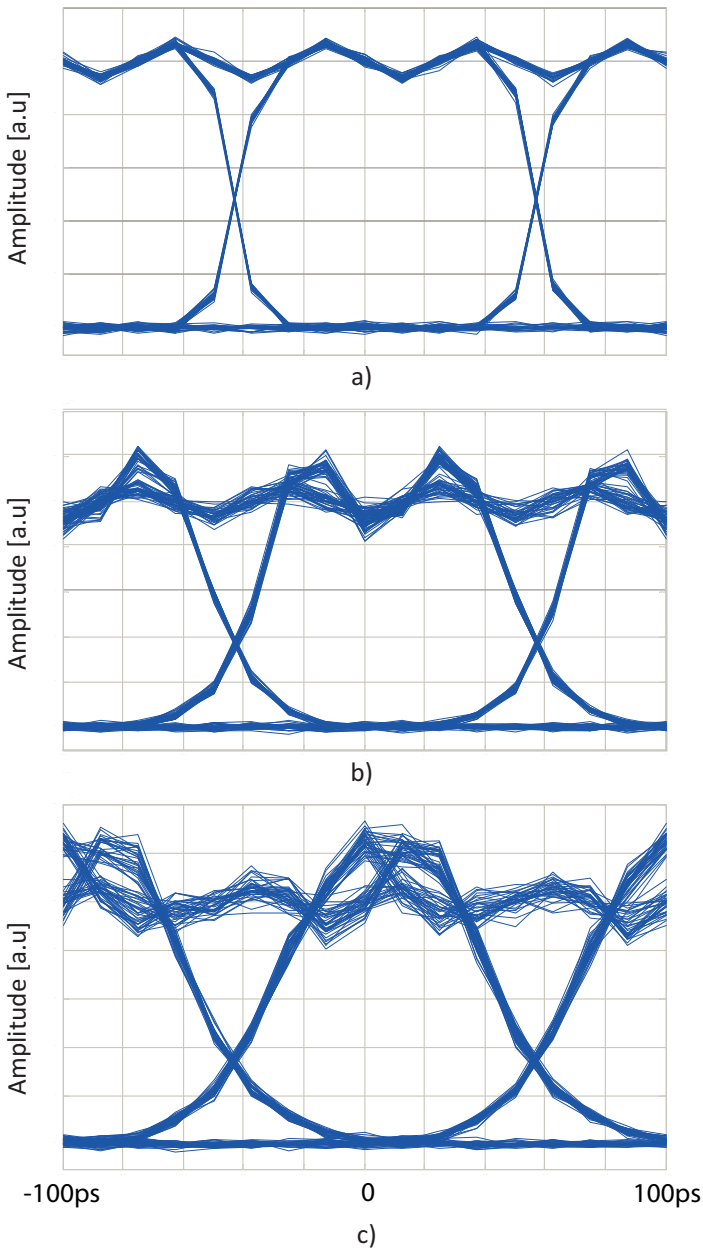

Figure 1.11: Evolution of simulated optical waveform of chirp-free 10-Gbps OOK transmitter during fiber transmission: a) transmitter output, b) after 10-km SMF, c) after 20-km SMF.

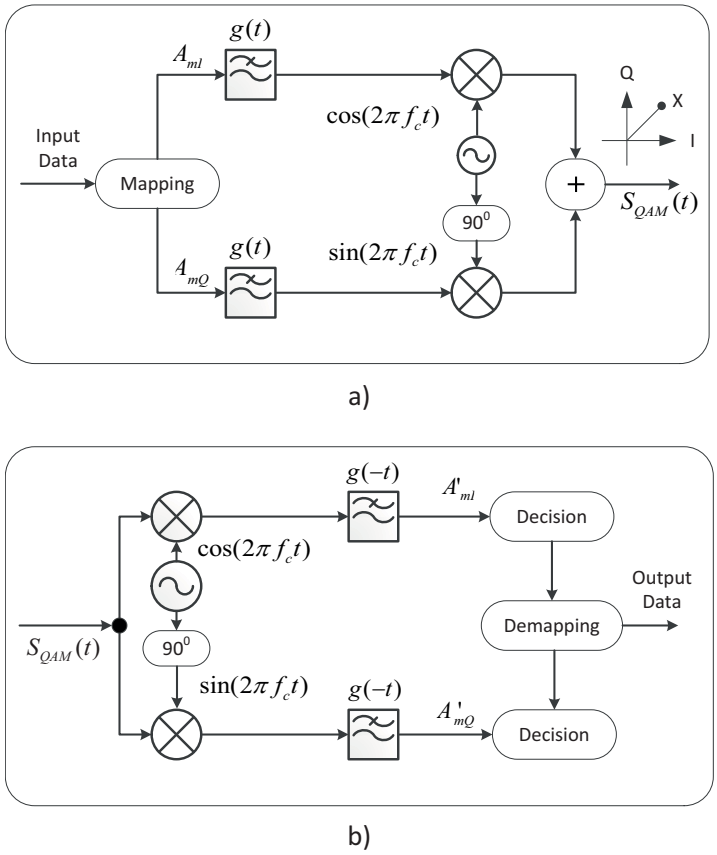

Figure 1.12: Structure of a) QAM transmitter and b) QAM receiver

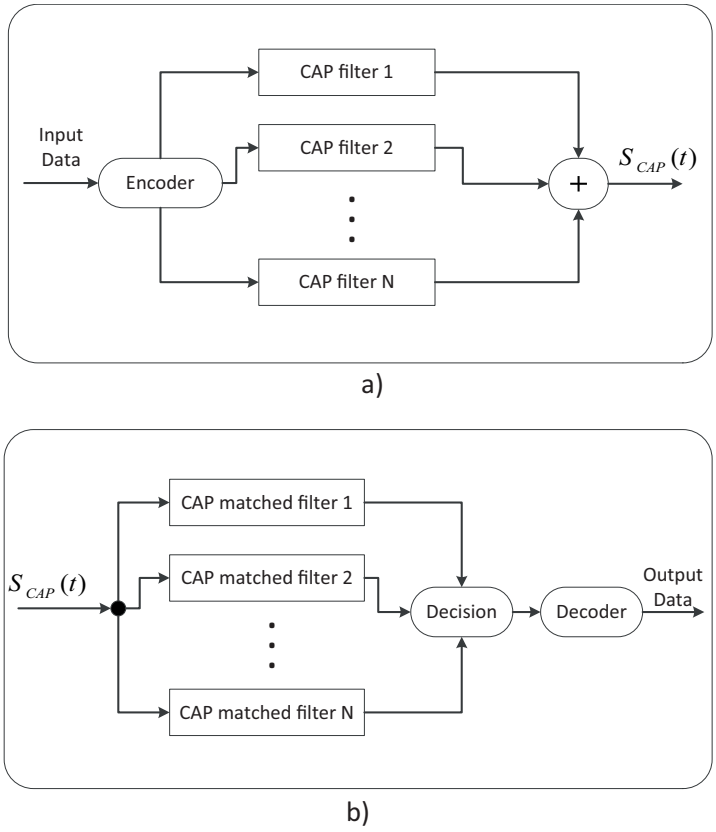

Figure 1.13: Structure of multi-dimensional CAP a) transmitter and b) receiver

1.6 State-of-the-art

In this section, analysis of state-of-the-art related to the topics of this Ph.D. thesis is presented.

1.6.1 Photonic UWB signal generation and transmission

Since UWB communication was approved by the FCC in 2002, it has been considered to be used for different applications such as radar-imaging technology, time-of-arrival-based localization, sensing [40–42]. For telecommunication, the low allowed EIRP of UWB signals limits the communication distance. Therefore, UWB is suitable for use in PANs. The classification of UWB appears in the IEEE 802.15.3a PAN standard [43]. There are two basic approaches to implement UWB signals: impulse radio (IR) single band UWB and OFDM multiband UWB. In the framework of this Ph.D. project, we only focus on IR-UWB.

To increase the reach of UWB, UWB-over-fiber (UWBoF) has been proposed by Wad in 2003 [44]. Some high-speed UWB communication systems were demonstrated after that [45,46]. In UWBoF systems, UWB signals are generated in the CS and distributed to the access points via optical fibers. UWBoF adopts several advantages of photonic technologies including light weight, small size, large tunability, and immunity to electromagnetic interference. One of the key advantages of an UWBoF system is that the UWB signals can be generated directly in the optical domain with no need for extra electrical to optical conversion. Several approaches have been proposed to generate and distribute IR-UWB signals in optical domain. Typically, these methods can be divided into two broad classes: time delay and nonlinear signal processing. In the first class, two Gaussian pulses with different phases are combined at the receiver side by controlling the delay time between them [47]. Different implementations of optical delay lines have been exploited and applied for the generation of UWB pulses, such as fiber Bragg grating (FBG) [48–50], differential group delay (DGD) module [51], dispersion medium [52], semiconductor optical amplifier (SOA) [53, 54], gain switching technique [55]. The second class is based on the nonlinear optical signal processing, after which the derivative of a Gaussian pulse is achieved. For example, a microwave differentiator [56, 57], nonlinear pulse shaping with FBG [58] and nonlinear modulation of electro-optical modulators [59, 60], and optical pulse compression [61] have been proposed. Photonic UWB generation based on direct intensity modulation of a laser has also been experimentally demonstrated by our group [62, 63].

The integration of UWBoF systems into existing baseband PONs will greatly reduce the complexity of PONs and cost of installing a new fiber link for extra UWB wireless services. In addition, the co-existence of baseband and UWB in the same infrastructure can significantly increase the spectrum efficiency of PONs and optical in-home networks. Some work has been performed to demonstrate the simultaneous transmission of baseband and the electrically generated UWB signals over PON [64, 65]. However, to further take advantage of photonic technologies, it is desirable to develop the WDM-PON compatibility of photonic UWB generation methods and directly integrate the UWB signal into the optical domain. In [66, 67], the integration of photonically generated gigabit UWB signal into WDM-PONs using dedicated wavelengths is demonstrated.

1.6.2 60-GHz radio-over-fiber systems

Several key front-end millimeter-wave (mmW) components such as transceiver modules, power amplifiers have been developed using the mature integrated-circuit (IC) technology for wireless communication in the V (50–75 GHz) and W (75–110 GHz) bands and commercially available by companies such as Gotmic AB., Millitech Inc., HXI. This encourages the research of mmW RoF, particularly at the 60-GHz band. Recently, many research groups have proposed and demonstrated several optical mmW generation, upconversion, and transmission techniques for mmW RoF systems. For instance, three main methods with different variants are proposed for the generation of 60-GHz subcarriers in optical links: direct intensity modulation with RF signals [68], frequency multiplication using an external modulator and a reference RF frequency synthesizer [69], and remote heterodyning [71]. Multi-gigabit links with different modulation formats have been demonstrated recently. By using photonic up-conversion and OFDM techniques, bitrates over 30 Gbps within the 7 GHz of available bandwidth can be achieved [70]. Our group also has demonstrated a 24-Gbps QPSK link at the 60-GHz band [71] and a 100-Gbps link at the 75-100 GHz band [72] using optical OFDM, remote heterodyning for the transmitter and coherent detection for the receiver.

However, lowering the cost of end-to-end mmW RoF system while still meeting customer demand for bandwidth and performance will be one of the dominating factors to achieve successful RoF deployments in the real networks in the near future. For that purpose, all parts of the system such as CS, BSs, transport networks need to be taken into account. For instance, the main function of CS is to generate mmW subcarrier, optically up-convert

the digital baseband or analog IF signal into the mmW band so that a cost-effective and simple method of optical mmW signal generation is critical. Additionally, because several BSs are required to cover a geographic area, the structure and cost of BS are also keys to achieve a cost-effective mmW RoF system.

Regarding the optical fiber plant, SMF is well studied in proposed mmW RoF systems in [68–72] and references therein. On the other hand, for in-building optical networks, MMFs were predominantly deployed and are continuously being deployed as a backbone for broadband LANs (approximately from 85% to 90%) [74]. When developing a system to meet the increasing demand for high-bandwidth wireless services, it is greatly encouraged to efficiently utilize that legacy infrastructure. Together with SMFs in access networks, the reuse of MMF for distribution of mmW signals through in-building optical networks to WPAN networks will save fiber reinstallation cost. Both theoretical and experimental works on MMF based RoF systems have been intensively reviewed in [75] for low frequencies and [76] for high frequencies. State-of-the-art results for MMF based mmW RoF systems are reported in [76–79]. The highest reported frequency and data rate so far are 38.8 GHz and 900 Mbps over 100-m MMF [78]. Data transmission over a composite channel has been demonstrated at low bitrate and low RF frequency: 120 Mbps data at 31.14 GHz over 20-km SMF plus 300-m MMF and 3-m wireless link [79]. However, MMF based mmW RoF systems operating at 60-GHz or higher frequency bands have not been demonstrated yet. For future deployment of 60-GHz RoF systems, it is important to evaluate the performance of 60-GHz signals over such composite channels.

Investigating applications for the 60-GHz band is also an interesting research topic. Previous works in this area suggest to use uncompressed video signals for video transmission and some demonstrations have been reported in [80–82]. The main drawback of using uncompressed video signals is reduced flexibility in terms of bitrate: bitrates are fixed depending on resolution, number of bits per pixel, and frame rate of the video sequence. This therefore results in extremely complex adaptation of HDTV systems to the significant drops of signal-to-noise ratio (SNR) caused by either severe shadowing in non light-of-sight (NLOS) case or extremely high attenuation – problems that are typical for 60-GHz systems.

1.6.3 Advanced modulation formats for VCSEL based links

VCSELs are optical light sources which have several advantages compared to edge-emitting lasers. They provide high modulation speed, low thresh-

old current and power consumption, high output power and high slope efficiency. They can be produced in small size in a planar process that allows testing and characterization on wafer stages, giving low-cost production. Furthermore, low-cost parallel devices are possible with the VCSELs produced in 2-D arrays [83,84,90]. Those advantages make VCSELs attractive light sources for low-cost high-speed optical communication links in data centers and optical access networks using IM/DD technique. 850-nm VCSELs and MMFs are used widely for local area network (LAN) and storage area network (SAN). Much of the recent development in VCSEL technology has been driven by short-range optical data links. VCSELs operating at up to 40 Gbps have been developed [85,86]. Recently, however, thanks to the development of GaInNAsSb and InAs quantum dots long-wavelength VCSELs in the range 1.3–1.55 μm have been realized [87,88,90]. Operation of a 1.5-μm VCSEL up to 40 Gbps also has been demonstrated [91]. Long-wavelength VCSELs are now available in the market by several companies such as Alight Technologies (Denmark), Vertilas GmbH (Germany), and RayCan (Korea). The key advantages of VCSELs at short wavelengths still remain at long-wavelength VCSELs. Additionally, long-wavelength VCSELs have even lower voltage operation. Because long wavelength such as 1.5-μm is used widely for communication links, long-wavelength VCSELs are now emerging as an attractive alternative to conventional lasers for high-speed links in metro-access networks.

Short-wavelength VCSEL based optical links suffer from modal dispersion of MMFs while links that use directly modulated long-wavelength VCSELs and OOK modulation are limited in transmission reach by chromatic dispersion of optical fibers due to frequency chirping caused by direct modulation of the VCSEL and large occupied bandwidth of signals. For 10-Gbps data transmission using 1.5-μm VCSELs, a 3-dB power penalty after 10-km SMF transmission was experimentally observed [92] and a 11-dB power penalty after 20-km SMF was observed after numerical simulations [**PAPER 15**]. To deal with the effect of chromatic dispersion for OOK systems, dispersion management and dispersion mitigation methods have been proposed: dispersion managed links [92, 93], optical injection locking [94] and offset filtering [**PAPER 15**].

Advanced modulation formats have also been proposed to reduce the bandwidth of the signals. High-speed PAM using a single VCSEL has been demonstrated: transmission of a 25-Gbaud 4-PAM signal over 100-m MSF using a 1.5-μm VCSEL in [95], a 15-Gbaud 4-PAM signal over 200-m MMF using a 850-nm VCSEL in [96]. Its scalability is limited because it is single

dimension modulation. DMT and OFDM, are promising technologies for both increasing spectral efficiency and dispersion tolerance. High speed data transmission of DMT signals using VCSELs has been demonstrated recently. In [97], 24-Gbps data was transmitted over 730-m MMF using a 850-nm VCSEL while in [98], authors demonstrated real-time transmission of 11.25 Gbps data over 25-km SMF using a 1.5-μm VCSEL. However, such DMT systems require fast digital-to-analog converter (DAC) and analog-to-digital converter (ADC) converters to support high-speed data transmission. Additionally, DMT transceivers consume high power for signal processing compared to conventional OOK transceivers. A simpler method, single-cycle subcarrier QAM was proposed in which the subcarrier frequency is equal to the symbol rate. Transmission of a 10-Gbaud 16-QAM signal in 20-GHz bandwidth over 200-m MMF using a 850-nm VCSEL has been reported [99].

Another low-cost possible solution for IM/DD system is carrierless amplitude phase modulation (CAP). Up to 40-Gbps optical communication system employing two-dimension CAP has been demonstrated in [100]. Application of multi-dimensional, multi-level CAP for high-SE VCSEL-based optical links has been intensively investigated by our group. Important results can be found in **PAPER 17, PAPER 18, PAPER 19, PAPER 20** and [101].

1.7 Thesis contributions beyond state-of-the-art

In this section, I highlight the achievements of my Ph.D. thesis to show how my works have significantly extended the state-of-the art reviewed in section 1.6. The achievements are divided into three topics in conjunction with the discussed state-of-the-art including photonic UWB signal generation and integration, low-cost 60-GHz radio over fiber links and advanced modulation formats for VCSEL based systems.

1.7.1 UWB signal generation and integration into existing optical networks

In the area of photonic generation of UWB signals, my work presented in **PAPER 1-2** improves previous results in [62, 63]. Two simpler and more flexible methods are proposed to optically generate FCC compliant Gigabit UWB signals by employing a single DML. In **PAPER 1**, multiple-subcarrier up-conversion was proposed to up-convert baseband spectrum to all allocated UWB spectrum. In **PAPER 2**, offset-filtering is introduced to shape the spectrum of UWB pulses to meet FCC regulation. This solution requires less active optical devices than other methods proposed up to date. In **PAPER 1**, a 2-Gbps UWB signal is transmitted over 46-km SMF and 0.5-m wireless link. In **PAPER 2**, transmission of a 1-Gbps UWB signal over 23-km SMF and 0.4-m wireless link is reported. Our methods in those two papers are also wavelength independent resulting a cost-effective solution to generate and distribute UWB signals in future WDM-PON access networks.

Additionally, several applications scenarios of UWB signals in next-generation optical access networks are first demonstrated in this Ph.D. project.

Two architectures for integration of UWB signals into baseband WDM-PON are demonstrated. Both the UWB signal and baseband signal share the same wavelength to improve overall SE of the systems. In **PAPER 1**, the 2-Gbps data is carried in both baseband and UWB frequency band. This provides to end-users flexible access to wired or wireless services. In **PAPER 2**, two different 1-Gbps signals are transmitted in the baseband and UWB frequency band, separately.

PAPER 3 reports the transport of a 2-Gbps UWB signal using a phase-modulated RoF link assisted with coherent detection, which has attracted much interest for high-speed wireless signal detection [73]. The effect of chromatic dispersion on the performance of the UWB signal in a metro-

access optical link up to 80-km fiber and the capability of a DSP-enabled coherent receiver to compensate for the effect are investigated. In **PAPER 4**, we further investigate the performance of that UWB signal in a long-reach heterogeneous hybrid wireless-wired access network supporting different data formats, bit rates. The phase modulated 2-Gbps BPSK UWB signal is seamless integrated into a WDM-PON with a 5-Gbps OOK signal, a 20-Gbps QPSK signal and a 500-Mbps OFDM signal at 5-GHz RF frequency. All signals were demodulated using a single reconfigurable digital coherent receiver.

UWB has been proposed and demonstrated for separate applications such as broadband communication, sensing and localization. In **PAPER 5**, for the first time, we demonstrate the utilization of an UWB signal for both communication and motion sensing in a converged optical network. A 1.5-μm VCSEL is used to distributed a 2-Gbps UWB signal for high-speed communication. The UWB signal is simultaneously used to estimate the speed of a spinning blade without interrupting communication service.

1.7.2 60-GHz radio-over-fiber systems

In collaboration with Valencia Nanophotonics Technology Center of the Universidad Politécnica de Valencia, we looked into possibilities to simplify the configuration of a 60-GHz RoF system in all parts of the system: mmW signal generation, data modulation, transport and detection to reduce the cost of the overall system. In the meantime, it still meets near future customer requirements for bandwidth and performance. In **PAPER 6**, we demonstrated error-free end-to-end transmission of 2-Gbps data in the 60-GHz band over a composite optical channel including 10-km SMF and 1-km MMF. This is the very first time that performance of a wireless signal at the 60-GHz band over a MMF is experimentally reported. The results show that it is possible to reuse the legacy MMF networks which have been deployed widely in buildings to reduce the CAPEX and OPEX for future mmW RoF systems.

We not only looked into the performance of the physical layer of a mmW RoF system but also the performance of the application layer, particularly video signal quality. In **PAPER 7** we explored the notion of joint optimization of physical layer parameters of a RoF link including power levels, distance and the codec parameters comprising quantization, error-resilience tools based on peak signal-to-noise ratio (PSNR) as an objective video quality metric. We focus on the trade-off between the distortion introduced by the source (lossy compression) and distortion introduced by channel for high

quality HD video transmission over 60-GHz RoF links. Our experiment and simulation shows that it is possible to achieve significant extension of wireless distance employing low complexity physical layer solution for mmW RF signal generation and detection. For instance, at a PSNR of 33 dB, wireless transmission distance is almost doubled from 3 m to 5.5 m when the compression ratio of the video signal changes from 10 to 3. Additionally, robustness and reach of simplified converged fiber-wireless RoF communication links can be significantly improved by employing video coding to reduce the data rate for transmission.

1.7.3 Advanced modulation formats for VCSEL based links

As a result of the external stay at University of California, Berkeley during my Ph.D. study, I proposed, theoretically analyzed and demonstrated the utilization of sub-cycle subcarrier frequencies for QAM modulation including half-cycle and quarter-cycle subcarriers to improve SE. By using subcarrier at half the baud rate, the SE of the QAM signal is 2/3 symbol/s/Hz while the SE of single-cycle QAM signal proposed in [99] is 1/2 symbol/s/Hz. Compared to DMT modulation with approximately the SE of 1 symbol/s/Hz, the SE is lower. However, implementation of half-cycle QAM is much simpler with lower power consumption because no DAC is required for the transmitter, the receiver can be implemented using current technologies for non return-to-zero (NRZ), PAM signals without a high-speed ADC. The concentration of the spectral power of sub-cycle signals at low frequencies also makes it suitable for optical systems employing DMLs such as VCSELs or DFBs. The first experimental result, transmission performance of a 10-Gbps half-cycle 4-QAM signal over 20-km SMF using 1.5-μm VCSEL is presented in **PAPER 8**. The power penalty after 20-km fiber transmission is only 2.5 dB at the BER of 10^{-5}. It is the most tolerant signal to chromatic dispersion (CD) for 10-Gbps links using a free-running 1.5-μm VCSEL without employing any dispersion compensation methods.

In **PAPER 9**, we extend **PAPER 8** by theoretically investigating the principle and characteristics of sub-cycle QAM signals. We also experimentally compare the performance of the half-cycle QAM signal with NRZ signals at the same bit rate and same baud rate to further confirm advantages of half-cycle QAM signals.

Half-cycle QAM signals are also tolerant to modal dispersion. The performance of a 9-Gbps 4-QAM signal in the comparison with a 9-Gbps NRZ signal after 1-km MMF transmission using a 850-nm VCSEL is reported **PAPER 10**. In all of those works, we only used 4-QAM, which results a

relatively low data rate. This is because the limited performance of available equipment we used to generate QAM signals at the time of experiments.

In the framework of GiGaWaM, an EU project that I have been involved in [8], L-band VCSELs have been produced by Vertilas, a project consortium member. Beside exploring applications of L-bands VCSEL for further-proof WDM-PON systems, we also experimentally investigated the possibility of migrating multiple-lane link into a single compact WDM system based on advanced L-band VCSELs for future data-centers. Four L-band VCSELs are directly modulated with 4-PAM signals at 7 Gbauds to generate a total data nominal rate of 56 Gbps. The results is reported in **PAPER 11**.

Several other works performed during this Ph.D. project also contribute to push forward the state-of-the-art of data transmission techniques for short-range optical communication systems: dispersion tolerance improvement for OOK signals in **PAPER 15, 23**, high SE optical links employing CAP in **PAPER 17-20**.

Chapter 2

Description of papers

This thesis is based on a set of articles already published or submitted for publication in peer-reviewed journals and conference proceedings. These articles present the results obtained during the course of my doctoral studies, combining theoretical analysis, simulation and experimental results. The papers are grouped in three categories: the generation and integration of ultra-wide band (UWB) signals into optical networks (**PAPER 1** to **PAPER 5**), simplifying 60-GHz band signal generation and transmission links (**PAPER 6** to **PAPER 7**) and advanced modulation formats for vertical-cavity surface-emitting laser (VCSEL) based optical networks (**PAPER 8** to **PAPER 11**).

2.1 Generation and integration of UWB signals into PONs and short-range optical Links

PAPER 1 In this paper, we propose a novel and simple scheme to realize wavelength-independent flexible access for gigabit wireline and impulse radio (IR)-UWB wireless services. The UWB signals are generated by multi-carrier up-converting and reshaping the baseband signals. The proposed system is experimentally demonstrated with the performance assessment of 2.0-Gbps data in both baseband and UWB formats after 46-km single-mode fiber (SMF) transmission and further 0.5-m wireless for UWB data. The bandwidth allocation flexibility of the system to support different data rates including 1.0 and 1.6 Gpbs is demonstrated by simply tuning the clock signal.

PAPER 2 We propose a compact integration system to simultaneously provide wireline and wireless (baseband and UWB) services to end-users in a wavelength division multiplexing (WDM)-passive optical network (PON). A 1-Gbps UWB signal is optically generated using a directly modulated laser (DML) and offset filtering. The UWB signal then shares the same wavelength with a 1-Gbps baseband signal. The integration of UWB signals into baseband WDM-PON increases electrical/optical spectrum efficiency of the whole systems. Two signals are transmitted over a 23-km SMF and the UWB signal is additionally transmitted over a 0.4-m wireless link. The trade-off between the performance of UWB and baseband signals is also analyzed.

With the development of digital coherent receivers, in **PAPER 3**, we consider optical phase-modulated transmission and coherent detection of an IR-UWB-over-fiber system in a coherent-detection PON scenario. We demonstrate an uplink transmission of a 2-Gbps keying binary phase shift keying (BPSK) IR-UWB signal. The influences of the chromatic dispersion of various SMF links (from 20 km in conventional access networks to up to 78 km in long-reach access networks) are experimentally investigated. With less than 1-dB power penalty when using digital signal processing (DSP)-based dispersion compensation, the result proves the robustness of coherent detection based UWB-over-fiber system.

PAPER 4 In this paper, we investigate the integration of an IR-UWB signal into a heterogeneous WDM metro-access network using a reconfigurable digital coherent receiver. The unified heterogeneous metro access network included the following subsystems: 1) 5-Gbps OOK directly modulating VCSEL. 2) Baseband 20-Gbps non return-to-zero (NRZ)-quadrature phase shift keying (QPSK). 3) Optically phase-modulated 2-Gbps IR-UWB and 4) Optically phase-modulated radio-over-fiber (RoF) link with 500-Mbps OFDM at 5-GHz RF frequency. Four signals are wavelength multiplexed onto the same optical fiber, transported through 78 km of installed optical fiber and detected using a single reconfigurable digital coherent receiver.

PAPER 5 presents the very first experimental demonstration of a simultaneous gigabit UWB telecommunication and wireless UWB sensing application. A 1.550-μm VCSEL-generated IR-UWB signal is used for 2-Gbps wireless data distribution over 800-m and 50-km SMF links which present short-range in-building and long-reach access network applications, respec-

tively. The IR-UWB signal is also used to simultaneously measure the rotational speed of a blade spinning between 18 and 30 Hz without interrupting communication service.

2.2 Simplifying 60-GHz band signal generation and transmission links

PAPER 6 we propose and experimentally demonstrate a simple, cost-effective hybrid gigabit fiber-wireless system operating at the 60-GHz band for in-building wireless access. Simplicity and cost-effectiveness are achieved in all parts of the system by utilizing direct laser modulation, optical frequency up-conversion, combined SMF and multimode fiber (MMF) transmission and envelope detection. Error-free transmission of 2-Gbps data in the 60-GHz band over a composite channel including 10-km standard SMF/1-km MMF and 6.5-m air transmission is successfully achieved.

PAPER 7 This paper addresses the problem of distribution of high-definition video over a fiber-wireless network. We explore the notion of joint optimization of physical layer parameters of a RoF link (power levels, distance) and the codec parameters (quantization, error-resilience tools) based on peak signal-to-noise ratio (PSNR) as an objective video quality metric. The physical layer architecture with the low complexity envelope detection solution is investigated. We present both experimental studies and simulation of high quality high-definition compressed video transmission over a 60-GHz fiber-wireless link.

2.3 Advanced modulation format for VCSEL based optical networks

PAPER 8 we propose and demonstrate the first experimental results of sub-cycle QAM modulation for spectrally efficient VCSEL-based optical links. We point out that the subcarrier frequency can be reduced to half the symbol rate to improve spectral efficiency while the simplicity of the

transceiver is maintained. By using a subcarrier frequency at half the symbol rate, the spectral width, defined as the frequency of the first null in the spectrum, of the QAM signal is reduced by 25% compared to conventional QAM signals. We demonstrate the generation and detection of 10-Gpbs and 16-Gbps 4-QAM signals transmitted over 20-km SMF and 3-km SMF, respectively using an un-cooled commercially available 10-GHz, 1.5-μm VCSEL. Bit error ratio (BER) below the limit of forward error correction (FEC) is achieved. 2.5-dB power penalty is observed for the 10-Gbps 4-QAM signal after 20-km fiber transmission.

PAPER 9 is an extended work of **PAPER 8** to explain the theory of QAM signal generation, detection with the subcarrier frequency lower than the baudrate including a quarter and a half the baudrate. The performance comparison with on-off keying (OOK) signals at the same datarate (10 Gbps) and the same baudrate (5 Gbaud) is also presented to further demonstrate the advantages of sub-cycle QAM signals.

PAPER 10 presents another application of half-cycle QAM signal for short-range optical systems using MMF. Transmission of a 6-Gbaud 4-QAM signal over 1-km MMF using 9-GHz bandwidth was successfully achieved with a bit error rate (BER) below the limit of the FEC. The performance comparison with an OOK signal at the same data rate shows that the half-cycle QAM signal improves 1.5-dB power penalty after 1-km MMF transmission.

In **PAPER 11** paper, we look into high-speed, cost-efficient and power-efficient VCSEL-based WDM system oriented towards short-range optical fiber connectivity. Four novel L-band VCSELs are directly modulated with 4-pulse amplitude modulation (PAM) signals at 7 Gbauds to generate a total data nominal rate of 56 Gbps. Experimental validation achieves successful transmission over 10 km of SMF at 4x14 Gbps. Inter-channel crosstalk penalty is observed to be less than 0.5 dB and a transmission penalty around 1 dB. The power budget margin ranges within 6 dB and 7 dB.

Chapter 3

Conclusions

3.1 Conclusions

The demand for bandwidth of both wired and wireless services continuously keeps increasing and places tremendous pressure on communication infrastructures. In particular, it has generated a "broadband bandwidth bottleneck" in the access networks, both wired and wireless ones. Deployment of optical fibers and photonic technologies in access and in-building networks as the transmission medium for both wired and wireless services is considered as the key solution to meet that growing demand. In this Ph.D. study, I have comprehensively investigated applications of photonic techniques for cost-effective high-speed communications supporting both wired and wireless services in two main areas: optical/wireless integration and advanced modulation formats. All in all, optical techniques proposed and demonstrated in this thesis have shown great potential to enable future broadband cost-effective converged wired/wireless access networks.

3.1.1 Optical/wireless integration for high-capacity converged networks

In this Ph.D. project, first of all, applications of optical technologies to enable high-speed wireless ultra-wide band (UWB) communication has been intensively investigated. Two novel methods have been proposed to optically generate gigabit UWB signals employing a single directly modulated laser (DML). Gigabit UWB communication in several applications and scenarios of future broadband access networks is investigated: integrated wired/wireless wavelength division multiplexing (WDM)-passive op-

tical network (PON), converged communication/sensing networks. UWB signals are distributed over various lengths of optical fibers to represent different types of optical networks: in-building network, typical access network and long-reach access network. Wireless transmission of UWB signals is also demonstrated in the range of a wireless personal area network (WPAN) to fully prove the capabilities of end-to-end service distribution.

The subsequent research work for this topic has focused on the study of 60-GHz radio-over-fiber (RoF) links. We investigated the performance of a very low-cost 60-GHz system. All parts of the system are simplified with less electrical and optical components involved: direct modulation for baseband data, double sideband carrier suppression for millimeter-wave (mmW) subcarrier generation and envelope detection for data down-conversion. We demonstrated the possibility of utilizing widely-deployed multimode fiber (MMF) networks in homes, buildings for 60-GHz signal distribution. It greatly help to reduce capital expenditure (CAPEX) and operating expense (OPEX) to deploy new mmW RoF services. We also analyzed and optimized the quality of video signals for a given link budget. The contributions of this Ph.D. thesis for optical/wireless integration topic are summarized in Table 3.1.

Employing optical technologies for signal generation and distribution will be the key for future broadband wireless access networks. Optical techniques discussed in this thesis for optical/wireless integration have great potential in satisfying increasing bandwidth demands for various wired and wireless services. Additionally, they significantly decrease network hardware costs which enables relatively cheap mass production and possibly contribute to quick large-scale deployments. Therefore, they will be very strong candidates to build a ubiquitous broadband access network.

3.1.2 Advanced modulation formats for VCSEL based links

Advanced modulation formats play an important role in the design of high-speed short-range and access optical networks where low cost and low energy consumption is the key for practical deployment. In this research, we have discussed generation, transmission and detection of some key modulation schemes for intensity modulation (IM)/direct detection (DD) links focusing on pulse amplitude modulation (PAM), single subcarrier quadrature amplitude modulation (QAM) and carrierless amplitude phase modulation (CAP). We proposed employing subcarrier frequencies at quarter the baudrate and half the baudrate for QAM modulation. Half-cycle QAM modulation improves SE by 25% as compared to conventional single-cycle

Table 3.1: Summary of contributions for optical/wireless integration

PAPER	Data	Transmission	Contributions
1	2-Gbps UWB 2-Gbps NRZ	46-km SMF 0.5-m wireless	- Generation of UWB signal - Integration into WDM-PON
2	1-Gbps UWB 1-Gbps NRZ	23-km SMF 0.4-m wireless	- Generation of UWB signal -Integration into WDM-PON
3, 4	2-Gbps UWB 20-Gbps QPSK 500-Mbps OFDM 5-Gbps OOK	80 km MSF 1 m wireless	- Seamless integration - Universal digital coherent receiver
5	2-Gbps UWB	46-km SMF 800-m SMF 2.5-m wireless	- Converged comm./sensing
6	2-Gbps 60 GHz	10-km SMF +1-km MMF 6.5-m wireless	- Simplified 60-GHz system -MMF for 60-GHz signal distribution
7	Compressed video	20-km SMF 6-m wireless	- Simplified 60-GHz system - Performance optimization

Table 3.2: Summary of contributions for advanced modulation formats for VCSEL based systems

PAPER	Modulation format	Bitrate	VCSEL	Fiber link
8, 9	half-cycle 4-QAM	10 Gbps	1.5-μm	20-km SMF
		16 Gbps		3-km SMF
10	half-cycle 4-QAM	9 Gbps	850-nm	1-km MMF
11	4-PAM	4 x 14Gbps	L-band	20-km SMF

QAM and spectrum concentrates in low frequency region which is suitable for DML based IM/DD. The high dispersion tolerance of half-cycle QAM modulation compared to on-off keying (OOK) modulation is demonstrated in both single-mode fiber (SMF) and MMF based systems. It has been observed the 10-Gbps 1.5-μm VCSEL based link has improved chromatic dispersion tolerance by 3 dB while the 9-Gbps 850-nm VCSEL based link has improved modal dispersion tolerance by 1.5 dB. Table 3.2 presents the key contributions of this Ph.D. project for the topic.

In summary, advanced modulation formats such as half-cycle QAM modulation are attractive solutions for next-generation access networks because of low complexity of transceiver implementation and high dispersion tolerance even with large frequency chirping of VCSELs. Furthermore, the successful demonstration of systems employing VCSELs opens prospects of the wide deployment of VCSELs for future low cost and low power consumption access networks.

3.2 Future work

3.2.1 High-capacity converged optical/wireless networks

There are still many issues of RoF systems that need to be identified and studied in the future. First, the full-duplex demonstration with real-traffic to prove capability of systems to support different services is necessary. The media access control (MAC) layer design, network architecture are also very important for successful development of both wired and wireless systems. Integrability of wireless signals other than UWB and 60-GHz signals need to be investigated. Particularly, for RoF system, handover, radio resource management are also very critical. Finally, the demonstration presented in this thesis used lab equipment. Therefore, a further step before field trials, developing integrated prototypes also should be considered.

3.2.2 Towards Tbps datacom and client optics

In our work, inherent low performance of the XOR gate as an QAM modulator only allowed us to investigate half-cycle QAM signals at a low modulation level (4-QAM). Therefore, investigation of half-cycle QAM signals at higher modulation level as well as improving the half-cycle QAM modulator should be interesting for further research.

The most promising applications where low-cost advanced modulation format solution be used in near future are datacom and client optics. For

the next data rate beyond 100G, technology for 100G products (25 Gbps per lane) is feasible for rates up to 400 Gbps, however not practical for 1 Tbps and above due to connector complexity, printed circuit board (PCB) routing, switch application-specific integrated circuit (ASIC) input/output and cost limitations [102]. High SE modulation format is an practical approach to reduce the numbers of transceivers. Investigation of CAP, single-subcarrier QAM and PAM at such high speed and high density is a potential future research.

Paper 1: WDM-PON-compatible system for simultaneous distribution of gigabit baseband and wireless ultrawideband services with flexible bandwidth allocation

T. T. Pham, X. Yu, T.B. Gibbon, L. Dittmann and I.Tafur Monroy, "WDM-PON-compatible system for simultaneous distribution of gigabit baseband and wireless ultrawideband services with flexible bandwidth allocation," *IEEE Photonics Journal*, vol. 3, no. 1, pp. 13—19, 2011.

IEEE Photonics Journal
An IEEE Photonics Society Publication

A WDM-PON-Compatible System for Simultaneous Distribution of Gigabit Baseband and Wireless Ultrawideband Services With Flexible Bandwidth Allocation

Volume 3, Number 1, February 2011

Tien-Thang Pham, Member, IEEE
Xianbin Yu, Member, IEEE
Timothy Braidwood Gibbon, Member, IEEE
Lars Dittmann, Member, IEEE
Idelfonso Tafur Monroy, Member, IEEE

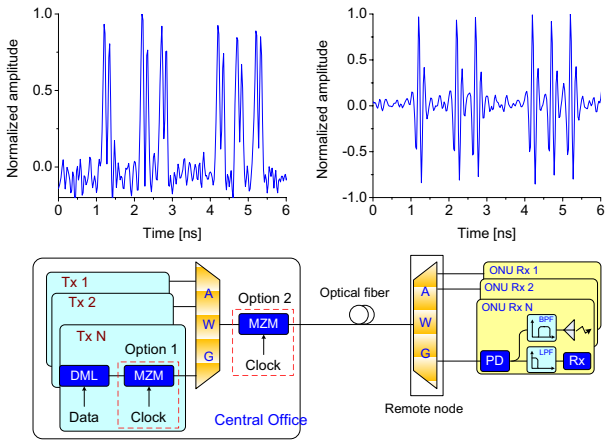

DOI: 10.1109/JPHOT.2010.2095834
1943-0655/$26.00 ©2010 IEEE

A WDM-PON-Compatible System for Simultaneous Distribution of Gigabit Baseband and Wireless Ultrawideband Services With Flexible Bandwidth Allocation

Tien-Thang Pham, *Member, IEEE*, Xianbin Yu, *Member, IEEE*, Timothy Braidwood Gibbon, *Member, IEEE*, Lars Dittmann, *Member, IEEE*, and Idelfonso Tafur Monroy, *Member, IEEE*

DTU Fotonik, Department of Photonics Engineering, Technical University of Denmark, DK-2800 Kgs. Lyngby, Denmark

DOI: 10.1109/JPHOT.2010.2095834
1943-0655/$26.00 ©2010 IEEE

Manuscript received October 27, 2010; accepted November 20, 2010. Date of publication November 29, 2010; date of current version January 24, 2011. Corresponding author: T. T. Pham (e-mail: ptit@fotonik.dtu.dk).

Abstract: In this paper, a novel and simple scheme to realize flexible access for gigabit wireline and impulse radio ultrawideband (IR-UWB) wireless services is proposed. The UWB signals are generated by multi-carrier upconverting and reshaping the baseband signals. The proposed system was experimentally demonstrated with the performances of 2.0-Gb/s data in both baseband and UWB formats after 46-km single mode fiber transmission and further 0.5-m wireless for UWB data. The flexibility of the system is confirmed by investigating the system performance at different data rates including 1.0 and 1.6 Gb/s. Optical wavelength independency and data-rate variability of UWB signal generation makes the system attractive for potential wireline and wireless applications in existing wavelength division multiplexing (WDM)-passive optical network (PON) systems.

Index Terms: Microwave photonics, ultrawideband (UWB), radio over fiber, wavelength division multiplexing (WDM), passive optical network (PON).

1. Introduction

Ultrawideband (UWB) is finding its application in high-speed wireless communication systems as well as sensor applications [1]. Regulated by the U.S. Federal Communications Commission (FCC) for the spectral band from 3.1 to 10.6 GHz, the power spectral density (PSD) of a UWB transmitter is limited to −41.3 dBm/MHz [2], which is below the noise level of other wireless communication systems such as the Global Positioning System (GPS), Global System for Mobile Communications (GSM), and Worldwide Interoperability for Microwave Access (WiMAX). The low emitted PSD causes the wireless transmission distance to be limited to within a few meters. In this context, UWB-over-fiber is a promising technology for extending the coverage of UWB services. Recently, several techniques have been proposed to optically generate impulse radio UWB (IR-UWB) signals using a fiber-Bragg-grating-based frequency discriminator [4], a gain-switch laser [5], or relaxation oscillations of a laser [6].

On the other hand, passive optical networks (PONs) are highly recognized as the most promising candidates for next-generation optical access systems to satisfy the increasing bandwidth demand

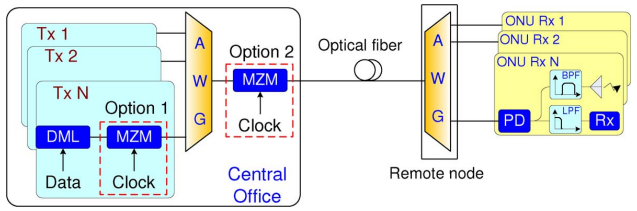

Fig. 1. Proposed WDM-PON system for photonic UWB generation and distribution. DML: directly modulated laser, MZM: Mach–Zehnder modulator, AWG: arrayed waveguide gratings, PD: photodetector, HPF: high-pass filter, LPF: low-pass filter. MZM can be used by a single channel (placed after the DML—option 1) or shared by many WDM channels (placed after the AWG—option 2) if they operate at the same data rate.

from households as well as enterprises [8]. The convergence of distributing wireline and wireless services including IR-UWB service over a common PON architecture is regarded as a potential solution to exploit cost-efficiently and, with a high degree of flexibility, the benefits of low-loss and high-bandwidth optical fiber access plants. However, to realize this vision, it is mandatory to conceive simple approaches for photonic generation of IR-UWB signals with common photonic PON components as well as to develop simple and flexible methods for service differentiation and dynamic bandwidth allocation. Recently, Pan *et al.* have demonstrated an electrically generated UWB signal that can share a single wavelength with a baseband signal in a wavelength division multiplexing-PON (WDM-PON) system [9]. The authors also have demonstrated the seamless integration of UWB service in a WDM-PON system that supports a variety of wireline and wireless services [10].

In this paper, we propose and experimentally demonstrate a novel, simple, and flexible method to generate gigabit FCC-compliant IR-UWB signals by optically upconverting baseband signals using their clock signal as a source of multiple sinusoidal signals. Assisted by a digital signal processing (DSP) receiver, the data in both the baseband and UWB formats at 1, 1.6, and 2 Gb/s are recovered without error bits after 46-km single mode fiber (SMF) and further 0.5-m wireless for the UWB signal. The fact that the baseband bandwidth for the wireline service can be shared with the wireless service just by switching on the clock signal enables flexible access connectivity for end-users with a less-complex architecture. Additionally, wavelength-independent operation makes our proposed system compatible with existing WDM-PONs.

2. Proposed System and Operation Principle

Fig. 1 depicts the proposed WDM-PON supporting UWB and wireline baseband service distribution. The operation principle of this scheme is based on the use of the same wireline baseband data source for UWB service. At the central office (CO), for each end-user, an electrical baseband signal drives a directly modulated laser (DML). The baseband data is then mixed with multiple optical-intensity-modulated sinusoidal signals at a Mach–Zehnder modulator (MZM). Due to the nature of the sum of sinusoidal signals at different frequencies, the clock signal is utilized to drive the MZM. The are two options for the position of the MZM, as shown in the figure. If the MZM and the clock signal is used separately by a single channel, it is placed after the DML (Option 1). Optical signals from all WDM channels are combined by an array waveguide grating (AWG). The MZM and clock signal also can be shared by several WDM channels if they operate at the same data rate (Option 2). In this case, the MZM is placed after the AWG. The combined optical signal is transmitted to an AWG-based remote node (RN) through a fiber. At the output of the photodiode (PD) of each optical network unit (ONU), there are copies of the data at both the baseband and the harmonic frequencies of the modulating sinusoidal signals. Therefore, by using appropriate electrical filtering at the ONU, both wireline baseband and FCC-compliant wireless IR-UWB signals are achieved for service distribution. This scheme provides wireless service dynamically as connectivity to the UWB service is simply enabled by switching the clock signal on or off.

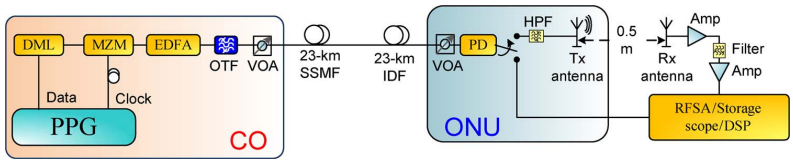

Fig. 2. Experimental setup of photonic UWB generation, distribution, and detection. DML: directly modulated laser, MZM: Mach–Zehnder modulator, PPG: pulse pattern generator, EDFA: erbium-dropped fiber amplifier, OTF: optical tunable filter, SSMF: standard single mode fiber, IDF: inverse dispersion fiber, VOA: variable optical attenuator, PD: photodetector, RFSA: radio frequency spectrum analyzer, DSP: digital signal processing, Amp: electrical amplifier. HPF: high-pass filter.

3. Experimental Setup

The experiment setup of the proposed system is shown in Fig. 2. A 4-Gb/s programmed pattern from a pulse pattern generator (PPG) was used to drive a DML. The reversed lasing threshold and bias currents of the DML were −11 mA and −31 mA, respectively. A sequence of 2 bits from the PPG was used to generate one UWB bit. Due to the negative bias of the DML, "0" and "1" UWB bits are represented by the sequences of "11" and "10," respectively. The data from the PPG is thus 50% inverted return-to-zero (RZ), and the effective bit rate of the UWB signal is 2 Gb/s. The output of the DML was then launched into a 10-GHz MZM. The clock signal from the PPG at 4 Gb/s was used as a multiple-subcarrier source to drive the MZM. The MZM biased at 3 V operated at a nonlinear region to modify the amplitude of subcarriers and consequently shape the waveform of the generated UWB signal. An Erbium-dropped fiber amplifier (EDFA) and a tunable optical filter (TOF) with 0.9-nm 3-dB bandwidth were employed to amplify the optical signal and reject out-band amplified spontaneous emission (ASE) noise. The optical signal was transmitted over a 46-km link including 23-km standard SMF and dispersion-matched 23-km inverse dispersion fiber (IDF) and then detected by a PD with 12-GHz bandwidth. The losses of SMF and IDF fibers were 5.1 dB and 7.7 dB, respectively. The detected signal was filtered by a commercially available high-pass filter (HPF) with 3.1-GHz cutoff frequency to form UWB pulses. The detected signal was also used to recover the transmitted data in the baseband. The UWB signal was radiated into the free space by an Omni-directional antenna (Skycross SMT-3TO10M-A). The wireless transmission distance was set at 0.5 m. The radiated UWB signal was received by a directive antenna (Geozondas AU-3.1G10.6G-1). Data in both the UWB and baseband formats were sampled, stored at 40 GSa/s by a digital sampling scope (DSO Agilent Infiniium 8000B), and then processed offline by using a DSP receiver.

4. Experimental Results and Discussions

Fig. 3(a) and (b) illustrate the electrical spectra of the UWB signals with a $2^7 - 1$ pseudorandom binary sequence (PRBS) pattern length after 46-km fiber transmission at −19 dBm received optical power with and without the HPF. The effective mask is the allowed mask when the frequency response of the transmitting antenna is taken into account [3]. As shown in the figure, the obtained UWB signals were fully compliant with the FCC mask. Fig. 3(c) and (d) show the detected electrical spectra when the clock signal and data were off, respectively. When the clock signal was off, some frequency components (<−50 dBm/MHz) could be observed in the UWB frequency band, which was caused by the relaxation oscillations of the DML operating close to the threshold current. When the clock signal was applied to the MZM, PSD at high-frequency band increased over 10 dB, and the generated UWB signal met the FCC requirements from 3.1 to 10.6 GHz. Fig. 4(a) and (b) show the detected waveform of the sequence "001011001110" before and after the HPF. We can notice that the waveform of the generated UWB pulse is similar to a fifth-order Gaussian derivative, which is known to agree well with the FCC spectra requirements for UWB systems [6]. Fig. 4(c) illustrates the waveform of the received UWB signal after wireless transmission.

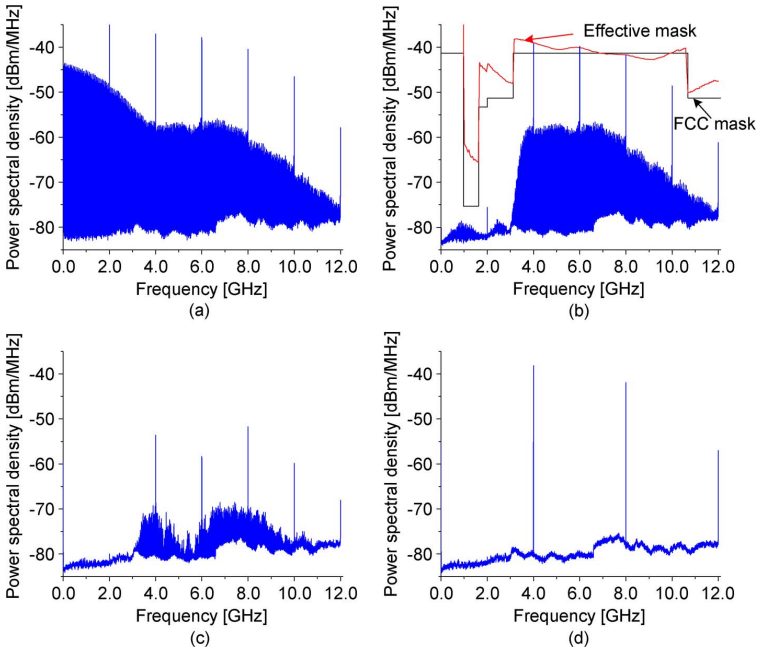

Fig. 3. Electrical spectra of detected 2-Gb/s baseband and UWB signals at −19 dBm after fiber transmission. (a) Without the HPF, (b) with the HPF, (c) with the HPF and clock off, and (d) with the HPF and data off.

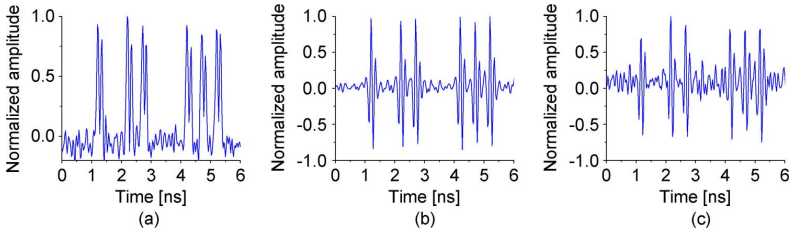

Fig. 4. Waveforms of the pattern "001011001110" at 2 Gb/s (a) without the filter, (b) with the filter (inside the mask), and (c) after 0.5-m wireless transmission.

4.1. Performance of 2-Gbps UWB Signal

To assess the performance of the UWB signal, 100 000 UWB bits were recorded and processed offline using a DSP algorithm. The DSP comprises of noise filtering, bit correlation, and threshold detection functions [7]. In the final step, value of each detected UWB bit was determined by comparing the sum of some sampled points within each bit slot to an optimally determined decision threshold. The measured bit-error-rate (BER) curves of the UWB data at back-to-back (B2B), after 46-km fiber transmission, and 0.5-m wireless transmission are shown in Fig. 5(a). Without wireless transmission, errors appeared when optical power was −25 dBm. The inset is the eye-diagram of the UWB signal at this optical power after 46-km fiber. There was no power penalty after fiber transmission as the dispersion induced by the SMF was completely compensated by the IDF. After

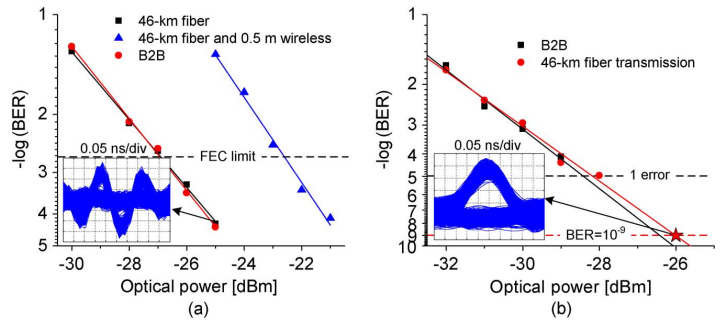

Fig. 5. Transmission performance of both 2-Gb/s data in (a) UWB and (b) baseband formats.

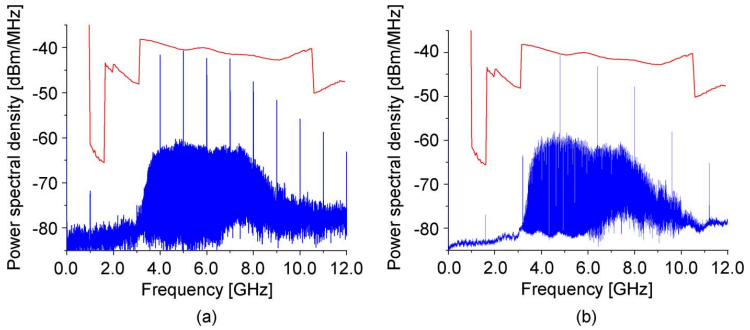

Fig. 6. Electrical spectra of detected (a) 1.0-Gb/s data and (b) 1.6-Gb/s UWB signals after fiber transmission.

wireless transmission, errors were recorded at -21 dBm. The received optical power to achieved the forward error correction (FEC) limit $(\mathrm{BER} = 2 \times 10^{-3})$ was approximately -22.7 dBm. Therefore, at this BER requirement, 0.5-m wireless transmission introduced about a 4.5-dB power penalty.

4.2. Performance of 2-Gb/s Baseband Signal

For the baseband data, the corresponding DSP algorithm includes low-pass filtering and threshold decision functions to demodulate the received signal. The cutoff frequency of the digital low-pass filter was 4 GHz. Unlike the UWB data, the logic value of each bit was determined by comparing the value at only one sampled point to an optimally determined decision threshold. This process emulated a conventional receiver. The measured BER curves of 100 000-bit baseband data with and without fiber transmission are also shown in Fig. 5(b). Similar to the performance of the UWB signal, there was no power penalty after 46-km fiber transmission. The required optical power to achieve the same BER for the baseband signals was about 4 dB lower than for the UWB signals without wireless transmission, because the baseband signals had higher signal-to-noise ratio (SNR), as shown in Fig. 3(a). Moreover, by extrapolating the linearized BER curves, $\mathrm{BER} < 10^{-9}$ of the baseband can be approximately achieved at -26 dBm for both B2B and fiber transmission, which is compatible with existing WDM-PON systems. The inset displays the eye-diagram of the baseband data at -26 dBm.

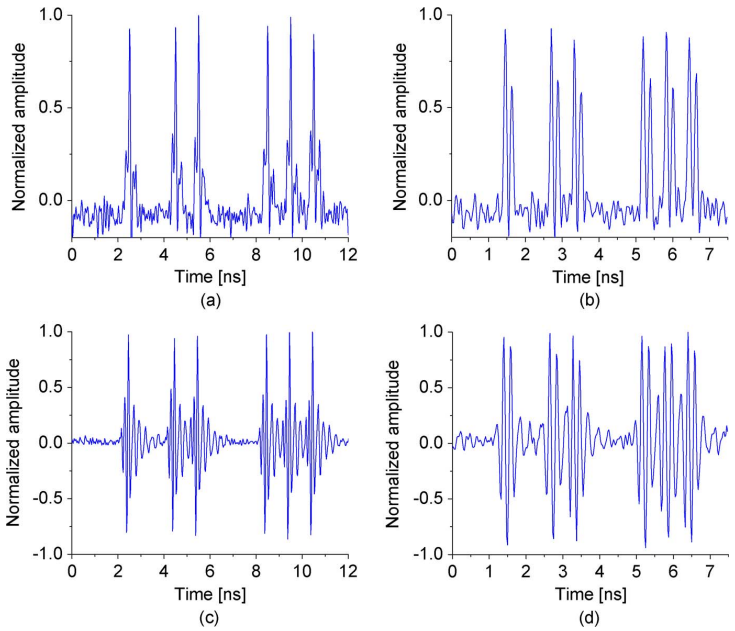

Fig. 7. Waveforms of the pattern "001011001110" at (a) 1.0 Gb/s and (b) 1.6 Gb/s without the HPF (Baseband), (c) 1.0 Gb/s and (d) 1.6 Gb/s with the HPF (UWB).

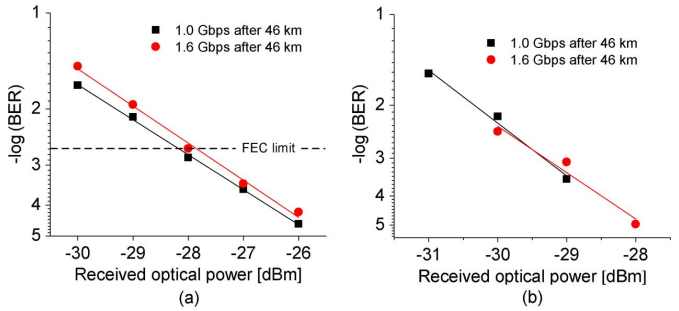

Fig. 8. Transmission performance of both 1.0-Gb/s and 1.6-Gb/s data in (a) UWB and (b) baseband formats.

4.3. Flexible Data-Rate Allocation

To investigate the data-rate flexibility of our proposed method, we varied the frequency of the PPG to 3.2 GHz and 2 GHz with no other changes of the setup, and thus, the data rates of both the baseband and UWB signals were lowered to 1.6 and 1.0 Gb/s. The maximum received optical powers to fit the FCC mask were approximately −20 dBm for both 1.6- and 1.0-Gb/s data. The electrical spectra of detected UWB signals at this optical power level are shown in Fig. 6. The corespondent waveforms of the sequence "001011001110" at these bit rates with and without HPF are displayed in Fig. 7. The transmission performances of both the baseband and UWB signals are illustrated in Fig. 8. Compared with the 2-Gb/s case, the baseband signals had similar performance.

However, the sensitivities of the 1.6-Gb/s and 1.0-Gb/s UWB signals at BER of $< 2 \times 10^{-3}$ were about 1.0 and 1.3 dB better, respectively, because they required received optical power to fit the mask about 1 dB lower than the 2-Gb/s case. Longer wireless transmission distances for the UWB signals at these bit rates can be achieved at the same received optical power and BER requirement.

5. Conclusion

A simple system supporting flexible gigabit wireline and IR-UWB wireless access for IR-UWB-over-fiber based on multi-subcarrier upconversion has been proposed and experimentally demonstrated. The same wireline baseband data is used for the UWB service. The FCC-compliant UWB signals were generated by multi-carrier upconverting and reshaping the baseband signals. This method offers very simple UWB generation and efficiently improves access flexibility. Both wireline and UWB wireless connectivity to end-users can be easily realized using a common PON component and fiber plant. The performance of the proposed system was evaluated by the BER of both the wireline baseband and wireless UWB signals. Additionally, optical wavelength independency and data-rate flexibility of UWB signal generation makes the system compatible with existing WDM-PON systems.

References

[1] D. Porcino and W. Hirt, "Ultra-wideband radio technology: Potential and challenges ahead," *IEEE Commun. Mag.*, vol. 41, no. 7, pp. 66–74, Jul. 2003.
[2] Fed. Commun. Comm., *Revision of Part 15 of the Commission's Rules Regarding Ultra-Wideband Transmission Systems*, 2002.
[3] M. Abtahi, M. Mirshafiei, S. LaRochelle, and L. A. Rusch, "All-optical 500-Mb/s UWB transceiver: An experimental demonstration," *J. Lightw. Technol.*, vol. 26, no. 15, pp. 2795–2802, Aug. 2008.
[4] F. Zeng and J. Yao, "Ultrawideband impulse radio signal generation using a high-speed electrooptic phase modulator and a fiber-Bragg-grating-based frequency discriminator," *IEEE Photon. Technol. Lett.*, vol. 18, no. 19, pp. 2062–2064, Oct. 2006.
[5] A. Kaszubowska-Anandarajah, P. Perry, L. P. Barry, and H. Shams, "An IR-UWB photonic distribution system," *IEEE Photon. Technol. Lett.*, vol. 20, no. 22, pp. 1884–1886, Nov. 2008.
[6] X. Yu, T. B. Gibbon, M. Pawlik, S. Blaaberg, and I. T. Monroy, "A photonic ultra-wideband pulse generator based on relaxation oscillations of a semiconductor laser," *Opt. Express*, vol. 17, no. 12, pp. 9680–9687, Jun. 2009.
[7] T. B. Gibbon, X. Yu, and I. T. Monroy, "Photonic ultra-wideband 781.25 Mbit/s signal generation and transmission incorporating digital signal processing detection," *IEEE Photon. Technol. Lett.*, vol. 21, no. 15, pp. 1060–1062, Aug. 2009.
[8] G. K. Chang, A. Chowdhury, Z. Jia, H. C. Chien, M. F. Huang, J. Yu, and G. Ellinas, "Key technologies of WDM-PON for future converged optical broadband access networks," *IEEE/OSA J. Opt. Commun. Netw.*, vol. 1, no. 4, pp. C35–C50, Sep. 2009.
[9] S. Pan and J. Yao, "Simultaneous provision of UWB and wired services in a WDM-PON network using a centralized light source," *IEEE Photon. J.*, vol. 2, no. 5, pp. 712–718, Oct. 2010.
[10] K. Prince, J. B. Jensen, A. Caballero, X. Yu, T. B. Gibbon, D. Zibar, N. Guerrero, A. V. Osadchiy, and I. T. Monroy, "Converged wireline and wireless access over a 78-km deployed fiber long-reach WDM PON," *IEEE Photon. Technol. Lett.*, vol. 21, no. 17, pp. 1274–1276, Sep. 2009.

Paper 2: Integration of Optically Generated Impulse Radio UWB Signals into Baseband WDM-PON

T. T. Pham, X. Yu, L. Dittmann and I.Tafur Monroy, "Integration of optically generated impulse radio UWB signals into baseband WDM-PON," *IEEE Photonics Technology Letters*, vol. 23, no. 8, pp. 474–476, 2012.

Integration of Optically Generated Impulse Radio UWB Signals Into Baseband WDM-PON

Tien-Thang Pham, *Member, IEEE*, Xianbin Yu, *Member, IEEE*, Lars Dittmann, *Member, IEEE*, and Idelfonso Tafur Monroy, *Member, IEEE*

***Abstract*—We propose a compact integration system to simultaneously provide wireline and wireless [baseband and ultra-wideband (UWB)] services to end-users in a wavelength-division-multiplexed–passive optical network (WDM-PON). A 1-Gb/s UWB signal is optically generated and shares the same wavelength with the baseband signal. Error-free performance was achieved after 23-km single-mode-fiber (SMF) transmission for both signals and additional 0.4-m wireless transmission for the UWB signal. The low complexity and high spectrum efficiency of this system makes it attractive for deployment of in wireline/wireless converged gigabit optical access networks.**

***Index Terms*—Microwave photonics, passive optical network (PON), radio over fiber (RoF), ultra-wideband (UWB), wavelength-division multiplexing (WDM).**

I. Introduction

RECENTLY, there is a increasing demand from service providers to simultaneously support multiple wireline/wireless broadband services to end-users in a converged optical access network. A wavelength-division-multiplexed–passive optical network (WDM-PON) is considered as the backbone of a converged network for provision of both wireline and wireless services because it offers several advantages such as large bandwidth, long reach, high power budget, excellent security and easy upgradeability [1], [2].

Ultra-wideband (UWB) is a promising technology for short range wireless communication systems due to its low complexity, low cost, low power consumption and coexistence with other radio communication systems. Regulated by the Federal Communications Commission (FCC), UWB operating within the spectrum band 3.1–10.6 GHz has extremely low emission power at -41.3 dBm/MHz [3]. As a result, achievable wireless transmission distance is limited in a few meters. To extend the reach of UWB services, UWB-over-fiber technologies with different schemes have been proposed recently [4]–[8]. Additionally, some works have demonstrated the possibility to increase the spectrum efficiency of WDM-PON networks and optical in-home networks by simultaneously transmitting baseband and the electrically generated UWB signals [9], [10]. The baseband signal is combined with the UWB signal using electrical combiner and then modulates an optical source. To further exploit the advantages of photonic technologies such as high-speed generation and no requirement of combining electrical signals, it is desirable to directly generate and integrate the UWB signal in the optical domain.

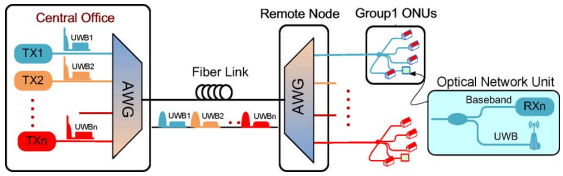

Fig. 1. Schematic of proposed WDM-PON system for simultaneous provision of wireline and UWB wireless services. TXn: nth channel transmitter. RXn: nth channel receiver. AWG: Arrayed waveguide grating.

In this letter, we propose and experimentally demonstrate a WDM-PON system that simultaneously provides gigabit baseband service and gigabit impulse UWB (IR-UWB) service on a single wavelength. The UWB signal is optically generated based on relaxation oscillations of a directly modulated laser (DML). Both signals were transmitted over 23 km of single-mode fiber (SMF). The detected UWB signal was further transmitted over 0.4-m wireless link. Offline digital signal processing (DSP) receivers were employed to demodulate the signals and assess their bit-error-rate (BER) performance.

II. Network Architecture and Experimental System

Fig. 1 depicts the downlink topology of a WDM access network supporting wireline and UWB wireless services. A central office (CO) is composed of a laser array with n transmitters (TXs) which offer WDM wavelengths for downlink. Two arrayed waveguide gratings (AWGs) operate as a wavelength multiplexer and a demultiplexer, respectively. At the optical network unit (ONU) side, after a SMF link, a downstream receiver is used to demodulate the baseband signal, and a transmitting antenna is employed to radiate the UWB signal to the air. In this scenario, a number of ONUs in a cluster can share a single wavelength and broadcast services on this wavelength.

Fig. 2 shows the experimental system supporting optically generated IR-UWB and wireline baseband services. At the CO, for a channel, a high-speed baseband signal drove a directly modulated laser (DML) to generate a UWB signal based on relaxation oscillations [5]. The lightwave from the laser was launched into a March–Zehnder modulator (MZM) which was driven by the second baseband signal. Two optical tunable filters (OTFs) were used to emulate AWGs. The optical carrier was located at the right side slope of the OTF1 to modify the pulse shape of the UWB signal to better comply with the FCC mask [4]. The low frequency RF components can be greatly

Manuscript received September 27, 2010; revised December 23, 2010; accepted January 22, 2011. Date of publication January 31, 2011; date of current version March 23, 2011.

The authors are with DTU Fotonik, Department of Photonics Engineering, Technical University of Denmark, 2800 Kgs. Lyngby, Denmark (e-mail: ptit@fotonik.dtu.dk; xiyu@fotonik.dtu.dk; ladit@fotonik.dtu.dk; idtm@fotonik.dtu.dk).

Color versions of one or more of the figures in this letter are available online at http://ieeexplore.ieee.org.

Digital Object Identifier 10.1109/LPT.2011.2109943

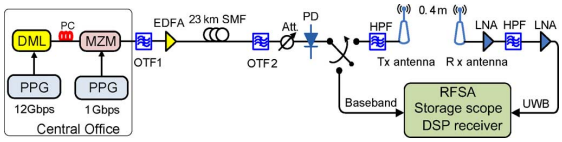

Fig. 2. Experimental setup of the proposed fiber-wireline/wireless transmission system. PPG: Pulse pattern generator. DML: Directly modulated laser. EDFA: Erbium-doped fiber amplifier. MZM: March–Zehnder modulator. PD: Photodetector. Att: Tunable optical attenuator. HPF: High-pass filter. LNA: Low-noise amplifier. RFSA: RF spectrum analyzer.

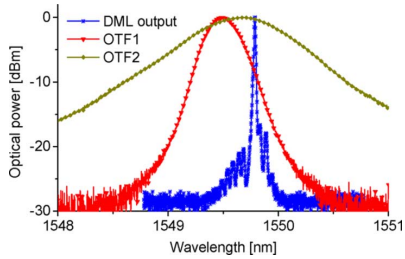

Fig. 3. Normalized optical spectrum of DML output and bandwidth profiles of two optical tunable filters (OTFs).

suppressed for the integration of baseband signals. The OTF2 simply suppressed amplified spontaneous emission (ASE) noise from erbium-doped fiber amplifier (EDFA). At the ONU, both the UWB and baseband data were recovered by a single photodetector (PD) and separated by proper filters. The UWB signal was then radiated into the air through a transmitting antenna.

Both the baseband and UWB data were demodulated offline employing a DSP receiver composed of a 40-GSa/s digital storage oscilloscope (DSO) and offline DSP algorithms. For the baseband data, the unfiltered detected signal from the PD was recorded. For the UWB data, the signal from the receiving antenna was amplified, filtered and then stored by the DSO.

III. Experimental Results

In the experiment, lasing threshold current and bias current of the DML -21 mA and -34 mA, respectively. The DML was driven by a pulse pattern generator (PPG) at 12-Gb/s and 0.625-V peak-to-peak voltage ($V_{p\text{-}p}$) with a pattern "1010 0000 0000" to present UWB bit "1" and a pattern "0000 0000 0000" to present UWB bit "0". The effective bit rate for the generated UWB signal was thus 1 Gb/s. The output optical carrier is then externally modulated by a 1-Gb/s baseband PRBS with a word length of $2^{15}-1$ from the second PPG at the MZM. 3-dB bandwidth of two OTFs was 0.308 nm and 0.948 nm, respectively. The offset between the transmission wavelength and the central wavelength of OTF1 was 0.3 nm. The optical spectrum of the DML output and the bandwidth profiles of two OTFs are shown in Fig. 3. The bandwidth of the PD was 12-GHz. The UWB signal was radiated into the free space by an Omni-directional antenna (Skycross SMT-3TO10M-A). The wireless transmission distance was set at 0.4 m for demonstration purpose. The radiated UWB signal was received by a directive antenna (Geozondas AU-3.1G10.6G-1) pointed towards the transmitting antenna.

No electrical amplifier was used after the PD. In this condition, to ensure UWB spectrum was FCC-compliant, the maximum optical power launched to the PD was -12.5-dBm.

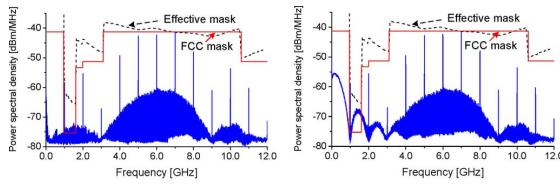

Fig. 4. Detected electrical spectra at -12.5-dBm optical power (a) without baseband signal and (b) with baseband signal.

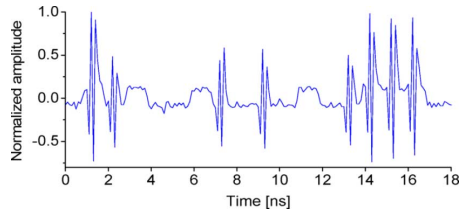

Fig. 5. Hybrid (baseband and IR-UWB) waveform of the detected signal.

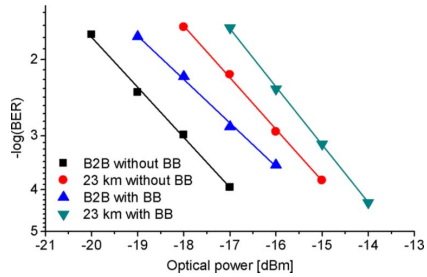

Fig. 6. Measured BER of the UWB signal after 0.4-m wireless transmission.

Fig. 4 shows the electrical spectra after fiber transmission at this power. The effective mask is the allowed mask when the frequency response of the transmitting antenna was taken into account [8]. The baseband signal did not alter the spectrum of the UWB signal in the main frequency region (3–9 GHz). The detected hybrid waveform is shown in Fig. 5. There were two levels for the pulse amplitude of UWB bits "1" when they coexisted with baseband bits. Baseband bits "1" increased the pulse amplitude of UWB bits "1" when they overlapped in time domain. It is because the baseband signal modulated the intensity of the optical carrier after the UWB signal.

A. Performance of the UWB Data

The DSP demodulation algorithm for the UWB signal comprised four steps: high-pass filtering, bit correlation, bit synchronization and threshold gating [6]. Fig. 6 illustrates the transmission performance of 50,000 generated UWB bits after 0.4-m wireless transmission, with and without the copropagation of 0.5-V baseband data. There were no errors detected in all cases when the optical power was higher than -14 dBm. We can notice that 23-km fiber transmission introduced about 2-dB power penalty which is mainly caused by fiber chromatic dispersion. It was because relaxation oscillations of direct modulation broadened the spectrum of the optical signal from the DML and the UWB signal occupied a broad bandwidth. Moreover, the copropagation of baseband signal caused approximately 1-dB power penalty.

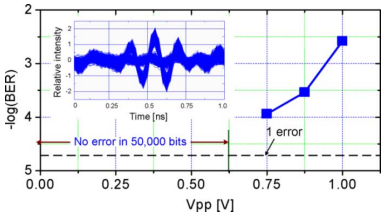

Fig. 7. BER of the UWB signal at different $V_{p\text{-}p}$ of the baseband signal. Inset: measured eye-diagram with 0.5-V baseband signal.

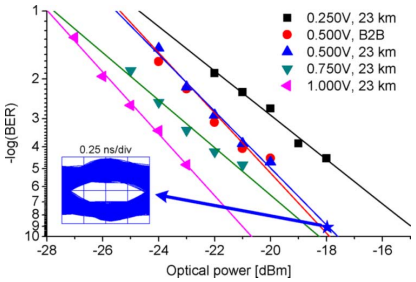

Fig. 8. Measured BER of the baseband signal. Inset: Eye diagram at −18 dBm after 23-km transmission.

As two signals share the same optical carrier, there is a trade-off between their performances [2]. To further assess the effect of the baseband signal on the performance of the UWB signal, we varied the $V_{p\text{-}p}$ of the baseband data while the optical power at the receiver was fixed at -12.5 dBm. No error was detected in 50,000 bits when the $V_{p\text{-}p}$ was below 0.625 V as presented in Fig. 7. When the $V_{p\text{-}p}$ increased from 0.75 V to 1.0 V, BER of the UWB signal increased from 1.26×10^{-4} to 2.51×10^{-3}. At this optical power level, for the baseband data, BER $< 10^{-9}$ could be achieved at 0.250-V $V_{p\text{-}p}$ as presented in next section. The inset shows the eye-diagram after DSP processing for the case with the baseband data.

B. Performance of the Baseband Data

The DSP algorithms for baseband signal included low-pass filtering with 900-MHz cutoff frequency, synchronization and threshold decision. This cutoff frequency ensures that the repetition frequency at 1 GHz of the UWB signal is rejected to reduce the interference from the UWB signal. Fig. 8 shows the measured BER curves of 100,000-bit baseband data at different $V_{p\text{-}p}$. We can notice that at the same optical power to the PD, BER decreased with the increase of $V_{p\text{-}p}$. In a linear transmission system, $\log(-\log(\mathrm{BER}))$ is proportional to the received optical power, therefore by extrapolating the BER curve, error-free transmission (BER $< 10^{-9}$) is predicted to be able to achieve at -21 dBm to -15 dBm when the $V_{p\text{-}p}$ was decreased from 1.0 V to 0.25 V. The power penalty induced by after 23-km fiber transmission is negligible as it can be seen from the 0.5-V modulation case. The inset shows the measured eye-diagram after transmission at -18-dBm optical power. At this optical power, BER $< 10^{-9}$ could be achieved.

The experimental results show the existence of the trade-off between the performance of the baseband and UWB signals. The higher modulation index of the baseband signal, the better the performance of baseband data but the worse the performance of the UWB data. We also can notice that the required optical power for the baseband data to reach the forward error correction (FEC) limit (BER $< 2\times10^{-3}$) was always lower than that for the UWB service even at the driving voltage of 0.25-V. To satisfy performance requirement for both the data at a fixed optical power level, the $V_{p\text{-}p}$ of the baseband signal can be further reduced. With such low modulation depth, the optical carrier can be reused for uplink baseband data transmission in reflective semiconductor optical amplifier (RSOA) based WDM-PON systems [1], [2]. On the other hand, to improve the performance of the UWB signal at low optical power, an electrical amplifier with a power control mechanism can be used for the UWB signal. In this condition, the optical power budget for splitting and transmission is increased.

IV. Conclusion

A novel scheme for simultaneous provision of optically generated gigabit UWB and baseband services on a single wavelength of a WDM-PON system was proposed and experimentally demonstrated. No error was observed for 1-Gb/s baseband data and 1 Gb/s IR-UWB data after 23-km fiber transmission. The existence of the baseband data caused about 1-dB power penalty on the performance of the UWB data. The integration of the UWB signals into the baseband WDM-PON increases electrical/optical spectrum efficiency of the whole systems, and thus it has great potential for applications in supporting the development of wireline/wireless convergence in optical access networks.

References

[1] W. Lee, M. Y. Park, S. H. Cho, J. Lee, C. Kim, G. Jeong, and B. W. Kim, "Bidirectional WDM-PON based on gain-saturated reflective semiconductor optical amplifiers," *IEEE Photon. Technol. Lett.*, vol. 17, no. 11, pp. 2460–2462, Nov. 2005.

[2] T. T. Pham, H. S. Kim, Y. Y. Won, and S. K. Han, "Colorless WDM-PON based on a Fabry-Pérot laser diode and reflective semiconductor optical amplifiers for simultaneous transmission of bidirectional gigabit baseband signals and broadcasting signal," *Opt. Express*, vol. 17, no. 19, pp. 16571–16580, 2009.

[3] Revision of Part 15 of the Commission's Rules Regarding Ultra-Wideband Transmission Systems Federal Communications Commission, Feb. 2002.

[4] F. Zeng and J. P. Yao, "Ultrawideband impulse radio signal generation using a high-speed electrooptic phase modulator and a fiber Bragg grating based frequency discriminator," *IEEE Photon. Technol. Lett.*, vol. 18, no. 19, pp. 2062–2064, Oct. 1, 2006.

[5] X. Yu, T. B. Gibbon, M. Pawlik, S. Blaaberg, and I. T. Monroy, "A photonic ultra-wideband pulse generator based on relaxation oscillations of a semiconductor laser," *Opt. Express*, vol. 17, no. 12, pp. 9680–9687, 2009.

[6] T. B. Gibbon, X. Yu, and I. T. Monroy, "Photonic ultra-wideband 781.25-Mb/s signal generation and transmission incorporating digital signal processing detection," *IEEE Photon. Technol. Lett.*, vol. 21, no. 15, pp. 1060–1062, Aug. 1, 2010.

[7] R. Llorente, T. Alves, M. Morant, M. Beltran, J. Perez, A. Cartaxo, and J. Marti, "Ultra-wideband radio signals distribution in FTTH networks," *IEEE Photon. Technol. Lett.*, vol. 20, no. 11, pp. 945–947, Jun. 1, 2008.

[8] M. Abtahi, M. Mirshafiei, J. Magn, S. LaRochelle, and L. A. Rusch, "All-optical 500-Mb/s UWB transceiver: An experimental demonstration," *J. Lightw. Technol.*, vol. 26, no. 15, pp. 2795–2802, Aug. 1, 2008.

[9] S. Pan and J. Yao, "Simultaneous provision of UWB and wired services in a WDM-PON network using a centralized light source," *IEEE Photon. J.*, vol. 2, no. 5, pp. 711–718, Oct. 2010.

[10] J. B. Jensen, R. Rodes, M. Beltran, and I. T. Monroy, "Shared medium 2 Gbps baseband & 2 Gbps UWB in-building converged optical/wireless network with multimode fiber and wireless transmission," in *Proc. 36th Eur. Conf. Optical Commun.(ECOC) 2010*, Italy, Sep. 2010.

Paper 3: Robust BPSK Impulse Radio UWB-over-Fiber Systems Using Optical Phase Modulation

T. T. Pham, N. G. Gonzalez, X. Yu, D. Zibar, L. Dittmann and I. T. Monroy, "Robust BPSK impulse radio UWB-over-fiber systems using optical phase modulation," in *Proc. Optical Fiber Communication Conference and Exposition*, *OFC/NFOEC 2011*, paper OTuF6, Los Angeles, CA, 2011.

Robust BPSK Impulse Radio UWB-over-Fiber Systems Using Optical Phase Modulation

Tien-Thang Pham, Neil Guerrero Gonzalez, Xianbin Yu, Darko Zibar, Lars Dittmann, and Idelfonso Tafur Monroy

DTU Fotonik, Department of Photonics Engineering, Technical University of Denmark, DK-2800 Kgs. Lyngby, Denmark.
Tel: + +45 45 25 37 77, Fax: +45 45 93 65 81, E-mail: ptit@fotonik.dtu.dk

Abstract: The impact of fiber dispersion on the performance of optical phase modulated impulse-radio-ultrawideband (IR-UWB) signals is experimentally investigated. 2Gbps BPSK IR-UWB over 78km fiber transmission is successfully achieved by using digital coherent detection.

OCIS codes: (060.1660) Coherent communications, (060.5625) Radio frequency photonics.

1. Introduction

With the recent development of integrated electronic circuits and digital signal processing (DSP), optical coherent receivers using DSP are becoming a practical and feasible solution for high speed systems. Digital coherent detection is a dominating approach for long-haul high capacity transmission systems [1]. Recently, it has also been proposed for optical access networks due to its very good channel selectivity, including optical phase modulated radio-over-fiber (RoF) systems which have several advantages compared to intensity-modulated RoF systems, such as no need of bias voltage, no fundamental limit on modulation depth, high linearity [2, 3], and 6 dB receiver performance advantage over intensity modulation counterpart [4].

On the other hand, ultrawideband (UWB) has been considered as a promising technology for short-range, high-speed wireless communication systems [5]. Regulated by the U.S. Federal Communications Commission (FCC), power spectral density of UWB signals is limited below -41.3dBm/MHz. Therefore, wireless transmission distance is very limited. In this context, UWB-over-fiber, similar to radio-over-fiber technology, is a potential technology to extend the reach with assistance of flexible UWB generation and distribution. Several approaches have been proposed to optically generate impulse radio (IR) UWB signals at the central office (CO) and distribute to end-users [6, 7, 8]. Recently, we also demonstrated that UWB-over-fiber could be integrated seamlessly into a WDM-PON that supports both wireline and wireless services [9]. In fact, in such long reach UWB-over fiber transmission systems, fiber chromatic dispersion will critically affect the signal performance, since UWB signals occupy a large bandwidth up to 6.5 GHz. Therefore it is important to conceive a robust IR-UWB optical fiber signal distribution approach with seamless integration with the major trend of employing advanced digital coherent receivers for universal support of several services and modulation formats.

In this paper we consider optical phase-modulated transmission and coherent detection of IR-UWB-over-fiber in a coherent-detection PON scenario. We demonstrate an uplink transmission of 2-Gbps binary phase shift keying (BPSK) IR-UWB signals. The influences of the chromatic dispersion of various single mode fiber links (from 20 km in conventional access networks to up to 78 km in long-reach access networks) are experimentally investigated. The result proves the robustness of our system and its integration capability into a digital coherent receiver structure.

2. Coherent optical access networks

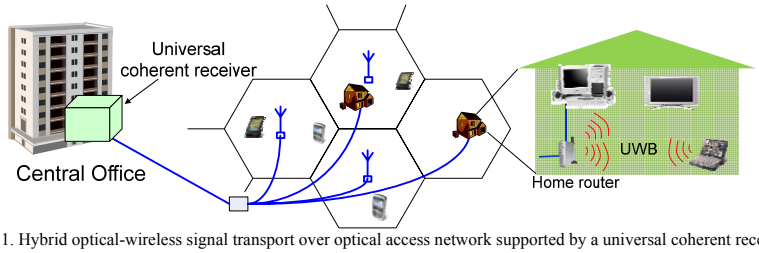

Fig. 1. Hybrid optical-wireless signal transport over optical access network supported by a universal coherent receiver.

Fig. 1 shows a schematic diagram for a prospective converged wireless-optical network. Both wireline and wireless services are transported in the same fiber infrastructure. With the advantages of DSP, a universal and reconfigurable coherent-detection based DSP receiver can be employed in the CO to detect all types of signals. Moreover, the utilization of the universal receiver allows the CO to adaptively tackle the requirements for large number of users,

diversity of services and reach extension, as it has potential to support large number of channels with very close channel spacing and increased receiver sensitivity.

3. Experimental setup

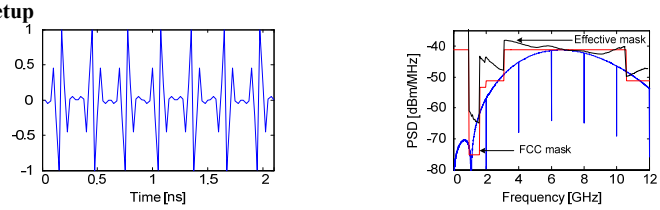

Fig.2. a) BPSK-modulated UWB sequence (1 0 1 1 0 0 1). b) Spectrua of the 2Gbps BPSK-UWB signals.

To emulate a UWB wireless signal generation terminal, an arbitrary waveform generator (AWG) with a 24-GSa/s sampling rate was used. The generated UWB pulse is a 5th derivative Gaussian shape for its good compliance with the FCC mask [6]. In the experiment, a pseudo-random bit sequence (PRBS) at a bit rate of 2 Gbps with a word length of 2^{11}-1 was used. Bipolar modulation is employed for the UWB signal in order to avoid spectral lines at multiplication of pulse repetition frequency for on-off-keying modulation [10], and thus to be able to radiate further wirelessly. Fig. 2 shows an example of UWB sequence and the UWB spectra generated by the AWG. We can see PI phase shift is perfectly introduced between bit '1' and '0', and no spectral spike lines are observed. The effective mask is the allowed mask when the frequency response of the transmitting antenna is taken into account.

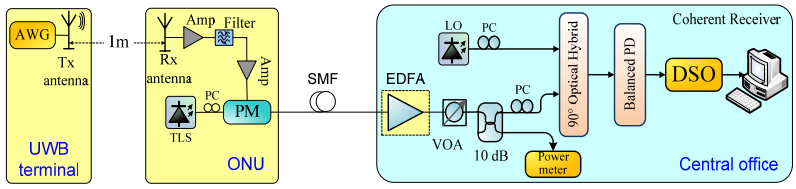

Fig. 3. Experimental setup. AWG: arbitrary waveform generator, TLS: tunable laser source, PM: phase modulator, EDFA: Erbium doped fiber amplifier, SMF: single mode fiber, VOA: variable optical attenuator, LO: local oscillator, DSO: digital storage oscilloscope.

Fig. 3 shows the experimental setup. The UWB signal from the AWG was transmitted wirelessly through an Omni-antenna (SMT-3TO10M-A) and received by a directive antenna (AU-3.1G10.6G-1). The wireless transmission distance was set at 1 m. The received UWB signals from the receiver antenna were amplified and filtered out by a high-pass filter, to remove frequency components below 3.1 GHz before driving an optical phase modulator (PM). The lightwave launched into the PM with 4 dBm power was emitted from a tunable laser source (TLS). The modulated optical signals were then transmitted over a spool of single mode fibers (SMF) with different length (23, 40, 58 and 78 km fiber). The 78-km long link is a deployed fiber; in this case an erbium doped fiber amplifier (EDFA) was used as pre-amplifier to compensate 25 dB losses of the optical link.

In the coherent receiver, a tunable external cavity laser with a linewidth of 100 kHz was used as local oscillator (LO). The in-phase and quadrature signals after a 90° optical hybrid were detected by two pairs of balanced photodiodes with 7.5 GHz full-width-half-maximum (FWHM) bandwidth. The detected photocurrents were digitized by a sampling scope at 40 GSa/s for offline digital signal processing (DSP). The employed single digital receiver included a digital dispersion compensation module, which is followed by an optical carrier-recovery digital phase-locked loop (PLL) [9] and a linear signal demodulator. In the digital linear demodulation module, the DSP algorithm performs functions of high-pass filtering, matched filtering with the original UWB pulse, synchronization and threshold decision [10]. The dispersion parameter for dispersion compensation (DC) module was 17ps/nm/km.

4. Experimental results

In the experiment, 70,000 UWB bits were used to assess the performance of the UWB signals in each case. Fig. 4a shows the BER curves in cases of back-to-back (B2B), after 23, 40 and 58 km fiber transmission, with and without dispersion compensation as well. As illustrated in the figure, 23, 40 and 58 km fiber without DC caused approximately 1.4, 3.1 and 4.3 dB power penalties at a BER of 10^{-4}, respectively. When digital DC was applied in the digital domain, power penalties were then less than 0.5 dB for all the transmission cases. Fig.4b shows the comparison of the measured BER performance between B2B and 78 km fiber transmission cases. The use of the EDFA introduced about 1 dB power penalty while 78-km fiber caused about 7 dB. However, similar to the shorter

transmission distances, this power penalty can also be compensated completely by using digital dispersion compensation. Fig. 4c simply summaries the measured power penalties caused by the chromatic dispersion.

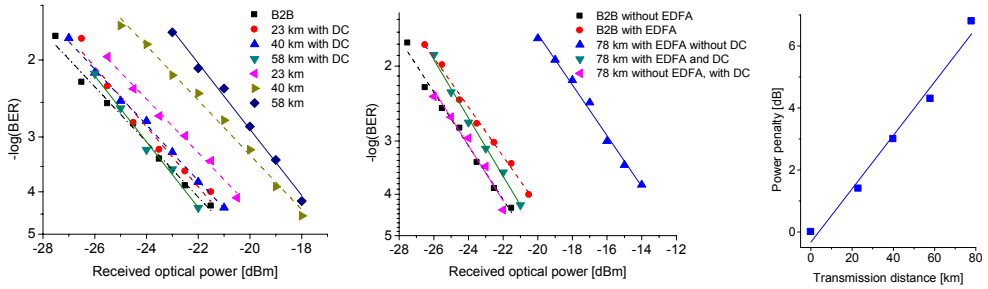

a) b) c)

Fig. 4. BER performance of the UWB signals with and without dispersion compensation after (a) 23km, 40km and 58km and (b) 78km fiber transmission, c) Summarized power penalties caused by chromatic fiber dispersion.

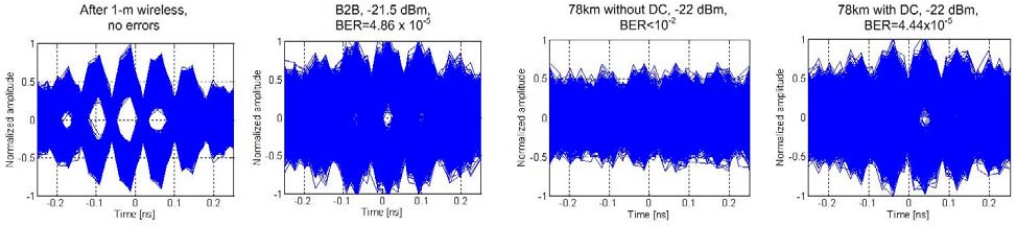

Fig. 5. Eye-diagrams of the received BPSK UWB signals

Fig. 5 illustrates the eye-diagrams of 10,000 UWB bits at different positions in the 78-km transmission system. The eye diagram after wireless transmission but before fiber transmission was clear and open. After 78-km fiber transmission, the eyes at -22-dBm optical power were completely close due to the chromatic dispersion. However, after using digital dispersion compensation, the eye-diagrams and the transmission performance were similar to B2B.

5. Conclusions

We experimentally demonstrated an optical phase modulated UWB-over-fiber system using digital coherent detection for the transport of 2-Gbps BPSK IR-UWB signals in a coherent detection PON. Our experimental results indicate that a DSP receiver has the capability of overcome fiber transmission impairments, and the power penalty caused by the chromatic fiber dispersion is completely compensated in the digital coherent receiver. Therefore, it can be foreseen that a universal, reconfigurable DSP receiver will make it possible to seamlessly integrate also IR-UWB into the diverse services supported in next generation high capacity optical access networks.

6. References

[1] J. Renaudier, G. Charlet, O. Bertran-Pardo, et al, "Transmission of 100Gb/s Coherent PDM-QPSK over 16x100km of standard fiber with allerbium amplifiers," *Opt. Express* **17**, 5112-5119 (2009).

[2] D. Zibar, et al, "Digital coherent receiver for phase-modulated radio-over-fiber optical links," *IEEE Photon. Techn. Lett.* **21**, 155-157, (2009).

[3] T. R. Clark, M. L. Dennis,"Coherent optical phase-modulation link," *IEEE Photon. Techn. Lett.* **19**, 1206–1208, (2007).

[4] F. Gardner, "Phase-lock techniques," 3rd edition, (John Wiley and Sons, 2004).

[5] D. Porcino, W. Hirt, "Ultra-wideband radio technology: Potential and challenges ahead," *IEEE Comm. Mag.*, **41**, 66–74, (2003).

[6] X. Yu, T. B. Gibbon, M. Pawlik, S. Blaaberg and I. T. Monroy, "A photonic ultra-wideband pulse generator based on relaxation oscillations of a semiconductor laser," *Optics Express* **17**, 9680–9687, (2009).

[7] S. Pan, J. P. Yao, "Switchable UWB pulses generation using a phase modulator and a reconfigurable asymmetric Mach-Zehnder interferometer," *Opt. Lett.* **34**,160-162, (2009).

[8] A. K.-Anandarajah, P. Perry, et al, "An IR-UWB photonic distribution system," *IEEE Photon. Techn. Lett.* **20**, 1884 – 1886, (2008).

[9] K. Prince, J. B. Jensen, A. Caballero, et al, "Converged wireline and wireless access over a78-km deployed fiber long-reach WDM PON," *IEEE Photon. Technol. Lett.* **21**, 1274–1276, (2009).

[10] T. B. Gibbon, X. Yu, I. T. Monroy, "Photonic ultra-wideband 781.25 Mbit/s signal generation and transmission incorporating digital signal processing detection," *IEEE Photon. Techn. Lett.* **21**, 1060-1062, (2009).

Paper 4: Reconfigurable Digital Coherent Receiver for Metro-Access Networks Supporting Mixed Modulation Formats and Bit-rates

N. G. Gonzalez, A. Caballero, R. Borkowski, V. Arlunno, **T. T. Pham**, R. Rodes, X. Zhang, M. B. Othman, K. Prince, X. Yu, J. Jensen, D. Zibar, I.T. Monroy, "Reconfigurable digital coherent receiver for metro-access networks supporting mixed modulation formats and bit-rates," in *Proc. Optical Fiber Communication Conference and Exposition*, *OFC/NFOEC 2011*, paper OMW7, Los Angeles, CA, 2011.

Reconfigurable Digital Coherent Receiver for Metro-Access Networks Supporting Mixed Modulation Formats and Bit-rates

Neil Guerrero Gonzalez, Antonio Caballero Jambrina, Robert Borkowski, Valeria Arlunno, Tien Thang Pham, Roberto Rodes, Xu Zhang, Maisara Binti Othman, Kamau Prince, Xianbin Yu, Jesper Bevensee Jensen, Darko Zibar, and Idelfonso Tafur Monroy

DTU Fotonik, Department of Photonics Engineering, Technical University of Denmark, DK-2800 Kgs. Lyngby, Denmark.
nggo@fotonik.dtu.dk.

Abstract: Single reconfigurable DSP coherent receiver is experimentally demonstrated for mixed-format and bit-rates including QPSK, OFDM, IR-UWB for wireline and wireless signal types. Successful transmission over a deployed fiber link is achieved.
OCIS codes: (060.1660) Coherent communications, (120.5060) Phase modulation

1. Introduction:

Next generation metro-access networks will need to support diverse broadband services including converged wireless and wireline optical access over a unified fiber platform, satisfying bandwidth requirements [1] as well as fulfilling stringent power budget and chromatic dispersion constrains [2]. Another important attribute of future metro-access networks is agile re-configurability to seamlessly accommodate for emerging new services and increased bandwidth requirements [1]. Furthermore, the introduction of mixed modulation formats, bit-mixed rates, support for burst mode transmission into the metro-access networking scenario is creating a highly heterogeneous environment that represents a new challenge to tackle in the near future. Approaches looking for solutions to one or more of the above issues are radio-over-fiber systems for integrating baseband and wireless service delivery over optical fiber access networks [3]. Another approach is developing multi-rate receivers for optical network units (ONUs) from 2.5 Gbit/s-40 Gbit/s to accommodate for mixed bit-rate or service bit-rate on demand [4]. Another promising approach proposed recently is coherent detection based passive optical networks to support closely spaced channels with increased receiver sensitivity to cope with the required large number of users and to extend the reach of metro-access networks [5]. Although experimental demonstrations of converged service delivery have been reported in the literature [2, 3] they use a dedicated receiver for each modulation or bit-rate. In this paper we present and experimentally demonstrate a single, reconfigurable, digital receiver supporting mixed modulation formats, baseband and wireless-over-fiber, with reconfiguration in the digital signal processing domain. We successfully demonstrate its operation for 20 Gbps non-return-to-zero quadrature phase-shift keying (NRZ-QPSK), optically phase-modulated 5 GHz OFDM radio-over-fiber and 2 Gbps impulse radio ultrawideband (IR-UWB), and 5 Gbps directly modulated vertical cavity surface emitting laser (VCSEL) after 78 km of deployed fiber link.

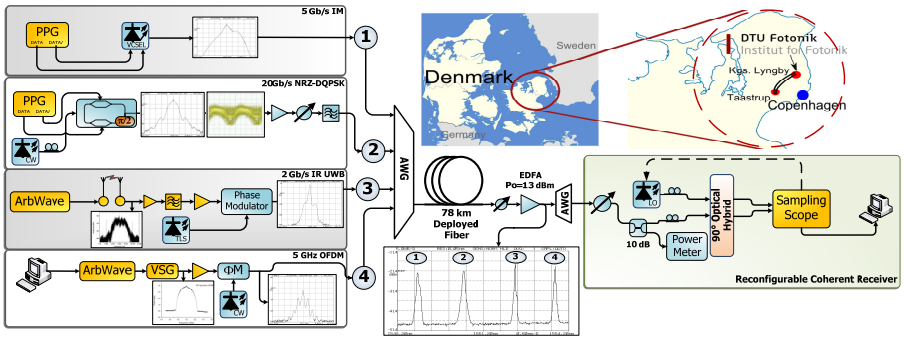

Fig.1 Experiment layout, showing optical and electrical RF spectra at key points; route of installed optical fiber are also shown. Reconfigurable receiver construction allows local oscillator (LO) tuning for channel selection. PPG: pulse pattern generator; ArbWave: arbitrary waveform; VSG: vector signal generator.

2. System description

Fig. 1 shows a block diagram of the heterogeneous optical network and setup used in the experiment. The field-deployed fiber connects the Kgs. Lyngby campus of the Technical University of Denmark (DTU) and the Taastrup suburb of Copenhagen. The fiber is a G.652 standard single-mode fiber (SMF) type (16.5 ps/nm km chromatic dispersion, 0.20 dB/km attenuation). The total link loss was 27 dB. ITU standard operating wavelengths were used for all channels at 200 GHz separation due to equipment availability. Total launch power into the deployed fiber was kept to +4 dBm. At the receiver side, emulating the central office, an erbium doped fiber amplifier (EDFA) was used as preamplifier followed by an optical bandpass filter to reduced ASE noise. The optical power level to the receiver was set to -11 dBm. A tunable external cavity laser was used as local oscillator (LO) for all the received signal types; with a linewidth of 100 kHz. The in-phase and quadrature signals after the 90° optical hybrid were detected with two pairs of balanced photodiodes, having full width at half maximum bandwidth of 7.5 GHz. The detected photocurrents were digitized using a sampling oscilloscope at 40 GSa/s for offline processing. The employed single digital receiver used a digital dispersion compensation module followed by an optical carrier-recovery digital phase-locked loop (PLL) and linear signal demodulation [6] for phase-modulated OFDM and IR-UWB RoF subsystems. Instead of a DPLL, a frequency offset compensation module was used for the NRZ-QPSK optical signal. Reconfiguration for each modulation format was performed by digitally switching between the signal demodulation DSP blocks. Below we present the set-up for each of the signal formats considered.

Gbps Intensity-modulated VCSEL: a pulse pattern generator (PPG) at 5 Gbps directly modulated a 1550 nm VCSEL. Single drive configuration was used for the VCSEL with a driving peak-peak voltage of 1 V. A pseudo random binary sequence (PRBS) with a length of 2^{15}-1 was used for this experiment. The bias current of the VCSEL was used to tune the wavelength to the assigned AWG channel. Bias current was set to 14 mA. The output power of the VCSEL launched into the fiber was measured to be 0.5 dBm.

20 Gbps QPSK baseband: the transmitter of the baseband QPSK subsystem included a PPG to providing a PRBS (215-1) and a MZ modulator to generate a QPSK signal at the wavelength of 1550.5 nm. The value of the signal laser linewidth was 2 MHz.

2 Gbps phase-modulated IR-UWB: an Arbitrary Waveform Generator (AWG) with 24 GSa/s sampling rate was utilized to program a 5th order derivative Gaussian pulse for good compliance with FCC mask [7]. A PRBS with a word length of 2^{11}-1 with bipolar modulation at a bit rate of 2 Gbps was used. The UWB signal was transmitted using a Skycross omni-directional antenna (SMT-3TO10M-A, 0dBi gain) and received after 1 m wireless transmission by a Geozondas directive antenna (AU-3.1G10.6G-1, from +4.65 dBi to +12.4 dBi gain within the UWB frequency range). The received signal was amplified by a low noise amplifier, filtered by a high-pass filter and then amplified again to drive the optical phase modulator. The wavelength of this channel was set at 1552.54 nm. The DSP algorithm in the receiver side included matched filtering and a decision block.

5 GHz OFDM RoF: the OFDM baseband signal was generated in software using a 2^{15}-1 PRBS as input data stream. 256 4-QAM subcarriers were used with 26 samples (10%) cyclic prefix per OFDM symbol. The OFDM frame is composed of two Schmidl training symbols [8] followed by eight data symbols. The signal was fed to an AWG with a 1.25 GSa/s rate which results in a bit rate of 500 Mbps. The signal is then upconverted to a frequency of 5 GHz using a free-running Vector Signal Generator (VSG) whose output is amplified to drive an optical phase modulator supplied with a continuous wave (CW) light at 1553.78 nm. At the receiver, the DSP algorithm implemented a digital PLL, timing offset estimation using a smoothed Schmidl timing metric followed by a carrier frequency offset estimation [8]. The training sequence enabled equalization of each OFDM sub-channel.

3. Results

To demonstrate the performance of our reconfigurable digital coherent receiver, we show in Fig. 2 the measured bit error rate (BER) curves for back-to-back (B2B) and after 78 km of deployed fiber transmission (considering both single and all simultaneous channel performance) as a function of the received optical power. For all four subsystems, a BER value below 10^{-3} (FEC threshold) is achieved for all considered scenarios. **5 Gbps coherently detected, intensity-modulated VCSEL:** as we can see in Fig. 2(a), the VCSEL coherently detected subsystem achieves a sensitivity of -24 dBm for both B2B and 78 km deployed fiber. Chromatic dispersion was completely compensated by DSP, and no penalty was appreciated compared with the B2B case. **20 Gbps QPSK baseband:** Fig. 2(b) shows that fiber transmission incurred 1 dB power penalty (at 10^{-3} BER) difference. Moreover in the simultaneous presence of the other three channels, there was an observable 0.5 dB penalty both for back to back and after transmission; however the reconfigurable receiver showed successful operation.

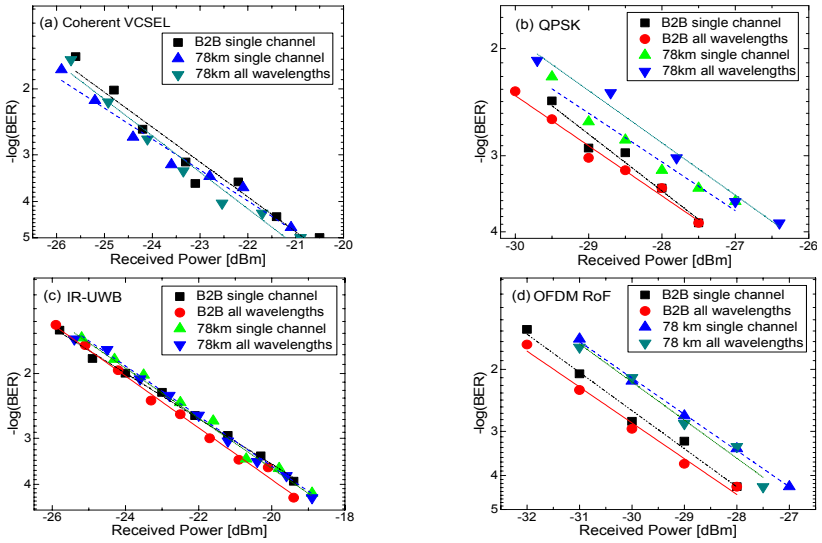

Fig.2 Measured BER performances for (a) 5 Gbps intensity-modulated VCSEL, (b) 20 Gbps QPSK baseband, (c) 2 Gbps phase-modulated IR-UWB, and (d) 5 GHz OFDM RoF.

2 Gbps phase-modulated IR-UWB: as shown in Fig. 2(c) the measured BER performances of the UWB subsystem were consistent for all cases. Errors occurred when the received optical power was less than -21.5 dBm. The BER performance is below the FEC limit when the received power was higher than -23 dBm. **5 GHz OFDM RoF:** Fig. 2(d) shows that for the case of four simultaneously integrated channels, OFDM suffered nearly 0.5 dB of power penalty, for both B2B and 78 km fiber transmission compared to single OFDM channel transmission yielding a receiver sensitivity at a BER of 10^{-4} of 28 dBm for the B2B system, and -27.5 dBm for the 78 km optical transmission link, respectively. The reconfigurable receiver showed stable operation for the 4-QAM OFDM RoF subsystem.

4. Conclusions

A single reconfigurable DSP enabled coherent receiver is experimentally demonstrated for mixed modulation formats and bit rates. In our reported experiment, four different types of wireline and wireless services including 20 Gbps QPSK baseband, 5Gbps OOK, 5 GHz OFDM RoF and 2 Gbps IR-UWB are successfully demodulated after transmission over 78 km deployed fiber link. The receiver used the same optical front-end, is able to switch among baseband and wireless types of signals by DSP reconfiguring to baseband only. This demonstrated digital reconfigurable coherent receiver has potential to enable unified support for signal detection on highly heterogeneous next generation metro- access networks.

5. References

[1]. K, Sato and H. Hasegawa, "Optical Networking Technologies That Will Create Future Bandwidth Abundant Networks", JOCN **1**, 81-83 (2009).

[2]. K. Prince, J. B. Jensen, A. Caballero, X. Yu, T. B. Gibbon, D. Zibar, N. Guerrero, A. V. Osadchiy, and I. Tafur Monroy, "Converged Wireline and Wireless Access Over a 78-km Deployed Fiber Long-Reach WDM PON", PTL **21**, 1274-1276, (2009).

[3]. M. Popov, "The Convergence of Wired and Wireless Services Delivery in Access and Home Networks", in Proc. OFC (San Diego, CA 2010), paper OWQ6.

[4]. H. Kimura, Y. Sakai, N. IIyama and K. Kumozaki, "Service Rate Matching Optical Receiver Module with Bit Rates Over 40Gb/s for PS-based WDM PON Systems", in Proc. LEOS (Newport Beach, CA 2008), pp. 669-70.

[5]. H. Rohde, S. Smolorz, E. Gottwald and K. Kloppe, "Next Generation Optical Access: 1 Gbit/s for Everyone", in Proc. ECOC (Vienna, Austria 2009), paper 10.5.5

[6]. D. Zibar, X. Yu, C. Peucheret, P. Jeppesen and I. Tafur Monroy, "Digital Coherent Receiver for Phase-Modulated Radio-Over-Fiber Optical Links", PTL **21**, 155-157 (2009).

[7]. X. Yu, T. B. Gibbon, M. Pawlik, S. Blaaberg, and I. Tafur Monroy, "A Photonic Ultra-Wideband Pulse Generator Based on Relaxation Oscillations of a Semiconductor Laser", Optics Express **17**, 9680-9687 (2009).

[8]. T. Schmidt and D. Cox, "Robust Frequency and Timing Synchronization for OFDM", IEEE Trans Commun **45**, 1613-1621. (1997).

Paper 5: VCSEL-based gigabit IR-UWB link for converged communication and sensing applications in optical metro-access networks

T. T. Pham, T. Braidwood Gibbon and I. Tafur Monroy, "VCSEL-based gigabit IR-UWB link for converged communication and sensing applications in optical metro-access networks," *Optics Communications*, vol. 285, no. 24, pp. 5068–5072, 2012.

Optics Communications 285 (2012) 5068–5072

Contents lists available at SciVerse ScienceDirect

Optics Communications

journal homepage: www.elsevier.com/locate/optcom

VCSEL-based gigabit IR-UWB link for converged communication and sensing applications in optical metro-access networks

Tien-Thang Pham *, Timothy Braidwood Gibbon, Idelfonso Tafur Monroy

DTU Fotonik – Department of Photonics Engineering, Technical University of Denmark, DK-2800 Kgs. Lyngby, Denmark

ARTICLE INFO

Article history:
Received 14 March 2011
Received in revised form
9 June 2012
Accepted 11 June 2012
Available online 4 August 2012

Keywords:
Vertical cavity surface emitting laser (VCSEL)
Ultrawide band (UWB)
Radio over fiber (RoF)
Sensing

ABSTRACT

We report on experimental demonstration of an impulse radio ultrawideband (IR-UWB) based converged communication and sensing system. A 1550-nm VCSEL-generated IR-UWB signal is used for 2-Gbps wireless data distribution over 800-m and 50-km single mode fiber links which present short-range in-building and long-reach access network applications. The IR-UWB signal is also used to simultaneously measure the rotational speed of a blade spinning between 18 and 30 Hz. To the best of our knowledge, this is the very first demonstration of a simultaneous gigabit UWB telecommunication and wireless UWB sensing application, paving the way forward for the development and deployment of converged UWB VCSEL-based technologies in access and in-building networks of the future.

1. Introduction

Vertical cavity surface emitting lasers (VCSELs) have long been promoted as a key future light source in short-range data communication networks such as Local Area Networks (LANs) and Storage Area Networks (SANs). For passive optical access networks (PONs), with the development of long-wavelength VCSELs, their relative low cost, low drive currents, high bandwidth, and wavelength tunability also make them as the idea for future widespread on-site and customer premises deployment [1–4]. It has been demonstrated that such VCSELs are suitable for high-speed long-reach next-generation PON systems [5].

On the other hand, ultrawide band (UWB) is a promising technology for short-range high-speed wireless communication systems due to its low complexity, low cost, low power consumption and coexistence with other radio communication systems such as Global System for Mobile Communications (GSMs), Worldwide Interoperability for Microwave Access (WiMAX), and the Global Positioning System (GPS) [6]. Currently, UWB systems can be implemented on a single chip architecture for hand-held devices with different pulse shapes such as third, forth and fifth orders at gigabit pulse rate [7–10]. Regulated by the Federal Communications Commission (FCC), UWB operating within the spectrum band 3.1–10.6 GHz has extremely low emission power at −41.3 dB m/MHz [11]. Such low emitted PSD causes the wireless transmission distance to be limited within a few meters. For extending the coverage of UWB services for both in-building and long-reach access network applications, optical technologies have been proposed recently. Electrical UWB signal modulates a light source and is delivered to remote UWB antennas through optical fiber [13–15]. Several all-optical solutions also have been proposed to generate, modulate as well as distribute UWB signals in an optical network [16–20,24]. The transmission performance of optically generated UWB signals at 500 Mbps over 63 cm wireless [21] and at 3.125 Gbps over 2.9 m wireless [22] were investigated. The comparison of the performance of electrical and photonic generation methods for 2 Gbps over 20-km fiber and 8 m wireless is presented in [23]. Additionally, there is an increasing trend to integrate UWB-over-fiber system into other wireline/wireless communication systems to build a converged communication access network [25–27]. Simultaneously, together with localization and tracking ability, UWB has also been used in numerous sensing applications ranging from indoor positioning, subsurface sensing, military through-wall motion detection to medical diagnosis and patient monitoring [30–33]. However, converged gigabit UWB telecommunication and wireless sensing applications have not yet been demonstrated. Practically, there are several applications where both high-speed communication and high-accuracy sensing are required. For example, in industrial machining and lathing applications controlled by bandwidth intensive genetic algorithms [34], high bandwidth data transmission can be used to interface remote servers running the algorithms that control the machinery, while simultaneous motion sensing provides real time feedback for the evolutionary algorithm. In medical diagnosis, sensing application can be used to monitor the

* Corresponding author.
E-mail address: ptit@fotonik.dtu.dk (T.-T. Pham).

0030-4018/$ - see front matter © 2012 Elsevier B.V. All rights reserved.
http://dx.doi.org/10.1016/j.optcom.2012.06.087

movement of patient body parts and data communication provide high resolution digital images for teleradiology and telepathology [35].

In this paper, we present the combination of VCSEL and UWB technologies by showing how VCSELs can be used to create an UWB signal for simultaneous high speed data transfer and remote sensing application. The demonstrated technique exploits the advantage of being able to directly modulate a VCSEL to simply and efficiently create a 2-Gbps optical UWB signal. The VCSEL performance is shown to be ideal for photonic UWB distribution over both short-range in-building/industrial fiber networks up to 800 m, as well as long-reach metro-access type applications up to 50 km. Following fiber distribution, the wireless UWB signal is subsequently simultaneously used in a 2-Gbps telecommunication and remote sensing application. This matches all requirements for an advanced in-building/industrial scenario: cheap and simple UWB generation, convenient extended UWB reach through optical fiber, accurate motion sensing, and simultaneous converged high speed uninterrupted 2-Gbps wireless communication channel. While photonic UWB generation through direct modulation of VCSELs has been demonstrated before at 850 nm over 100 m of multi-mode fiber [28] and at 1308/1564 nm over 1 km of standard single mode fiber (SMF) [29], this is the first report on UWB long-reach access and sensing applications featuring VCSELs. Additionally, our sensing approach is entirely DSP based, thus within an UWB data transmission environment, motion sensing can be performed without the need for additional hardware compared to conventional sensing techniques such as optical sensing.

2. Experimental setup

The experimental setup is shown in Fig. 1. To emulate a UWB source, a 24-GSample/s arbitrary waveform generator (AWG) is used to create a 2-Gbps UWB signal with pulse shape following a fifth-order Gaussian derivative which is known to demonstrate good agreement to the FCC requirements [12]. A 1550-nm uncooled VCSEL with output optical power of 0.5 dB m was directly driven by the UWB signal from the AWG. The UWB pulse shape for the UWB bit sequence '101100' at point A (before driving the VCSEL) is shown in Fig. 2. To verify the robustness of the VCSEL-UWB performance under different network scenarios, the UWB pulse is transmitted through two different types of optical links in two separate investigations. The first scenario (link A in Fig. 1) consists of 300 m of SMF followed by 500 m of bend-insensitive fiber (BIF) with 1.9 dB loss. This represents a typical in-building/industrial fiber plant case. The second scenario (link B

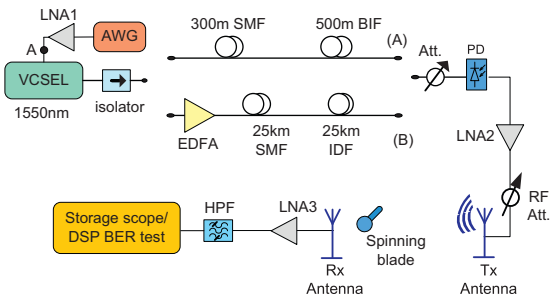

Fig. 1. Experimental setup for converged communication and sensing system. AWG, arbitrary waveform generator; VCSEL, vertical cavity surface emitting laser; EDFA, erbium doped fiber amplifier; SMF, standard single-mode fiber; IDF, inverse dispersion fiber; BIF, bend-insensitive fiber; PD, photodetector; TOA, tunable optical attenuator; LNA, low-noise amplifier; HPF, high-pass filter.

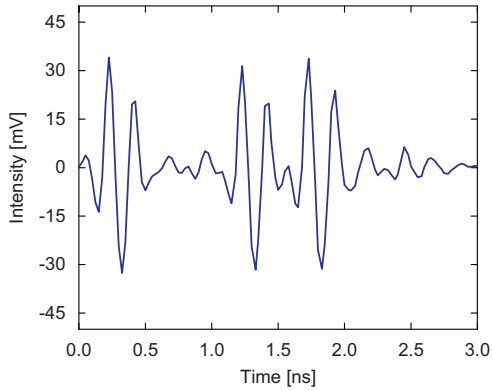

Fig. 2. UWB pulse shape for the bit sequence 101100 before driving the VCSEL.

in Fig. 1) mirrors an access network over 25-km SMF followed by 25 km of matching inverse dispersion fiber (IDF) with 15.4-dB combined loss. An erbium doped fiber amplifier (EDFA) with constant output power of 10 dB m was used to compensate the additional attenuation. After detection at the photodiode with a 12-GHz 3-dB bandwidth, the UWB signal power is matched to the FCC mask taking the antenna response into account, and the signal is transmitted wirelessly over 2.5 m using an omni-directional UWB antenna (Skycross SMT-3TO10M-A). The radiated UWB signal was received by a directive antenna (Geozondas AU-3.1G10.6G-1) pointed towards the transmitter antenna. The receiver antenna surface is 2.5×5 cm. For the sensing application a spinning metallic blade with 2.5 cm wide is placed 4 cm before the receiver antenna. After the directional receiver antenna, the signal is amplified, high-pass filtered to remove frequency components below 3.1 GHz and subsequently captured on a 40-GSample/s digital storage oscilloscope (DSO). For the sensing application, the frequency of the spinning blade is determined using wireless UWB signal through Fourier transform digital signal processing (DSP) analysis as described in the following section. The bit error rate (BER) of the communication channel is determined by an offline DSP algorithm incorporating matched filtering, synchronization and decision threshold optimization in a bit-for-bit comparison between the transmitted and received $2^{11}-1$ pseudo random binary sequence (PRBS) pattern length.

3. Photonic IR-UWB signal distribution

3.1. IR-UWB wireless communication

A prerequisite for high quality UWB wireless communication is that fiber transmission should not corrupt the signal as it is sent from the VCSEL source to the transmitting antenna. In order to validate the VCSEL UWB fiber transmission performance, we thus begin by presenting the electrical spectra of detected UWB signals at point A, back-to-back (B2B), after 800-m and 50-km fiber transmission as shown in Fig. 3. The effective mask is the allowed mask when the transmitter antenna is taken into account.

As shown in Fig. 3a, the spectra of detected UWB signal at B2B were different from those at point A. This is mainly due to the low frequency response of the VCSEL at frequencies higher than 9 GHz. However, the spectra after fiber transmission (in Fig. 3b) were found to be practically identical to those at B2B. It means that fiber transmission has negligible effect on the performance of the UWB signals. This is further confirmed by the measured BER

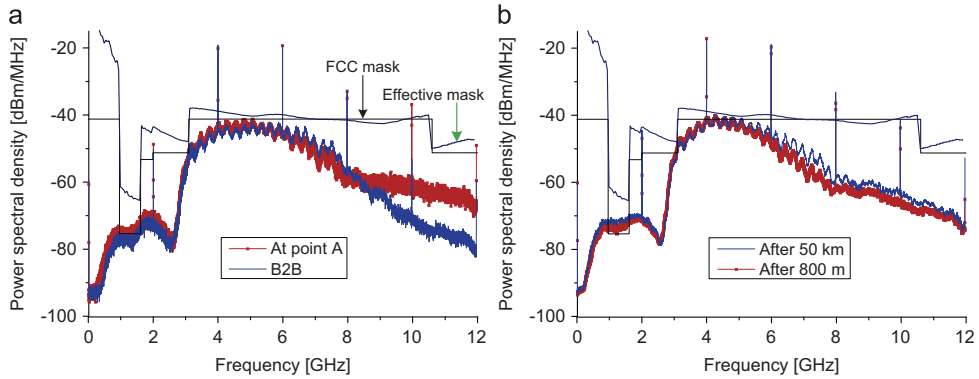

Fig. 3. Electrical spectral of UWB signal (a) before applied to VCSEL and at point A, (b) after 50-km and 800-m fiber transmission.

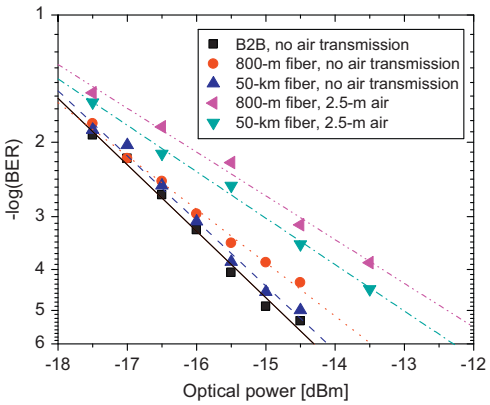

Fig. 4. Measured BER of the UWB signal over different optical and wireless links.

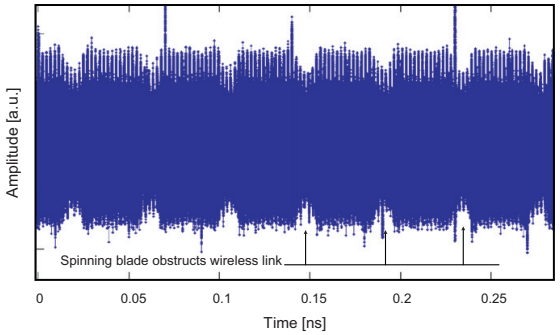

Fig. 5. Attenuation of UWB signal by spinning blade as it periodically passes receiver antenna.

which is shown below. The spikes in the spectrum with 2-GHz spacing originate from the on–off keying modulation and are spaced at the pulse repetition frequency, and the possible interference caused by the spikes higher than the FCC mask should be further considered for application in coexistence scenarios. The measured BER results are shown in Fig. 4. These BER measurements are determined directly after the photodiode with and without wireless transmission by using DSP on 200 kbits per plotted point. Without wireless transmission, in all three cases no errors were detected at receiver sensitivity of −14 dB m. Regarding the effect of chromatic dispersion, the performance of UWB-over-fiber system employing a continuous wavelength (CW) source has been theoretically analyzed [24]. In our proposed system, a directly modulated VCSEL is used. Therefore, frequency chirping and fiber transmission would cause the performance of the UWB signal to deteriorate. For the 50-km link B, negligible transmission penalty is observed in Fig. 4. In this case the use of IDF for dispersion management has added benefit compared to dispersion compensating fiber of being used as transmission fiber, thus extending network reach. For the 800-m link A, a small dispersion penalty of less than 0.5 dB is noticeable. However, this penalty is far offset by the cost-saving and elegance of using a VCSEL with no dispersion compensation or optical amplification in a simple to install and loss-tolerant BIF fiber plant for on-site and in-building applications. After 2.5-m wireless transmission, there were no errors detected when optical power was higher than −13.5 dB m. Compared to without wireless transmission cases, approximately 0.9-dB and 1.3-dB power penalties were observable in long-reach access and in-building scenarios at forward error correction (FEC) limit (BER $= 2 \times 10^{-3}$), respectively.

3.2. Motion sensing application

Results showing the converged UWB wireless communication and motion sensing are now presented and discussed. The scenario under consideration is that shown in Fig. 1 with the 800 m SMF/BIF link, and the received optical power at the photodiode set to −11.8 dB m. Fig. 5 illustrates the received UWB signal stored by the DSO with the spinning blade in motion.

As can be seen in Fig. 5, as the blade passes and partially obstructs the receiver antenna the UWB signal power is attenuated. The frequency of the spinning blade is determined by a second custom DSP algorithm that performs low pass filtering, down sampling, envelope detection, and a subsequent Fast Fourier Transform (FFT). Fig. 6(a) shows the FFT results for the blade spinning at different speeds for three different voltages applied to the motor driving the blade. In each case the fundamental frequency of the spinning blade and higher-order harmonics are clearly visible. Fig. 6(b) summarizes the measured frequencies of the spinning blade at different voltages between 6 and 12 V applied to the motor driving the blade. A parameter affecting the accuracy of measured spinning frequencies is the sampling frequency. Higher sampling frequency induces higher accuracy of the measurement. The sampling frequency for the sensing application with the current demonstration is 40 kSamples/s which is much higher than the frequencies of spinning blade. In real implementation, the sampling frequency can be adjusted to fit

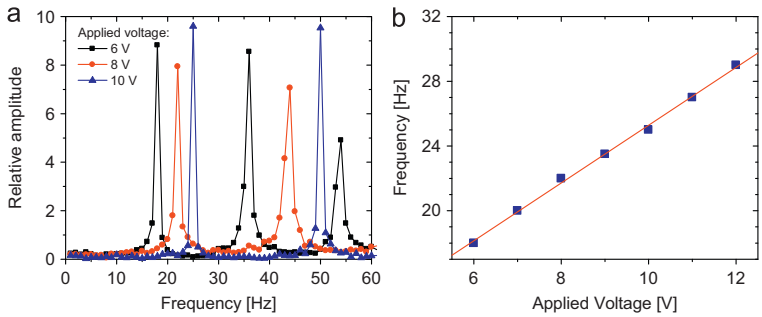

Fig. 6. Result for various voltages applied to the motor driving the spinning blade. (a) FFT-based DSP results for 6 V, 8 V and 10 V. (b) The measured spinning blade frequency as a function of motor voltage.

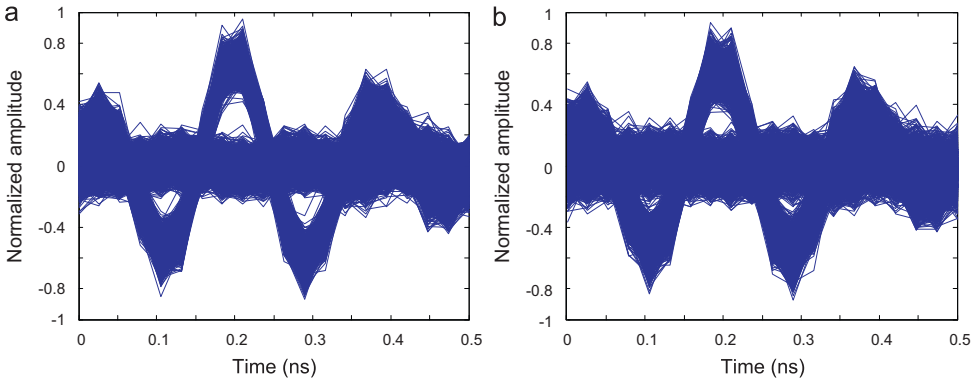

Fig. 7. Open eye diagrams for the spinning blade positioned at (a) minimum attenuation and (b) maximum attenuation of the wireless UWB signal.

with spinning frequencies and the requirement of sensing accuracy.

An important feature of our converged telecommunication/sensing application is that error-free 2-Gbps UWB wireless communication is achieved at all times while the sensing application is running. Fig. 7 shows the eye-diagrams of the UWB signal with the spinning blade positioned for maximum attenuation, and positioned for no attenuation of the received UWB wireless signal. The open eye diagrams are around 0.2 ns. As shown in the figure, the performance of the UWB signal would be affected when the blade is moving. However, in both cases no errors in 200 kbits were detected in analysis by the BER DSP algorithm. BERs of the UWB signal in these cases are still far away from the FEC limit. FEC has been intensively investigated [36,37] and also included in standard of UWB communication systems [38]. Therefore with the application of FEC, UWB communication can achieve the BER of below 10^{-12} even with longer wireless transmission distance when the sensing application is working.

4. Conclusion

We demonstrated the use of a 1550-nm VCSEL for the direct modulation generation of an FCC-compliant 2-Gbps UWB photonic signal. The VCSEL-UWB performance is shown to be robust over both 800 m of SMF/BIF representing an in-building network, as well as over 50 km of SMF/IDF representing a long-reach access network. In addition to 2-Gbps wireless UWB data transmission without errors, the wireless UWB signal is simultaneously used in conjunction with a custom DSP algorithm to determine the frequency of a blade spinning between 18 and 30 Hz. Highly sensitive, accurate motion sensing technology such as this finds application in industrial, manufacturing and early-warning failure notification processes. The results show the potential for UWB-based converged wireless communication and sensing technologies in access and in-building networks of the future using a low cost optical source.

Acknowledgment

The research leading to these results received partial funding from the European Commission Seventh Framework Programme FP7-ICT-2007-2 within the ICT project GigaWaM. The authors also thank Tektronix and Thomas Jul from Nortelco for the loan of the AWG7122B arbitrary waveform generator. The authors would also like to thank C. Neumeyr, E. Rönneberg and M. Ortsiefer from Vertilas GmbH for supplying high-quality VCSELs.

References

[1] K.D. Choquette, in: The 14th Annual Meeting of the IEEE Lasers and Electro-Optics Society (LEOS 2001), vol. 2, 2001, p. 594.
[2] M.V.R. Murty, X.D. Huang, G.L. Liu, C.C. Lin, D. Xu, C.L. Shieh, H.C. Lee, J. Cheng, IEEE Photonics Technology Letters 17 (6) (2005) 1286.
[3] A. Syrbu, A. Mereuta, V. Iakovlev, A. Caliman, P. Royo, E. Kapon, in: Proceedings of the Optical Fiber communication/National Fiber Optic Engineers Conference (OFC/NFOEC 2008), 2008.
[4] M.C. Amann, W. Hofmann, IEEE Journal of Selected Topics in Quantum Electronics 15 (3) (2009) 861.

[5] K. Prince, M. Ma, T.B. Gibbon, I. Tafur Monroy, in: Conference on Lasers and Electro-Optics (CLEO) and Quantum Electronics and Laser Science Conference (QELS2010), 2010, p. 1.
[6] D. Porcino, W. Hirt, IEEE Communications Magazine 41 (2003) 66.
[7] A. Medi, W. Namgoong, IEEE Journal of Solid-State Circuits 43 (4) (2008) 974.
[8] Y. Zhu, J.D. Zuegel, J.R. Marciante, H. Wu, IEEE Journal of Solid-State Circuits 44 (3) (2009) 808.
[9] X. Wang, S. Fan, H. Tang, L. Lin, J. Liu, Q. Fang, H. Zhao, A. Wang, L.W. Yang, B. Zhao, IEEE Transactions on Microwave Theory and Techniques 59 (4) (2011) 1109.
[10] L. Zhou, Z. Chen, C.C. Wang, F. Tzeng, V. Jain, P. Heydari, IEEE Transactions on Microwave Theory and Techniques 59 (4) (2011) 1117.
[11] Federal Communications Commission, Revision of Part 15 of the Commission's Rules Regarding Ultra-Wideband Transmission Systems, 2002.
[12] H. Sheng, P. Orlik, A.M. Haimovich, L.J. Cimini, J. Zhang, in: IEEE International Conference on Communications (ICC2003), vol. 1, 2003, p. 738.
[13] C.M. Tan, L.C. Ong, M.L. Yee, B. Luo, P.K. Tang, in: Proceedings of the IEEE Asia-Pacific Microwave Conference (APMC 2005), 2005.
[14] Y.L. Guennec, M. Lourdiane, B. Cabon, G. Maury, P. Lombard, in: 19th Annual Meeting of the IEEE Lasers and Electro-Optics Society (LEOS 2006), 2006, p. 518.
[15] R. Llorente, M.P. Thakur, M. Morant, S.D. Walker, J. Marti, in: 34th European Conference on Optical Communication (ECOC 2008), 2008.
[16] W.P. Lin, Y.C. Chen, IEEE Journal of Selected Topics in Quantum Electronics 12 (4) (2006) 882.
[17] A. Kaszubowska-Anandarajah, P. Perry, L.P. Barry, H. Shams, IEEE Photonics Technology Letters 20 (22) (2008) 1884.
[18] V. Torres-Company, K. Prince, I.T. Monroy, IEEE Photonics Technology Letters 20 (15) (2008) 1299.
[19] R. Llorente, T. Alves, M. Morant, M. Beltran, J. Perez, A. Cartaxo, J. Marti, IEEE Photonics Technology Letters 20 (11) (2008) 945.
[20] J. Yao, IEEE Microwave Magazine 10 (4) (2009) 82.
[21] M. Abtahi, M. Mirshafiei, S. LaRochelle, L.A. Rusch, Journal of Lightwave Technology 26 (15) (2008) 2795.
[22] T.B. Gibbon, X. Yu, R. Gamatham, N.G. Gonzalez, R. Rodes, J.B. Jensen, A. Caballero, I. Tafur Monroy, IEEE Microwave Theory and Wireless Component Letters 20 (2) (2010) 127.
[23] R.R. Lopez, A. Caballero, X. Yu, T.B. Gibbon, J.B. Jensen, I.T. Monroy, IEEE Photonics Technology Letters 22 (5) (2010) 263.
[24] S. Pan, J. Yao, IEEE Selected Areas in Communications 28 (6) (2010) 889.
[25] K. Prince, J.B. Jensen, A. Caballero, X. Yu, T.B. Gibbon, D. Zibar, N. Guerrero, A.V. Osadchiy, I.T. Monroy, IEEE Photonics Technology Letters 21 (17) (2009) 1274.
[26] S. Pan, J. Yao, IEEE/OSA Journal of Lightwave Technology 29 (20) (2011) 3025.
[27] T.T. Pham, X. Yu, L. Dittmann, I.T. Monroy, IEEE Photonics Technology Letters 23 (08) (2011) 1041.
[28] J.B. Jensen, R. Rodes, A. Caballero, X. Yu, T.B. Gibbon, I.T. Monroy, Optics Express 17 (19) (2009) 16898.
[29] M.P. Thakur, T.J. Quinlan, C. Bock, S.D. Walker, M. Toycan, S.E.M. Dudley, D.W. Smith, A. Borghesani, D. Moodie, M. Ran, Y. Ben-Ezra, IEEE/OSA Journal of Lightwave Technology 27 (3) (2009) 266.
[30] Z. Cemin, M.J. Kuhn, B.C. Merkl, A.E. Fathy, M.R. Mahfouz, IEEE Transactions on Microwave Theory and Techniques 58 (1) (2010) 9.
[31] J. Han, C. Nguyen, IEEE Sensors Journal 7 (1) (2007) 51.
[32] P. Withington, H. Fluhler, S. Nag, IEEE Microwave Magazine 4 (3) (2003) 51.
[33] X. Yong, in: Proceedings of the IEEE/ICME International Conference on Complex Medical Engineering (CME2007), 2007, p. 408.
[34] L.X. Wang, D.Y. Li, L.J. Du, in: Proceedings of the IEEE International Conference on Automation and Logistics (ICAL), 2011, pp. 452–455.
[35] DICOM Standard Committee, Working Groups 26, Pathology, 〈ftp://medical.nema.org/medical/dicom/supps/sup145_09.pdf〉.
[36] H. Karvonen, C. Pomalaza-Raez, M. Hamalainen, in: Proceedings of the IEEE International Conference on Ultra-Wideband, 2006, p. 357.
[37] S.W. Choi, S.S. Choi, H.H. Lee, in: Proceedings of the IEEE 64th Vehicular Technology Conference (VTC-2006), 2006.
[38] ECMA UWB Standard, 〈http://www.ecma-international.org/publications/files/ECMA-ST/ECMA-368.pdf〉.

Paper 6: Combined single-mode/multimode fiber link supporting simplified in-building 60-GHz gigabit wireless access

T. T. Pham, A. Lebedev, M. Beltran, X. Yu, R. Llorente, I. Tafur Monroy, "Combined single-mode/multimode fiber link supporting simplified in-building 60-GHz gigabit wireless access," *Optical Fiber Technology*, vol. 18, no. 4, pp. 226–229, 2012.

Optical Fiber Technology 18 (2012) 226–229

Contents lists available at SciVerse ScienceDirect

Optical Fiber Technology

www.elsevier.com/locate/yofte

Combined single-mode/multimode fiber link supporting simplified in-building 60-GHz gigabit wireless access

Tien-Thang Pham [a,*], Alexander Lebedev [a], Marta Beltrán [b], Xianbin Yu [a], Roberto Llorente [b], Idelfonso Tafur Monroy [a]

[a] DTU Fotonik-Department of Photonics Engineering, Technical University of Denmark, 2800 Kgs. Lyngby, Denmark
[b] Valencia Nanophotonics Technology Center, Universidad Politcnica de Valencia, Camino de Vera s/n, 46022 Valencia, Spain

ARTICLE INFO

Article history:
Received 20 January 2012
Revised 4 May 2012
Available online 2 July 2012

Keywords:
Millimeter wave (MMW)
Wireless personal area network (WPAN)
Multimode fiber (MMF)
Optical fiber communication
Radio over fiber (RoF)

ABSTRACT

In this paper, we propose and experimentally demonstrate a simple, cost-effective hybrid gigabit fiber-wireless system for in-building wireless access. Simplicity and cost-effectiveness are achieved in all parts of the system by utilizing direct laser modulation, optical frequency up-conversion, combined single mode/multimode fiber transmission and envelope detection. Error-free transmission of 2-Gbps data in 60-GHz band over a composite channel including 10-km standard single-mode fiber (SSMF)/1-km multimode fiber (MMF) and 6.5-m air transmission was successfully achieved.

1. Introduction

Millimeter wave (MMW) wireless communication is receiving increased research interests. It is aimed at exploring its potential of broadband wireless data transmission in future wireless personal area networks (WPANs), to support bandwidth-hungry services such as high-definition television (HDTV), 3D gaming and high-speed data access. Additionally, the 60-GHz band has been standardized for future WPAN networks by several working groups such as Ecma International - an European association for standardizing information and communication systems, WirelessHD and IEEE 802.15.3c [1–3]. In order to commercialize 60-GHz systems for next-generation high-speed wireless networks, it is highly desirable to develop a system with less complexity and low power consumption transceivers as a large number of remote antenna units (RAUs) and user terminals are to be deployed in such networks. Due to the high atmospheric loss of MMW signals, radio-over-fiber (RoF) technique is generally considered as an attractive solution to extend the reach of MMW wireless networks. In this context, supported by low loss and wide bandwidth transmission of optical fibers, several BSs is connected to one central office (CO) which has centralized functions such as MMW subcarrier generation, data up-conversion, amplification. Several MMW RoF systems have been proposed and demonstrated recently in the literature [4–10].

Regarding the optical fiber plant, standard single-mode fibers (SSMFs) have been widely deployed in optical core/metro/access networks, and well studied in proposed MMW RoF systems [4–10]. On the other hand, multi-mode fibers (MMFs) are predominantly deployed in in-building networks as a backbone for local area networks (LANs) (approximately from 85% to 90%) due to various advantages such as low cost, easy installation and maintenance [11]. Gigabit baseband links over hundred meters of MMF have been deployed [12]. When developing a system to meet the increasing demand for high-bandwidth wireless services, it is greatly encouraged to efficiently utilize this existing infrastructure. Together with SMFs in access networks, the reuse of MMF for distribution of MMW signals through in-building optical networks to WPAN networks will save fiber reinstallation cost. The schematic of such a system is presented in Fig. 1. MMW signal is optically generated at the CO and then distributed to user terminals through a composite channel including SMF, MMF and wireless links. Several experiments on MMF based RoF systems have been reported ([13–15, and references therein]). However, to the best of our knowledge, 60-GHz over MMF system has not been demonstrated yet. The reported highest frequency and data rate so far are 38.8 GHz and 900 Mbps over 100-m MMF [14]. Data transmission over a composite channel has been demonstrated at low bitrate and low RF frequency: 120-Mbps data at 31.14 GHz over 20-km SMF plus 300-m MMF and 3-m wireless link [15]. For future deployment of 60-GHz systems, it is important to evaluate the performance of 60-GHz signal over such composite channel.

* Corresponding author.
E-mail address: ptit@fotonik.dtu.dk (T.-T. Pham).

1068-5200/$ - see front matter © 2012 Elsevier Inc. All rights reserved.
http://dx.doi.org/10.1016/j.yofte.2012.06.001

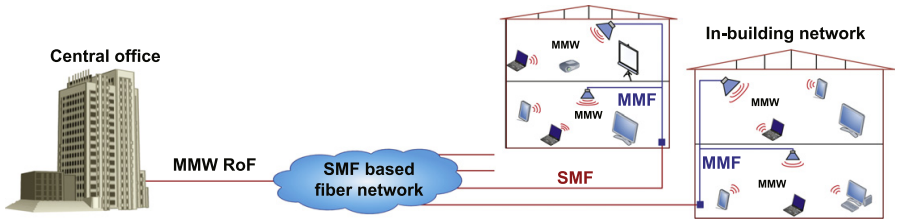

Fig. 1. Distribution of MMW RoF signals over combined SMF and MMF link for in-building broadband wireless access.

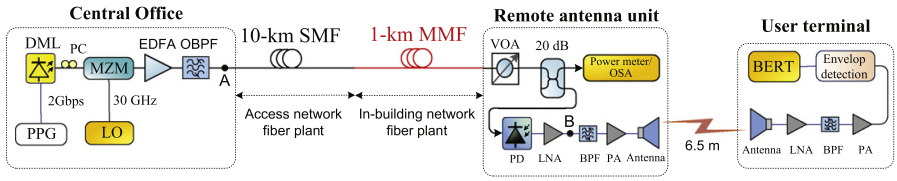

Fig. 2. Experimental setup: PPG: pulse pattern generator, DML: directly-modulated laser, PC: polarization controller, MZM: Mach–Zehnder modulator, EDFA: Erbium doped fiber amplifier, OBPF: optical band-pass filter, VOA: variable optical attenuator, OSA: optical spectrum analyzer, PD: photo-detector, LNA: low-noise amplifier, PA: power amplifier, BPF: band-pass filter, BERT: bit-error-rate tester.

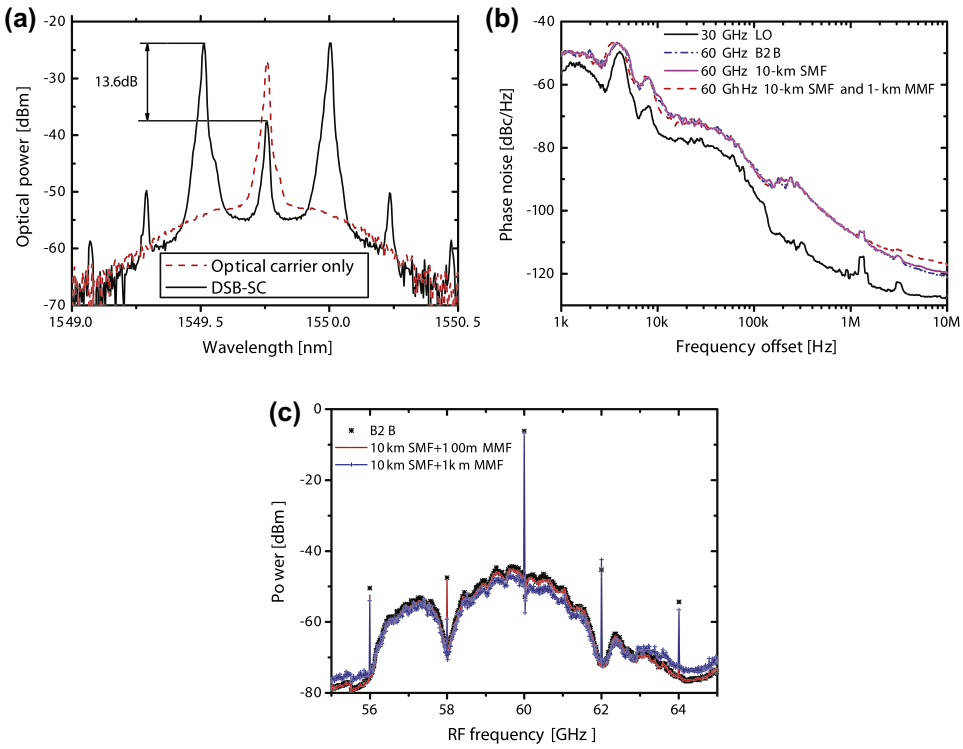

Fig. 3. (a) Optical spectra at point A in Fig. 2, (b) phase noise of RF subcarriers and (c) RF spectra of detected 60-GHz signals with 2-Gbps data at point B in Fig. 2 and −3.0-dBm received optical power.

In this paper, we report transmission of gigabit data at 60-GHz band with simplified transceivers in end-to-end composite RoF network scenario: access and in-building networks using different types of optical fibers. The link consists of 10-km SMF, 1-km MMF and 6.5-m wireless. Direct modulation and double-sideband suppressed carrier (DSB-SC) scheme are adopted in the CO to generate 60-GHz subcarrier while simple envelope detection is employed at user terminals. We show that error-free transmission of 2-Gbps

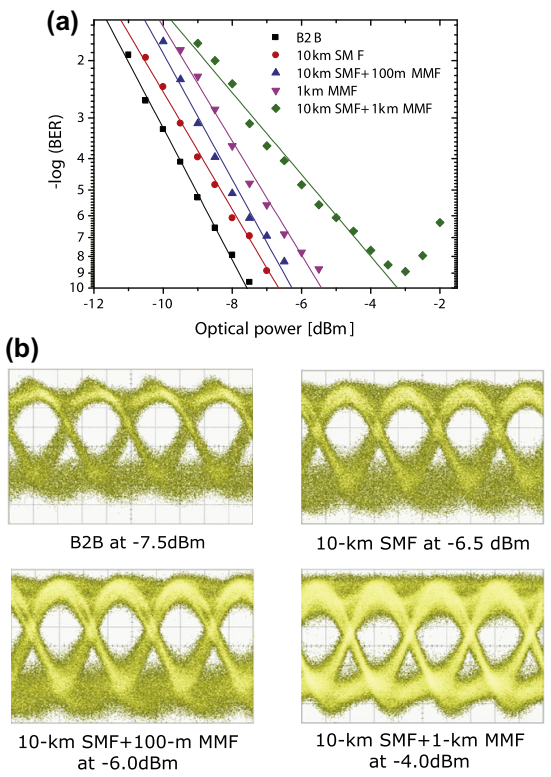

Fig. 4. Measured performance of the system: (a) BER and (b) eye-diagrams (amplitude: 83.5 mV/div and time: 200 ps/div).

data was successfully achieved over the link with less than 4-dB power penalty due to accumulated fiber dispersion.

2. Experimental setup

Fig. 2 illustrates the experimental setup of the in-building wireless access utilizing combined SMF/MMF and simplified wireless transceivers. At the CO, 2-Gbps Pseudo Random Binary Sequence (PRBS) baseband data from a pulse pattern generator (PPG) with a word length of 2^{31}-1 directly modulated a 1.55-μm laser. To generate a 60-GHz subcarrier, the well-known DSB-SC scheme was utilized. The output from the laser was launched into a Mach–Zehnder modulator (MZM) which was biased at the minimum transmission point and driven by a 30-GHz sinusoid signal from a local oscillator (LO). The output of the MZM was amplified and filtered out amplified spontaneous emission (ASE) noise by an optical band-pass filter (OBPF) with 0.8-nm 3-dB bandwidth. The optical signal was then distributed to a RAU over an optical fiber link composed of 10-km standard SMF and additional 100-m or 1-km MMF. The diameters of core and cladding of the MMF are 50 and 125 μm, respectively. The simple, conventional center-launching technique was used to couple the light from the SMF to the MMF [16]. At the RAU, the optical signal was detected by a broadband 75-GHz photo-detector (PD). The detected 60-GHz signal was amplified and radiated to the air by a horn antenna and received by another one. The wireless link was 6.5 m, which was limited by the available lab space. The received wireless signal was then again amplified and filtered. To simplify the end-user wireless terminal, electrical envelope detection was employed to down-convert 60-GHz band signal to the baseband. The output signal of the envelope detector was fed to a bit-error-rate tester (BERT) to evaluate the system performance. Both the antennas have 20-dBi gains in 50–75 GHz frequency range and 12 °C beam width. All the amplifiers have 10 GHz bandwidth (55–65 GHz). The power amplifiers (PA) have 28.7-dB gain and 14-dBm P1dB and the low noise amplifiers (LNA) have 16-dB gain. Bandwidth of the BPFs is 5.7 GHz (56.3–62 GHz).

Apart from the utilization of both SMF and MMF plants, this system architecture has some additional important features. Firstly, the use of direct modulation for data and optical frequency up-conversion to MMW band does not require high speed laser. Secondly, the DSB-SC scheme enables the use of low RF frequency LO and avoiding chromatic dispersion induced RF power fading [4–8]. In a wavelength-division multiplexing (WDM) system scenario to support multiple end-users, the MZM can be shared by many WDM channels. Thirdly, envelope detection is a simple demodulation method, which is transparent to RF frequency and does not require any phase-locked LO and mixer for down-conversion. Therefore, in connection with high transmission performance, this scheme is expected to be a very cost-effective solution for broadband 60-GHz in-building wireless networks with the use of simple transceiver, as well as long access reach. Finally, the same RF configuration can be used for uplink to realize a fully cost-effective bidirectional system. The 60-GHz wireless signal from an end-user terminal received by the antenna at the RAU can be down-converted to the baseband using the same envelope detection technique. Then the baseband signal can be transmitted to the BS through the combined MMF/SMF by directly modulating a light source such as a DFB laser or VCSEL.

3. Experimental results and discussion

Fig. 3a shows the optical spectra at the output of the MZM with and without the 30-GHz LO signal. When the LO signal was applied, two first-order sidebands were dominant and the original optical carrier at 1549.75 nm was suppressed approximately 13.6 dB. The influence of optical carrier suppression ratio on the power of the RF signal has been analyzed in [7].

In general, it is important to generate a high quality RF subcarrier to achieve high performance data transmission. The phase noise from the LO does not change the amplitude of a RF signal. However, fiber dispersion such as chromatic dispersion of the SMF, modal dispersion of the MMF causes the phase-to-intensity conversion that, in turn, makes the amplitude of the RF signal vary after fiber transmission. Fig. 3b shows the measured phase noise of the 30-GHz subcarrier from the LO as well as the generated 60-GHz subcarriers at back-to-back (B2B) and after fiber transmission. We can see that the quality of the 60-GHz subcarrier was maintained after fiber transmission due to the correlation of two sidebands [17]. For example, at 100-kHz offset, the phase noise of the 60-GHz subcarrier was only about 5 dB higher than that of the 30-GHz LO. Therefore, we can use a 30-GHz subcarrier from a LO which has similar phase-noise characteristic as the requirement for the 60-GHz subcarrier.

The electrical spectra of the signals at point B in Fig. 2 in cases of B2B and fiber transmission at −3-dBm optical power are shown in Fig. 3c. The RF spectrum was maintained after 10-km SMF and 100-m MMF. However, there was a slight distortion in the case of 10-km SMF and 1-km MMF due to large modal dispersion of the MMF.

Fig. 4 shows the measured BER curves and eye-diagrams of 2-Gbps data in different transmission cases: B2B, SMF only, MMF only and combined SMF/MMF. The optical power to the PD was controlled by a variable optical attenuator (VOA). We can observe

that chromatic dispersion of 10-km SMF introduced less than 1-dB power penalty. Additional 100-m MMF caused about 0.5-dB power penalty. Suffered from large modal dispersion, the BER performance after 1-km MMF transmission had about 2-dB power penalty. In the case of combined 10-km SMF and 1-km MMF transmission which has both large chromatic dispersion and modal dispersion, the BER curve shows a slightly different slope and the power penalty at a BER of 10^{-9} were approximately 4.3 dB. Additionally, we observed in the experiment that the BER performance rapidly became worse when the received optical power was higher than about −3.0 dBm. That is because the power of the 60-GHz signal was saturated with the RF configuration when high optical power was launched into the PD.

4. Conclusions

We have experimentally demonstrated a gigabit MMW system over a combined-SMF/MMF optical link with simple 60-GHz transceiver based on direct modulation and envelope detection. Error-free transmission was achieved for 2-Gbps data at 60-GHz after 10-km SMF, 1-km MMF and 6.5-m wireless. The experiment proves the feasibility of using SMF in optical access networks in combination with the existing MMF in buildings for distribution of 60-GHz signal direct from a CO to remote in-building antennas enabling a cost-effective solution for next generation gigabit in-building wireless access networks.

Acknowledgments

We would like to thank Thomas Jul from Rohde & Schwarz Danmark A/S for allowing us to use the FSU 67-GHz spectrum analyzer for the experiment.

References

[1] TC48 – High Rate Wireless Communications, Ecma International. <http://www.ecma-international.org/memento/TC32-TG20-M.htm>.
[2] WirelessHD Consortium. <http://www.wirelesshd.org>.
[3] IEEE 802.15 Working Group for WPAN. <http://www.ieee802.org/15/>.
[4] J. Yu et al., Optical millimeter-wave generation or up-conversion using external modulators, IEEE Photon. Technol. Lett. 18 (2006) 265–267.
[5] Z. Jia et al., Key enabling technologies for opticalwireless networks: optical millimeter-wave generation, wavelength reuse, and architecture, IEEE/OSA J. Lightw. Technol. 24 (2006) 1277–1282.
[6] M.K. Hong et al., Gigabit radio-over-fiber link for converged baseband and millimeter-wave band signal transmission using cascaded injection-locked Fabry–Prot laser diodes, Opt. Exp. 17 (2009) 7844–7852.
[7] M.-K. Hong et al., Gigabit optical access link for simultaneous wired and wireless signal transmission based on dual parallel injection-locked Fabry–Prot laser diodes, J. Lightw. Technol. 26 (15) (2008) 2725–2731.
[8] C. Lim et al., Fiber-wireless networks and subsystem technologies, IEEE/OSA J. Lightw. Technol. 28 (2010) 390–405.
[9] X. Yu et al., Bidirectional radio-over-fiber system with phase-modulation downlink and RF oscillator-free uplink using a reflective SOA, IEEE Photon. Technol. Lett. 20 (2008) 2180–2182.
[10] D. Zibar et al., 16 Gb/s QPSK wireless-over-fibre link in 75–110 GHz band with photonic generation and coherent detection, in: ECOC2010, Th.9.B.6, 2010.
[11] A. Flatman, In-premises optical fiber installed base analysis to 2007, in: IEEE 802.3 10 GBE over FDDI Grade Fiber Study, 2004.
[12] AIEEE 802.15 Working Group for Ethernet. <http://www.ieee802.org/3/>.
[13] A.M.J. Koonen, L.M. Garcia, Radio-over-MMF techniques. Part II: Microwave to millimeter-wave systems, IEEE/OSA J. Lightw. Technol. 26 (2008) 2396–2408.
[14] B.A. Khawaja, M.J. Cryan, Millimetre-wave radio-over-fibre data transmission over multimode fibre, Microw. Opt. Technol. Lett. 53 (2011) 254–256.
[15] A. Nkansah et al., Multilevel modulated signal transmission over serial single-mode and multimode fiber links using vertical-cavity surface-emitting lasers for millimeter-wave wireless communications, IEEE Trans. Microw. Theory 55 (2007) 1219–1228.
[16] D.H. Sim et al., High-speed multimode fiber transmission by using mode-field matched center-launching technique, IEEE/OSA J. Lightw. Technol. 27 (2009) 1018–1026.
[17] X. Yu et al., High carrier suppression double sideband modulation using polarization state rotation filter and optical external modulator, Opt. Commun. 267 (2006) 83–87.

Paper 7: Optimization of high-definition video coding and hybrid fiber-wireless transmission in the 60 GHz band

A. Lebedev, **T. T. Pham**, M. Beltran, X. Yu, A. Ukhanova, R. Llorente, I. Tafur Monroy, S. Forchhammer "Optimization of high-definition video coding and hybrid fiber," *OSA Optics Express*, vol. 19, no. 26, pp. B895–B904, 2011.

Optimization of high-definition video coding and hybrid fiber-wireless transmission in the 60 GHz band

Alexander Lebedev,[1,*] Tien Thang Pham,[1] Marta Beltrán,[2] Xianbin Yu,[1] Anna Ukhanova,[1] Roberto Llorente,[2] Idelfonso Tafur Monroy,[1] and Søren Forchhammer[1]

[1]*DTU Fotonik, Department of Photonics Engineering, Technical University of Denmark, 2800 Kgs. Lyngby, Denmark*
[2]*Valencia Nanophotonics Technology Center, Universidad Politécnica de Valencia, Camino de Vera s/n, 46022 Valencia, Spain*
**alele@fotonik.dtu.dk*

Abstract: The paper addresses the problem of distribution of high-definition video over fiber-wireless networks. The physical layer architecture with the low complexity envelope detection solution is investigated. We present both experimental studies and simulation of high quality high-definition compressed video transmission over 60 GHz fiber-wireless link. Using advanced video coding we satisfy low complexity and low delay constraints, meanwhile preserving the superb video quality after significantly extended wireless distance.

OCIS codes: (060.2330) Fiber optics communications; (060.5625) Radio frequency photonics.

References and links

1. M. Beltrán, J. B. Jensen, X. Yu, R. Llorente, and I. T. Monroy, "Experimental performance comparison of 60 GHz DCM OFDM and impulse BPSK ultra-wideband with combined optical fibre and wireless transmission," in ECOC, 1465–1467 (2010).
2. Z. Jia, H.-C. Chien, Y.-T. Hsueh, A. Chowdhury, J. Yu, and G.-K. Chang, "Wireless HD services over optical access systems: Transmission, networking, and demonstration," in OFC, 1–5 (2009).
3. M. Weiß, "60 GHz photonic millimeter-wave communication systems," thesis (2010).
4. A. Belogolovy, E. Belyaev, A. Sergeev, and A. Turlikov, "Video compression for wireless transmission: reducing the power consumption of the WPAN hi-speed systems," NEW2AN/ruSMART 2009, LNCS 5764, 313–322 (2009).
5. http://iphome.hhi.de/suehring/tml/.
6. T. Stockhammer, M. M. Hannuksela, and T. Wiegand, "H.264/AVC in wireless environments," IEEE Trans.Circuits Syst. Video Technol. **13**(7), 657–673 (2003).
7. I. E. Richardson, *The H.264 Advanced Video Compression Standard* (Wiley, 2010).
8. http://www.vpiphotonics.com/.
9. S.-K. Yong, *60 GHz Technology for Gbps WLAN and WPAN: From Theory to Practice* (Wiley, 2011), Chap. 2.
10. S. K. Yong and C.-C. Chong, "An overview of multigigabit wireless through millimeter wave technology: potentials and technical challenges," EURASIP J. Wireless Commun. Netw. **2007**(1), 078907 (2007).
11. K.-C. Huang and D. J. Edwards, *Millimetre Wave Antennas for Gigabit Wireless Communications: A Practical Guide to Design and Analysis in a System Context* (Wiley, 2008).

1. Introduction

The motivations for this work are three-fold. First, the unprecedented frequency range around 60 GHz (from 4 to 9 GHz within 57-66 GHz) has been regulated for unlicensed use in a number of countries around the world. Second motivation is the introduction of high quality video services such as high-definition (HD) video conferencing and distributed video gaming. These services define both the demand for increased data rates in the access networks and need for optimization of video compression schemes. Third, efficient convergence of wired and wireless technologies is required to enable the concept of "anytime anywhere" wireless

#155834 - $15.00 USD
(C) 2011 OSA
Received 3 Oct 2011; accepted 28 Nov 2011; published 8 Dec 2011

connectivity. Radio-over-fiber (RoF) is considered a promising example of such integration for optical networks [1].

Previous research in the area of 60 GHz RoF video transmission suggests the use of uncompressed video [2,3]. The main drawback of this approach is reduced flexibility in terms of bitrate: bitrates are fixed depending on resolution, number of bits per pixel, and frame rate of the video sequence. This therefore results in extremely complex adaptation of the HD video system to significant signal-to-noise ratio (SNR) drops caused by either severe shadowing in non-line-of-sight (NLOS) case or extremely high attenuation – problems that are typical for 60 GHz systems.

Source coding (compression) gives us desirable flexibility of bitrate but at the expense of introducing delay and increase of power consumption. However, there is a trade-off between the power needed to radiate larger bandwidth for uncompressed video and the power consumed for the computations of an encoder and a decoder for compressed video transmission. According to [4], low complexity compression can, in fact, bring about reduction in power consumption for a 60 GHz wireless video transmission system compared to the uncompressed case, while at the same time keeping delay under the acceptable limit.

In this work we explore the notion of joint optimization of physical layer parameters of a RoF link (power levels, distance) and the codec parameters (quantization, error-resilience tools) based on peak signal-to-noise ratio (PSNR) as an objective video quality metric. We experimentally demonstrate, first time to our knowledge, the combined optical access and wireless transmission of compressed HD video in the 60 GHz band employing simple envelope detection technique.

2. Experimental setup

The experimental setup of the 60 GHz optical-wireless RoF system is shown in Fig. 1. The binary sequence corresponding to compressed video file was uploaded in an arbitrary waveform generator (AWG). The non-return-to-zero (NRZ) electrical signal on the output of the AWG directly modulated a 1550 nm laser. After the baseband data modulation, frequency up-conversion to the 60 GHz band was performed by driving a Mach-Zehnder modulator (MZM) biased at the minimum transmission point with a 30 GHz sinusoidal signal. A polarization controller (PC) was used before the MZM to minimize its polarization-dependant losses. After the MZM, two sidebands with a frequency spacing of $2f_{LO}$ were generated according to the double sideband-suppressed carrier (DSB-SC) intensity modulation scheme (see Fig. 2). Optical carrier suppression of approximately 13.6 dB is achieved limited by the MZM extinction ratio. The generated sidebands have the same optical power and the locked phase. Subsequently, an Erbium doped fiber amplifier (EDFA) is employed to compensate the losses, and an optical band pass filter (OBPF) is used afterwards to mitigate the amplified spontaneous emission (ASE) noise produced by the EDFA. Then the signal is launched into a 20 km span of non-zero dispersion shifted fiber (NZDSF). We employ the NZDSF in order to minimize dispersion induced impairments. A variable optical attenuator (VOA) is employed to control the optical power impinging the photodiode (PD) in order to evaluate BER performance of the system as a function of the received optical power.

#155834 - $15.00 USD Received 3 Oct 2011; accepted 28 Nov 2011; published 8 Dec 2011

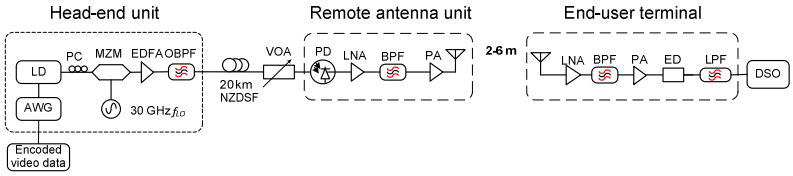

Fig. 1. Experimental 60 GHz optical-wireless RoF system with envelope detection, LD-laser diode, PC-polarization controller, MZM-Mach-Zehnder modulator, LO-local oscillator, EDFA-Erbium doped fiber amplifier, OBPF-optical band pass filter, PD-photodiode, LNA-low noise amplifier, PA-power amplifier, BPF-band pass filter, ED- envelope detector, LPF-low pass filter, DSO-digital sampling oscilloscope.

After photodetection the 60 GHz signal was amplified (gain of amplifiers – 16 dB and 28.7 dB) and filtered (58.1-61.9 GHz) before feeding it to an antenna for up to 6 meters of wireless transmission. After receiving the signal with an antenna and following filtering (58.1-61.9 GHz) and amplification (gain of amplifiers – 16 dB and 28.7 dB) envelope detection was employed for down-conversion. The detected envelope is low-pass filtered and digitized by a digital sampling oscilloscope (DSO). Both the transmitting and receiving antennas used throughout the experiment are commercially available horn antennas with 20 dBi gain and 12° beam width. Bitrates that were transmitted over the fiber are low compared to similar research setups. This explains a good performance to a certain extent, but we emphasize that reduction of bitrate does not lead to a significant video quality deterioration.

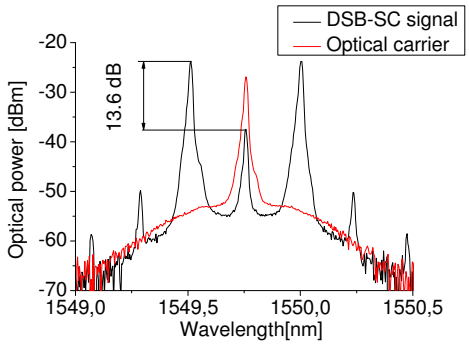

Fig. 2. Optical spectra on the input of the PD.

The encoding was performed using the Joint Model (JM) 17.0 reference software implementation of the H.264/Advanced Video Codec (AVC) [5]. It is a realistic scenario since H.264/AVC is one of the latest industrial video coding standards covering a wide range of applications, including, coding for transmission over wireless links and HDTV coding [6]. An Intra coding mode only and a frame slicing mechanism were employed to achieve the low delay requirement. Both mechanisms are improving the error-resilience as well [7]. Slicing was performed with the use of flexible macroblock ordering (FMO).

H.264 is not capable of coping with single-bit errors: its mechanisms of error-resilience on the encoding side and error concealment on the decoding side are adjusted to cope with packet loss when the packets affected by the errors are discarded such as usually occurs in networks. Packet error rate (PER) depends on the bit error rate (BER) and the size of the packet; in general, the noisier the transmission the shorter the length of the packet is desirable. Initially in the experiment we used the packet size equal to 2500 bytes, each packet containing a slice of the frame; afterwards we have been using packets of length of 3000 and 3500 bytes for

#155834 - $15.00 USD
Received 3 Oct 2011; accepted 28 Nov 2011; published 8 Dec 2011

simulation. The uncompressed HD test video sequence 'blue sky' was used for encoding and transmission. The sequence was originally shot in 4:2:0 format 8 bits per color 1920 × 1080 pixels. However, in order to model the most bitrate demanding case upsampling to 4:4:4 format was performed (uncompressed bitrate – 3 Gbps for the frame rate of 60 frames per second).

We use PSNR as an objective quality metric for video, which is defined as:

$$MSE = \frac{1}{N}\sum_{i=1}^{N}(x_i - y_i)^2, \tag{1}$$

$$PSNR = 10\log_{10}(\frac{L^2}{MSE}), \tag{2}$$

where MSE stands for mean squared error, N is the number of pixels in the image or video signal, and x_i and y_i are the i-th pixel values in the original and the distorted signals, respectively. L is the dynamic range of the pixel values. For an 8 bits/pixel signal, L is equal to 255. PSNR is evaluated for the luminance component of the transmitted video signal.

3. Composite fiber-wireless channel modeling for 60 GHz band

The difficulty of the modeling arises from the fact that we need to account for both the impairments induced by the wireless and the fiber-optic channels. We performed the modeling of the fiber-optic channel with VPI software [8]. The wireless channel model was implemented in Matlab and combined with VPI channel model afterwards. We combine below the description of the channel model with the excerpts from experimental measurements that allow us to simplify the model.

Noise processes in the optical part of the setup (such as amplified spontaneous emission (ASE) noise, Johnson noise, shot noise at the photodiode), attenuation and dispersion in the fiber are simulated in VPI software. We set the numerical values for these parameters according to the specifications of equipment we used in the experimental setup.

We performed the modeling of the wireless channel according to the physical parameters of the devices that have been used in the scheme and references on theoretical parameters taken from [9–11].

The path loss (attenuation) at 60 GHz is much more severe than the path loss at the frequencies that are currently employed for Wireless Personal Area Networks (WPAN). Theoretical description for this phenomenon is provided by Friis formula [9], according to which attenuation in the air is proportional to the frequency squared. It is known that the line-of-sight (LOS) attenuation of the 60 GHz wireless channel can be modeled with a log-normal model [11]. Parameters for this model have been defined through the extensive measurements presented in a number of publications. Summary on the parameters for different experimental environments can be found in [9]. We perform the modeling of the system without taking into account frequency dependency of the path loss. To the best of our knowledge, frequency dependent models for 60 GHz system have not yet been reported.

Influence of the noise on the signal can be modeled with the following formula [10,11]:

$$\begin{aligned} SNR = {} & P_{tx} + G_T + G_R + G_{LNA_{tx}+PA_{tx}} + G_{LNA_{rx}+PA_{rx}} - PL - \\ & -(10\log_{10}(KTB) + NF_{LNA_{tx}+PA_{tx}} + NF_{LNA_{rx}+PA_{rx}}), \end{aligned} \tag{3}$$

$$PL = PL(d_0) + 10n\log_{10}(\frac{d}{d_0}), \tag{4}$$

where P_{tx} in our case is the RF power on the output of the PD, G_T and G_R are the gain of transmitting and receiving antennas respectively, $G_{LNA_{tx}+PA_{tx}}$ and $G_{LNA_{rx}+PA_{rx}}$ are gains of

#155834 - $15.00 USD Received 3 Oct 2011; accepted 28 Nov 2011; published 8 Dec 2011

amplification cascades at transmitting and receiving parts of the scheme respectively, PL is the distance-dependent path loss (attenuation) in the air. The terms in brackets represent noise contributions. The first term represents the Johnson noise, second and third represents noise contributions from amplifiers. Parameters d_0 and d in Eq. (4) represent the reference distance (we used 1 m according to [9]) and the distance between a transmitter and a receiver respectively, n denotes path loss exponent.

The formula does not account for shadowing caused by LOS obstruction, but this resembles the experimental setting where we were working with the LOS scenario only.

Phase noise modeling for the channel was excluded after the experimental examination of the phase noise of the oscillator presented in Fig. 3. Figure 3 shows the high quality of the electrical oscillator for 3 cases: measuring the phase noise of LO, setup without fiber transmission up to a transmitting antenna (optical back-to-back) and after 20 km of NZDSF. Figure 3 also illustrates the fact that contribution from the system to the phase noise is insignificant. Moreover, it could be excluded from consideration, because after wireless transmission we finally recover with ED only the amplitude of the signal, and therefore discard information about phase or frequency.

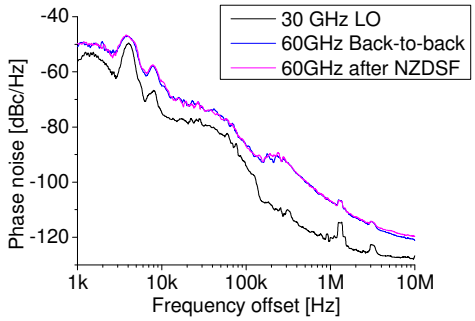

Fig. 3. Phase noise of RF subcarriers.

The model does not take into account the nonlinear effects that are reported for Power Amplifiers in [9]. Nevertheless we regard the model as feasible since the power after the PD is low, so we work in the linear region. Indeed, the power on the output of the PA at the transmitting side given the power at the photodiode of −10 dBm is around −6 dBm. Typically nonlinear effects are observed in the region above 0 dBm [9]. The RF-spectrum measured is depicted in Fig. 4. We refer to the power before the antenna, as the power before radiation P_{br}. Therefore the equation for wireless channel simulation based on Eq. (3) and Eq. (4) could be transformed into:

$$SNR = P_{br} + G_T + G_R + G_{LNA_{rx}+PA_{rx}} - PL(d_0) - 10n\log_{10}(\frac{d}{d_0}) - \\ -(10\log_{10}(KTB) + NF_{LNA_{rx}+PA_{tx}} + NF_{LNA_{rx}+PA_{rx}}). \quad (5)$$

#155834 - $15.00 USD
Received 3 Oct 2011; accepted 28 Nov 2011; published 8 Dec 2011

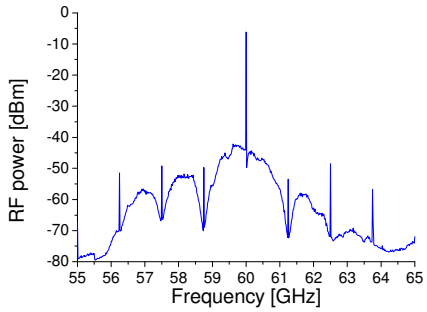

Fig. 4. RF spectrum measured before the antenna.

Typical parameters for the path loss at the reference distance and the path-loss exponent has been found in the references [9,10]. Values for the parameters that are used in modeling of the wireless channel are listed in the Table 1 below.

Table 1. System Parameters for Modeling

Parameter	Numerical value
Center frequency, GHz	60
Joint noise figure Tx amplifiers (LNA + PA), dB	(6 + 7) = 13
Joint noise figure Rx amplifiers (LNA + PA), dB	(6 + 7) = 13
Joint gain of Tx amplifiers (PA + LNA), dB	(28.7 + 16) = 44.7
Joint gain of Rx amplifiers (PA + LNA), dB	(28.7 + 16) = 44.7
Gain of the Tx antenna, dBi	20
Gain of the Rx antenna, dBi	20
Bit rate, Mbps	312.5/1250
Distance, m	2-6
Reference path loss at 1 meter, dB	57.5
Path loss exponent	1.77
Ambient temperature for Johnson noise modeling, K	298

We perform attenuation of the signal and addition of the Additive White Gaussian Noise (AWGN) in VPI, the noise power and attenuation to achieve SNR described in Eq. (5) are calculated in Matlab.

4. Results and discussion

Our goal for optimization is to achieve the best video delivery quality for a given link budget. With regards to the role of the quantization of transform coefficients of the coded video in the optimization, roughly speaking, the smaller the quantization parameter size, the smaller the source distortion (loss due to compression), but the larger the channel distortion it may cause. In the experiment we explored two cases. First, the chosen test video sequence ('blue sky' 4:4:4) was encoded with bitrate of 312.5 Mbps. Second, the tested video sequence was encoded in a high quality setting with the quantization parameter equal to 1, which gave us a compression ratio of 3.

#155834 - $15.00 USD Received 3 Oct 2011; accepted 28 Nov 2011; published 8 Dec 2011

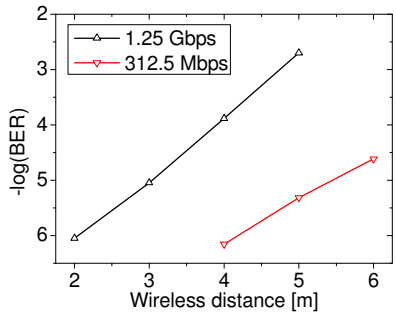

Fig. 5. BER as a function of the wireless distance.

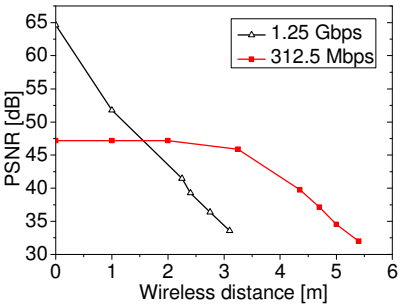

Fig. 6. PSNR as a function of the wireless distance.

On the Fig. 5 BER at the power level at the photodiode equal to −10 dBm as a function of the wireless distance is depicted. From the Fig. 5 we can see that in general the distortion induced by the wireless channel is severe in our system, but video coded with the use of higher quantization parameter has greater dynamic range of wireless distance, as shown in Fig. 6. The distance equal to 0 corresponds to the distortion introduced by the compression only. When we increase the wireless distance, in the beginning, the source distortion is dominant, and the use of lower quantization parameter is reasonable. Anyhow, we lose the advantage of lower distortion after around 2 m of transmission when video is evaluated based on the PSNR metric only. This shows the potential of optimization of the power budget of the system under the constraint of video quality. We obtain similar curves for changing optical power level at the photodiode at 5 m of wireless distance, as shown in Fig. 7 and Fig. 8. With the higher video compression we can work at lower optical power levels. At the same time, we should note that the video quality is high in both cases, and deterioration induced by the compression itself can be regarded as non-significant (PSNR of the video unimpaired by the channel is higher than 45 dB in both cases).

#155834 - $15.00 USD
Received 3 Oct 2011; accepted 28 Nov 2011; published 8 Dec 2011

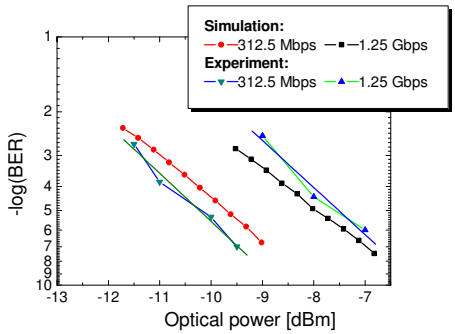

Fig. 7. BER as a function of the optical power at the photodiode.

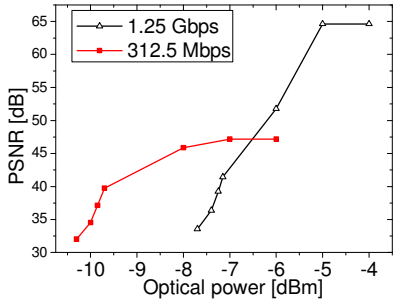

Fig. 8. PSNR as a function of the optical power at the photodiode.

Curves provided by simulation for 5 meters distance and dynamically changing optical power levels show close resemblance that verifies the correctness of the simplified wireless channel model employed. We do not provide simulation-based curves for PSNR, because our simulation is based on the analytical estimation of BERs with the use of VPI software, and we therefore do not have traces including erroneous bits to analyze video performance.

5. Video coding for 60 GHz radio-over-fiber

We employed video coding parameters in a simplified setting that is suitable for both conferencing applications and distributed video gaming. The main constraints for such type of an application are delay and energy consumption. As a part of simplified setting we were using Universal Variable Length Coding (UVLC) for entropy coding that is considered a lower complexity solution [7]. All coding experiments were performed in intra mode thus eliminating the need for long buffering time, and satisfying low delay requirement. The simulation below was performed with bit traces including erroneous bits.

H.264/AVC encoder employs the number of error-resilience tools: slicing of the frame, data partitioning, arbitrary slice ordering, and redundant coded slices [7]. Below we present simulation on two major tools providing error resilience: slices and Flexible Macroblock Ordering (FMO). On the decoder side, there are two error concealment tools used in JM 17.0 reference software implementation of H.264/AVC codec, one exploiting spatial information only, suitable for intra frames (the one used in the experiment and simulation), and one

#155834 - $15.00 USD
Received 3 Oct 2011; accepted 28 Nov 2011; published 8 Dec 2011

exploiting temporal information. Details on the error concealment algorithms used can be found in [5].

First we performed the simulation with a different size of the packet (each containing one slice of the frame). Employing the smaller slices enables us to receive acceptable video quality in the regions with higher BER, and therefore extends distance for acceptable quality of video transmission. Indeed, enabling packets of shorter length reduces the amount of information lost when the packet is discarded, enabling decoder to reconstruct impaired parts of the picture better from unimpaired blocks of neighboring pixels. The simulation results are illustrated on Fig. 9.

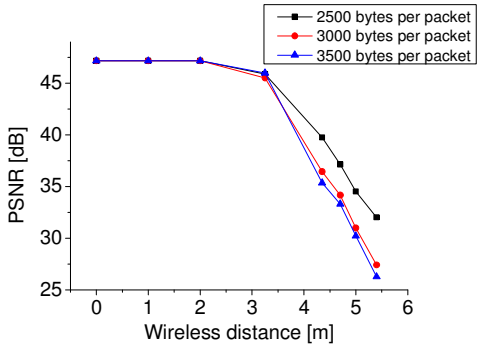

Fig. 9. PSNR as a function of the wireless distance for different packet sizes of the encoded video for the bitrate of 312.5 Mbps.

Below we also present the simulation results for enabling FMO in H.264 reference software [5]. H.264/AVC is the first standard defining this error-resilience tool [7]. In case if we do not use FMO, the images will be composed of a single slice groups with the macroblocks in a scan order. If we employ this algorithm, then when we lose a slice of the video frame, we can make better approximation with the neighboring blocks and therefore, presumably, can achieve gain in PSNR. Results of the simulation for the packet size of 3000 bytes are depicted in the Fig. 10. FMO shows up to 3 dB improvement of PSNR.

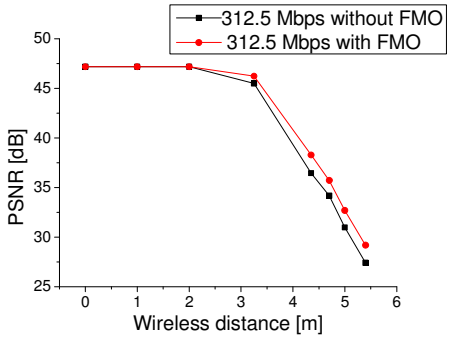

Fig. 10. PSNR performance as a function of the wireless distance for FMO effect estimation.

Coding simulations show the effect of employed source coding error-resilience mechanisms for a particular simplified setting of H.264/AVC and 60 GHz RoF setup as an example of physical layer architecture suitable for transmission high quality HD video

#155834 - $15.00 USD
Received 3 Oct 2011; accepted 28 Nov 2011; published 8 Dec 2011

content. Employed tools of H.264/AVC show the greater robustness of video provided by advanced video coding against impairments induced by 60 GHz fiber-wireless channel.

6. Conclusions

Our experiment and simulation demonstrates the trade-off between the distortion introduced by the source (lossy compression) and distortion introduced by channel for high quality HD video transmission over 60 GHz RoF fiber-wireless links. We have achieved significant extension of wireless distance employing low complexity physical layer solution for detection of RF modulated signal. Our work demonstrates the solutions for improving robustness and reach of simplified converged fiber-wireless RoF communication links provided by advanced video coding.

Acknowledgments

This work has been partly funded by the European Commission under FP7 ICT-249142 FIVER project and by the by the Spanish Ministry of Science and Innovation under the TEC2009-14250 ULTRADEF project.

#155834 - $15.00 USD Received 3 Oct 2011; accepted 28 Nov 2011; published 8 Dec 2011

Paper 8: Half-cycle QAM modulation for VCSEL-based optical fiber links

T. T. Pham, R. Rodes, J. Bevensee Jensen, C. J. Chang-Hasnain, and I. Tafur Monroy "Half-cycle QAM modulation for VCSEL-based optical fiber links," in *Proc. The 38th European Conference and Exhibition on Optical Communications*, *ECOC 2012*, paper Mo.1.B.3, Amsterdam, The Netherlands, 2012.

Half-cycle QAM modulation for VCSEL-based optical links

Tien-Thang Pham[1], Roberto Rodes[1], Jesper Bevensee Jensen[1], Connie. J. Chang-Hasnain[2] and Idelfonso Tafur Monroy[1]

[(1)] DTU Fotonik, Department of Photonics Engineering, Technical University of Denmark, DK2800 Kgs. Lyngby, Denmark, ptit@fotonik.dtu.dk
[(2)] Dept. of Electrical Engineering and Computer Science, University of California, Berkeley, CA 94720, USA, cch@eecs.berkeley.edu

Abstract *Novel spectrally efficient half-cycle QAM modulation is experimentally demonstrated. 10 Gbps 4-QAM signal in 7.5-GHz bandwidth was successfully transmitted over 20 km SMF using an un-cooled 1.5 μm VCSEL with no equalization applied.*

Introduction

Vertical cavity surface emitting lasers (VCSELs) have several attractive properties such as large modulation bandwidth, low driving voltage, wavelength tunability, wafer-scale testing, easy packaging, and low carbon footprint [1-4]. These advantages make VCSELs attractive light sources for high-speed optical communication links in data centers and optical access networks. Optical links that use long-wavelength VCSELs and on-off keying (OOK) modulation are limited in transmission reach by chromatic dispersion of optical fibers due to frequency chirping caused by direct modulation of the VCSEL and large occupied bandwidth of signals [5-8]. For 10-Gbps data transmission using 1.5-μm VCSELs, 3-dB power penalty after 10-km single mode fiber (SMF) was experimentally observed [6] and 11-dB power penalty after 20-km SMF was simulated [7]. To deal with the effect of chromatic dispersion for OOK systems, dispersion management and dispersion mitigation methods have been proposed [5-8]. Advanced modulation formats also have been proposed to reduce the bandwidth of the signals. Multi-tone modulation (DMT), a sub-class of orthogonal frequency division multiplexing (OFDM), is a promising technology for both increasing spectral efficiency and dispersion tolerance. High speed data transmission of DMT signal using VCSELs has been demonstrated recently [9-10]. However, to support high-speed data transmission, DMT requires fast analogue to digital (ADC) and digital to analogue (DAC) converters. Additionally, DMT transceivers consume high power for signal processing compared to conventional OOK transceivers. A simpler method, single-cycle subcarrier QAM modulation was proposed in which the subcarrier frequency is equal to the baud rate. Transmission of 10 Gbaud 16-QAM data in 20-GHz bandwidth over 200-m MMF using 850-nm VCSELs has been reported [11].

In this paper, we demonstrate half-cycle QAM modulation for spectrally efficient VCSEL-based optical links. By using a subcarrier frequency at a half the baud rate, the spectrum of the QAM signal is reduced 25% compared to conventional and single-cycle QAM modulation. We report the transmission of real-time generated 10-Gpbs and 16-Gbps 4-QAM signals over 20-km and 3-km SMFs respectively using an un-cooled commercially available 10-GHz 1.5-μm VCSEL. Bit error rate (BER) below the limit of the forward error correction (FEC) with 7% payload overhead was achieved for both cases. Only 2.5 dB power penalty was observed for 10 Gbps 4-QAM signal after 20-km fiber transmission.

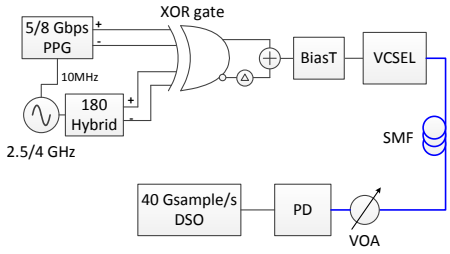

Fig. 1: Experimental setup: Pulse pattern generator (PPG), photodetector (PD), variable optical attenuator (VOA), single mode fiber (SMF), digital storage oscilloscope (DSO).

Experimental setup

Fig. 1 shows the experimental setup. There are two important parts in the setup: real time generation and transmission of a half-cycle 4-QAM signal.

a) Half-cycle 4-QAM signal generation

To generate the electrical half-cycle 4-QAM signal, we used the method proposed in [8]. However, in our case, the subcarrier frequency was equal to half the bit rate. 2.5/4-GHz subcarrier and synchronized 5/8-Gbps data with PRBS length of 2^{10}-1 were fed to a 13-GHz

bandwidth XOR gate (Inphi 13610XR) to create two BPSK signals in the two outputs of the XOR gate. One output of the XOR gate was delayed and then combined with the other one using a power combiner to form a 4-QAM signal. The delay time was optimized in order to secure that the two signals from the XOR outputs are uncorrelated and 90 degrees out of phase.

The half-cycle QAM signal has some special features. Firstly, the first null in the spectrum of the signal is at 1.5 times the symbol rate while the first null point of single cycle QAM modulation is at twice the symbol rate. This means that the spectral efficiency of half-cycle QAM modulation is improved by 25% compared to single cycle modulation. The spectra of the generated half-cycle and single-cycle 5-Gbaud 4-QAM signals are illustrated in Fig. 2. It is observed that the width of the first lobe of half-cycle modulation and single-cycle modulation is 7.5 and 10 GHz, respectively. Secondly, unlike the single-cycle QAM signal, most of the power of the half-cycle QAM signal is concentrated in the low frequency region. This makes the signal more tolerant towards high-frequency roll-off of VCSELs and photodiodes.

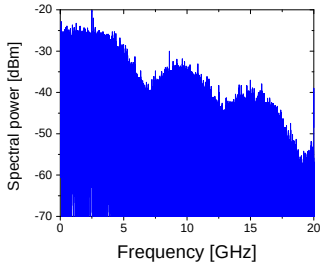

Fig.2: Spectrum of a) 5-Gbaud half-cycle 4-QAM signal and b) 5-Gbaud single-cycle 4-QAM signal

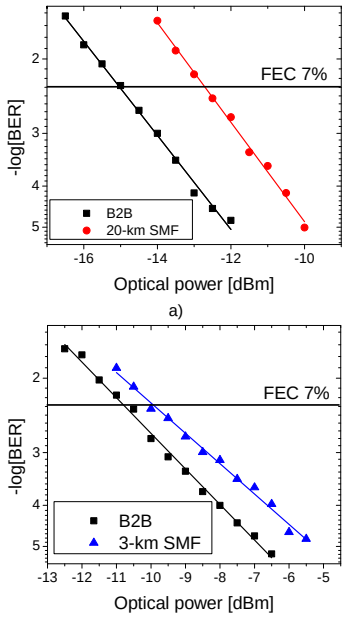

Fig.3: Performance of 4-QAM signals at B2B and after fiber transmission a) 5 Gbaud, b) 8 Gbaud

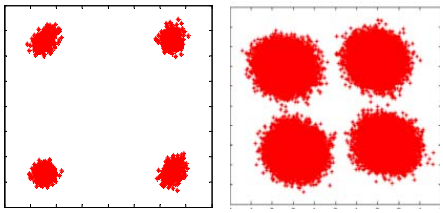

Fig.4- Constellation of 5-Gbaud signal, a) generated electrical signal and b) at -12.0 dBm B2B

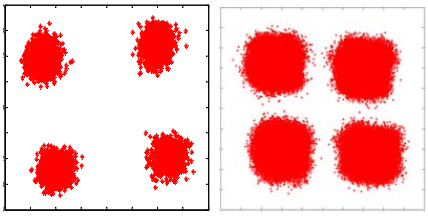

Fig. 5. Constellation of 8-Gbaud signal, a) generated electrical signal and b) at -6.5 dBm B2B

b) Half cycle QAM signal transmission

The generated 4-QAM signal was fed to an un-cooled 1.5-μm VCSEL using a BiasT. The threshold current of the VCSEL was 17 mA and

it is biased at 22.5 mA for the best performance. With 5-Gbaud data, the optical signal from the VCSEL was transmitted over 20-km standard SMF. The 8-Gbaud signal was transmitted through 3-km SMF. A variable optical attenuator (VOA) was utilized to vary the optical power level into the photodetector (PD). The 3-dB bandwidth of the VCSEL, evaluation board and PD was approximately 10 GHz. The photodetected signal was digitized using a 40-GSamples/s digital storage oscilloscope (DSO) for offline digital signal processing (DSP. The DSP algorithm was kept simple without any equalization technique. It includes clock recovery, I/Q detection, threshold detection and bit error rate (BER) calculation.

Experimental results

To assess the performance of the system, approximately 150k symbols (300k bits) were used to calculate the BER of the signals for both data rates. Fig. 3 shows the BER of the signals B2B and after fiber transmission. For the 5-Gbaud signal, there were no errors detected when the optical power was below -12 dBm and bellow -10 dBm for B2B and fiber transmission cases, respectively. Assuming that 7% payload is used for FEC header, the limit of pre-FEC BER aiming for after- FEC BER of 10^{-15} is $4.8x10^{-3}$ [12]. At the FEC limit, the receiver sensitivity B2B was approximately -15 dBm and the power penalty after 20-km SSMF transmission was only 2.5 dB.

For 8 Gbaud data B2B, as shown in Fig. 3.b, there were no errors detected at -6.0 dBm and the receiver sensitivity at the FEC limit was -11.0 dBm. Due to the increased bandwidth, the 8-Gbaud signal has higher transmission power penalty than the 5-Gbaud signal. After 3-km SMF, the power penalty was approximately 1.5 dB. In general, the receiver sensitivity was approximately 5 dB worse than the 5-Gbaud signal. This performance limitation are attributed the imperfection of the generated QAM signal before modulation and limited bandwidth of the transceivers. The generated 8 Gbaud signal had lower signal-to-noise ratio (SNR) than the 5-Gbaud signal and the bandwidth of the 8-Gbaud signal was 12 GHz. Examples of the constellations of both 5 Gbaud and 8Gbaud signals before modulating the VCSEL and at B2B are presented in Fig. 4 and Fig. 5.

Conclusions

We have investigated half-cycle subcarrier QAM modulation for VCSEL-based optical links with 25% better spectral efficiency than other QAM modulation. 10-Gbps data in 7.5-GHz bandwidth was transmitted through 20-km single mode fiber with BER below the FEC limit and only 2.5-dB power penalty. Half-cycle subcarrier QAM modulation has potential for applications in simple, spectrally efficient high-speed PON networks as well as high performance data centers.

Acknowledgements

The authors would also like to thank C. Neumeyr, E. Rnneberg and M. Ortsiefer from Vertilas GmbH for supplying high-quality VCSELs.

References

[1] W. Hofmann, Electronics Letters, 47, 270 (2011).
[2] P. Moser, et al., Proc. ECOC, (2011).
[3] W. Hofmann, et al., Proc. CLEO/QELS 2008, pp.1- 2, (2008).
[4] M. C. Y. Huang, IEEE J. Selected Topics in Quantum Electronics, 13, 374 (2007).
[5] B.Zhang, in Proc. OFC, OWT7 (2008).
[6] L. Xu, et al., Proc. CLEO-EQEC (2009).
[7] T. B. Gibbon, et al., Optical Fiber Tech., 17, 41, (2011).
[8] K. Prince, et al., IEEE/OSA JOCN, 3, 399, (2011).
[9] E. Hugues- Salas et al,. Optics Express, 19, 2979 (2011).
[10] S.C.J. Lee, et al,. Proc. OFC, PDP6, (2009).
[11] K. Szczerba et al., Proc. ECOC, We.7.B.2 (2011).
[12] J. Justesen, IEEE Trans. Commun. 59, 407 (2011).

Paper 9: Sub-cycle QAM modulation for VCSEL-based optical fiber links

T. T. Pham, R. Rodes, J. Bevensee Jensen, C. J. Chang-Hasnain, and I. Tafur Monroy "Sub-cycle QAM modulation for VCSEL-based optical fiber links," *OSA Optics Express*, accepted for publication, 2012.

Sub-cycle QAM modulation for VCSEL-based optical fiber links

Tien-Thang Pham,[1,*] Roberto Rodes,[1] Jesper Bevensee Jensen,[1] Connie J. Chang-Hasnain,[2] and Idelfonso Tafur Monroy[1]

[1]*DTU Fotonik, Department of Photonics Engineering, Technical University of Denmark, DK2800 Kgs. Lyngby, Denmark*

[2]*Dept. of Electrical Engineering and Computer Science, University of California, Berkeley, CA 94720, USA*

[*]*ptit@fotonik.dtu.dk*

Abstract: QAM modulation utilizing subcarrier frequency lower than the symbol rate is both theoretically and experimentally investigated. High spectral efficiency and concentration of power in low frequencies make sub-cycle QAM signals attractive for optical fiber links with direct modulated light sources. Real-time generated 10-Gbps 4-level QAM signal in a 7.5-GHz bandwidth utilizing subcarrier frequency at a half symbol rate was successfully transmitted over 20-km SMF using an un-cooled 1.5-μm VCSEL. Only 2.5-dB fiber transmission power penalty was observed with no equalization applied.

OCIS codes: (060.2330) Fiber optics communications; (060.4080) Modulation.

References and links

1. W. Hofmann, M. Müller, P. Wolf, A. Mutig, T. Gründl, G. Böhm, D. Bimberg, and M.-C. Amann, "40 Gbit/s modulation of 1550 nm VCSEL," Electron. Lett. **47**(4), 270–271 (2011).
2. P. Moser, W. Hofmann, P. Wolf, G. Fiol, J. A. Lott, N. N. Ledentsov, and D. Bimberg, "83 fJ/bit energy-to-data ratio of 850-nm VCSEL at 17 Gb/s," in *Proceedings of 37th European Conference on Optical Communication* (2011), pp. 1–3.
3. W. Hofmann, M. Görblich, G. Böhm, M. Ortsiefer, L. Xie, and M.-C. Amann, "Long-wavelength 2-D VCSEL arrays for optical interconnects," in *Proceedings of Lasers and Electro-Optics (CLEO) and Quantum Electronics and Laser Science Conference* (2008), pp.1- 2.
4. M. C. Y. Huang, K. B. Cheng, Y. Zhou, A. Pisano, and C. Chang-Hasnain, "Monolithic integrated piezoelectric MEMS-tunable VCSEL," IEEE IEEE J. Sel. Topics Quantum Electron. **13**(2), 374–380 (2007).
5. B. Zhang, X. Zhao, L. Christen, D. Parekh, W. Hofmann, M. C. Wu, M. C. Amann, C. J. Chang-Hasnain, and A. E. Willner, "Adjustable chirp injection-locked 1.55-μm VCSELs for enhanced chromatic dispersion compensation at 10-Gbit/s," in *Optical Fiber Communication Conference* (Optical Society of America, 2008) paper OWT7.
6. L. Xu, H. K. Tsang, W. Hofmann, and M.-C. Amann, "10-Gb/s colorless re-modulation of signal from 1550nm vertical cavity surface emitting laser array in WDM PON," in *Proceedings of Lasers and Electro-Optics (CLEO) and Quantum Electronics and Laser Science Conference* (2009), paper CI3_4.
7. T. B. Gibbon, K. Prince, T. T. Pham, A. Tatarczak, C. Neumeyr, E. Rönneberg, M. Ortsiefer, and I. T. Monroy, "VCSEL transmission at 10Gb/s for 20km single mode fiber WDM-PON without dispersion compensation or injection locking," Opt. Fiber Technol. **17**(1), 41–45 (2011).
8. K. Prince, M. Ma, T. B. Gibbon, C. Neumeyr, E. Rönneberg, M. Ortsiefer, and I. Tafur Monroy, "Free-running 1550 nm VCSEL for 10.7 Gb/s transmission in 99.7 km PON," IEEE/OSA JOCN. **3**, 399–403 (2011).
9. R. Rodes, J. Estaran, B. Li, M. Muller, J. B. Jensen, T. Gruendl, M. Ortsiefer, C. Neumeyr, J. Rosskopf, K. J. Larsen, M.-C. Amann, and I. T. Monroy, "100 Gb/s single VCSEL data transmission link," in *Optical Fiber Communication Conference* (Optical Society of America, 2012), paper PDP5D.
10. E. Hugues-Salas, R. P. Giddings, X. Q. Jin, J. L. Wei, X. Zheng, Y. Hong, C. Shu, and J. M. Tang, "Real-time experimental demonstration of low-cost VCSEL intensity-modulated 11.25 Gb/s optical OFDM signal transmission over 25 km PON systems," Opt. Express **19**(4), 2979–2988 (2011), http://www.opticsinfobase.org/oe/abstract.cfm?URI=oe-19-4-2979.
11. S. C. J. Lee, F. Breyer, S. Randel, J. Zeng, F. Huijskens, H. P. van den Boom, A. M. Koonen, and N. Hanik, "24-Gb/s transmission over 730 m of multimode fiber by direct modulation of an 850-nm VCSEL using discrete multi-tone modulation," in *Optical Fiber Communication Conference* (Optical Society of America, 2009), paper PDP5.

#176871 - $15.00 USD Received 2 Oct 2012; revised 11 Nov 2012; accepted 12 Nov 2012; published 17 Jan 2013

12. K. Szczerba, B.-E. Olsson, P. Westbergh, A. Rhodin, J. S. Gustavsson, A. Haglund, M. Karlsson, A. Larsson, and P. A. Andrekson, "37 Gbps transmission over 200 m of MMF using single cycle subcarrier modulation and a VCSEL with 20 GHz modulation bandwidth," in Proceedings of 36th European Conference on Optical Communication (2010), paper We.7.B.2.
13. J. Proakis and M. Salehi, *Digital Communications* (McGraw-Hill, 2007).
14. J. Justesen, "Performance of product codes and related structures with iterated decoding," IEEE Trans. Commun. **59**(2), 407–415 (2011).

1. Introduction

Vertical cavity surface emitting lasers (VCSELs) have several attractive properties such as large modulation bandwidth, low driving voltage, wavelength tunability, wafer-scale testing, easy packaging, and low carbon footprint [1–4]. These advantages make VCSELs attractive light sources for high-speed optical communication links in data centers and optical access networks using intensity modulation/ direct detection (IM/DD) technique. Optical links that use long-wavelength VCSELs and on-off keying (OOK) modulation are limited in transmission reach by chromatic dispersion of optical fibers due to frequency chirping caused by direct modulation of the VCSEL and large occupied bandwidth of signals [5–8]. For 10-Gbps data transmission using 1.5-μm VCSELs, a 3-dB power penalty after 10-km single mode fiber (SMF) transmission was experimentally observed [6] and a 11-dB power penalty after 20-km SMF was observed after numerical simulations [7]. To deal with the effect of chromatic dispersion for OOK systems, dispersion management and dispersion mitigation methods have been proposed [5–8]. Advanced modulation formats also have been proposed to reduce the bandwidth of the signals. High-speed pulse amplitude modulation (PAM) for VCSELs has been demonstrated [9]. Its scalability is limited because it is single dimension modulation. Multi-tone modulation (DMT), a sub-class of orthogonal frequency division multiplexing (OFDM), is a promising technology for both increasing spectral efficiency and dispersion tolerance. High speed data transmission of DMT signal using VCSELs has been demonstrated recently [10,11]. However, to support high-speed data transmission, DMT requires fast analogue to digital (ADC) and digital to analogue (DAC) converters. Additionally, DMT transceivers consume high power for signal processing compared to conventional OOK transceivers. A simpler method, single-cycle subcarrier quadrature amplitude modulation (QAM) was proposed in which the subcarrier frequency is equal to the symbol rate. Transmission of 10-Gbaud 16-QAM data in a 20-GHz bandwidth over 200-m MMF using 850-nm VCSELs has been reported [12].

In this paper, we analyze and demonstrate sub-cycle QAM modulation for spectrally efficient VCSEL-based optical links. We point out that the subcarrier frequency can be reduced to a quarter or a half of the symbol rate to improve spectral efficiency while the simplicity of the transceiver is maintained. For instance, by using a subcarrier frequency at half the symbol rate, the spectral width, defined as the frequency of the first null in the spectrum, of the QAM signal is reduced by 25% compared to conventional QAM modulation. We demonstrate the generation and detection of 10-Gpbs and 16-Gbps 4-QAM signals transmitted over 20-km and 3-km SMFs respectively using an un-cooled commercially available 10-GHz, 1.5-μm VCSEL. Bit error ratio (BER) below $4.8\text{x}10^{-3}$, the limit of forward error correction (FEC) with 7% payload overhead, was achieved for both cases. 2.5-dB power penalty was observed for 10-Gbps 4-QAM signal after 20-km fiber transmission.

2. Sub-cycle QAM modulation and demodulation

QAM is a two-dimensional signaling method which uses the in-phase and quadrature (cosine and sine waves, respectively). Two basis functions of QAM [13]:

$$\phi_1(t) = \sqrt{\frac{2}{\mathrm{E}_g}} g(t) \cos 2\pi f_c t \tag{1}$$

#176871 - $15.00 USD Received 2 Oct 2012; revised 11 Nov 2012; accepted 12 Nov 2012; published 17 Jan 2013

$$\phi_2(t) = -\sqrt{\frac{2}{\mathrm{E}_g}} g(t) \sin 2\pi f_c t \tag{2}$$

The corresponding signal waveform of M-QAM signals:

$$\begin{aligned} s_m(t) &= A_{mI}\sqrt{\frac{E_g}{2}}\phi_1(t) + A_{mQ}\sqrt{\frac{E_g}{2}}\phi_2(t), \qquad \text{m=1, 2,..., M} \\ &= A_{mI} g(t)\cos 2\pi f_c t - A_{mQ} g(t)\sin 2\pi f_c t \end{aligned} \tag{3}$$

where E_g is the energy of the signal with the lowest amplitude and $g(t)$ is a pulse shape. A_{mI} and A_{mQ} denote the set of M possible amplitudes for I and Q channels. The norms of two basis functions in a symbol duration [0, T]:

$$\begin{aligned} \langle \phi_1(t), \phi_1(t) \rangle &= \int_0^T \left(\sqrt{\frac{2}{\mathrm{E}_g}} g(t)\cos(2\pi f_c t + \varphi) \right)^2 \\ &= \int_0^T \frac{2}{\mathrm{E}_g} g^2(t)\cos^2(2\pi f_c t + \varphi) \end{aligned} \tag{4}$$

$$\begin{aligned} \langle \phi_2(t), \phi_2(t) \rangle &= \int_0^T \left(\sqrt{\frac{2}{\mathrm{E}_g}} g(t)\sin(2\pi f_c t + \varphi) \right)^2 \\ &= \int_0^T \frac{2}{\mathrm{E}_g} g^2(t)\sin^2(2\pi f_c t + \varphi) \end{aligned} \tag{5}$$

The inner product of two basis functions in a symbol duration [0, T]:

$$\begin{aligned} \langle \phi_1(t), \phi_2(t) \rangle &= \int_0^T \sqrt{\frac{2}{\mathrm{E}_g}} g(t)\cos(2\pi f_c t + \varphi) \sqrt{\frac{2}{\mathrm{E}_g}} g(t)\sin(2\pi f_c t + \varphi) \\ &= \int_0^T \frac{2}{\mathrm{E}_g} g^2(t)\sin 2(2\pi f_c t + \varphi) \end{aligned} \tag{6}$$

The two basis functions are orthogonal if integral of $\sin 4\pi f_c t$ is equal to zero in a symbol duration. We consider the cases subcarrier frequencies are lower than the symbol rate. There are two basic options to achieve that.

2.1. Subcarrier frequency is at half the symbol rate

If the carrier frequency is a half the symbol rate, $fc = \frac{1}{2T}$ (half-cycle modulation), the integral in Eq. (6) is taken in one cycle of $\sin(4\pi f_c t)$. It is equal to zero regardless the phase of basis functions. The two basis functions for half-cycle QAM modulation:

$$\phi_1(t) = \pm\sqrt{\frac{2}{\mathrm{E}_g}} g(t)\cos\left(2\pi\frac{1}{2T}t + \varphi\right) \qquad \text{t=[0, T]} \tag{7}$$

$$\phi_2(t) = \mp\sqrt{\frac{2}{\mathrm{E}_g}} g(t)\sin\left(2\pi\frac{1}{2T}t + \varphi\right) \qquad \text{t=[0, T]} \tag{8}$$

#176871 - $15.00 USD Received 2 Oct 2012; revised 11 Nov 2012; accepted 12 Nov 2012; published 17 Jan 2013

As in Eqs. (7) and (8), there are two available values for each basis function: positive and negative ones. When full cycle sine/cosine signals are used for data modulation. Those two values of each basis functions are alternately used for two consecutive bits. Nevertheless the two basis functions have unit norm regardless the sign. Therefore, they are an orthonomal set.

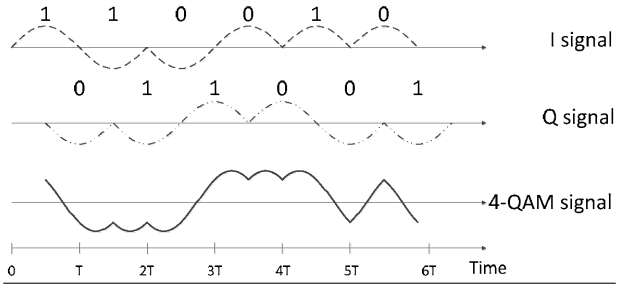

Fig. 1. Simulated waveforms of BPSK signals from I and Q channels and half-cycle 4-QAM signal. There is a half-period offset between the two signal components.

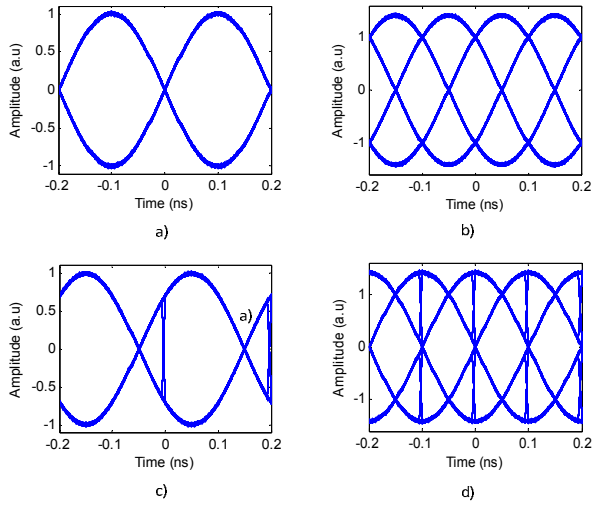

Fig. 2. Simulated eye diagram of 5-Gbaud BPSK signal from I channel and 4-QAM signal in two-baud duration (a,b): data bits start at ± kπ phase of subcarrier, (c,d): data bits start at a different phase.

#176871 - $15.00 USD Received 2 Oct 2012; revised 11 Nov 2012; accepted 12 Nov 2012; published 17 Jan 2013

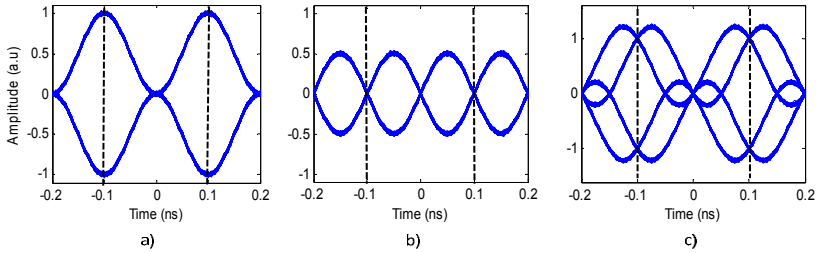

Fig. 3. Simulated eye diagrams of BPSK signal from a) I channel, b) Q channel and c) 4-QAM signal after multiplication with sine signal for detection. Dash lines indicate center of bits - the optimal sampling instant.

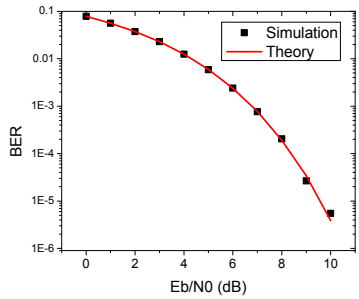

Fig. 4. Theoretical and simulated BER of half-cycle 4-QAM signal in AWGN channel.

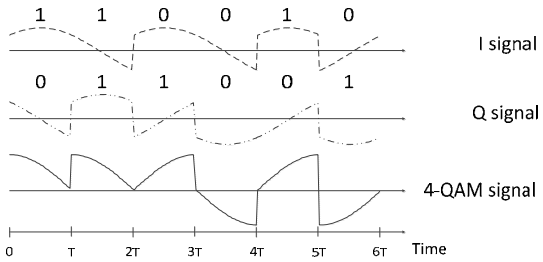

Fig. 5. Simulated waveforms of BPSK signals from I and Q channels and 4-QAM quarter-cycle signal.

#176871 - $15.00 USD Received 2 Oct 2012; revised 11 Nov 2012; accepted 12 Nov 2012; published 17 Jan 2013

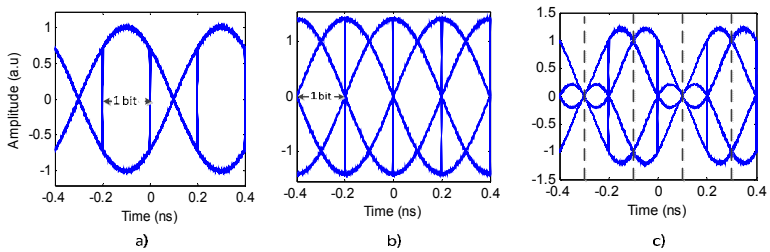

Fig. 6. Simulated eye diagram of 5-Gbaud quarter-cycle modulation signal in 4-baud duration. (a) BPSK signal, (b) 4-QAM signal, (c) 4-QAM signal after multiplication with sine signal. Dash lines indicate center of bits.

Examples of simulated waveforms of the BPSK signals from I and Q channels and half-cycle 4-QAM signal are depicted in Fig. 1. Simulated eye-diagrams of the BPSK signals and the 4-QAM signal are illustrated in Fig. 2. In Figs. 2(a) and 2(b), data bits start when the phase of subcarrier is $\pm k\pi$ (k = 0, 1, 2...) while in Figs. 2(c) and 2(d) data bits start at $\pm \pi/4 + k\pi$ of the subcarrier phase. Data in Q channel is half a bit delayed to make the half-cycle QAM signal consistent with the signal generated in the experiment which is presented in section 3.

The half-cycle QAM signal can be demodulated using a correlation receiver [13]. When multiplied with sine/cosine signals, two values of each basis function are again alternately used. It removes the effect of the sign of the basis functions on the demodulated data. Figure 3 shows the eye-diagrams for two symbols of the BPSK signals from I and Q channels and the 4-QAM signal after multiplication with a sine signal for detection. It shows clearly that the optimal sampling point for threshold gating is at the center of bits when the interference is zero. Therefore, the integration step can be eliminated. The theoretical BER for half-cycle QAM modulation is similar other subcarrier frequencies which is expressed in [13]. The theoretical and simulated BER of the half-cycle 4-QAM signal versus energy-per-bit-to-noise ratio (Eb/N0) in additive white Gaussian noise (AWGN) channel is presented in Fig. 4.

2.2. Subcarrier frequency is at a quarter of the symbol rate

In this case, the integral in Eq. (6) is taken in one half cycle of $\sin(4\pi f_c t)$ starting at $\pm\pi/2$ and ending at $\mp\pi/2$, precisely. It means that data bits must start at $\pm l\pi/2 + \pi/4$ (l = 1,2, ...). The two basis functions for quarter-cycle QAM modulation:

$$\phi_1(t) = \pm\sqrt{\frac{2}{\mathrm{E}_g}}g(t)\cos\left(2\pi\frac{1}{4T}t + \frac{k}{4}\pi\right) \quad \text{t=[0, T], k=1,3} \tag{9}$$

$$\phi_2(t) = \mp\sqrt{\frac{2}{\mathrm{E}_g}}g(t)\sin\left(2\pi\frac{1}{4T}t + \frac{k}{4}\pi\right) \quad \text{t=[0, T], k=1,3} \tag{10}$$

There are four possible values for each basis functions as expressed in Eqs. (9) and (10). However, these four values gives only two different norms. Different norms from different basis functions make the same symbols have different energy levels. Similarly to half-cycle modulation, when full cycle of sine/cosine signal is used for data modulation, all four values are alternately used. Example waveforms of BPSK signals from I and Q channels and quarter-cycle 4-QAM signal are depicted in Fig. 5. Eye-diagrams of the I channel output and the 4-QAM signal are illustrated in Figs. 6(a) and Fig. 6(b). Figure 6(c) represents the eye-diagram of 4-QAM signal after multiplication with the sine signal. As shown in the figure, the interference from the Q channel is zero at the center of the bits. However, the waveforms and

#176871 - $15.00 USD Received 2 Oct 2012; revised 11 Nov 2012; accepted 12 Nov 2012; published 17 Jan 2013

average levels of two consecutive bits are totally different. It means that quarter-cycle modulation not only requires strict phase condition alignment but also a more complicated method for detection.

3. Experimental setup

Due to the strict phase requirement for signal generation and complication of signal detection of quarter-cycle modulation, we chose only half-cycle modulation for the experiment. The experimental setup is illustrated in Fig. 4. There are two important parts in the setup: real time generation and transmission of a half-cycle 4-QAM signal.

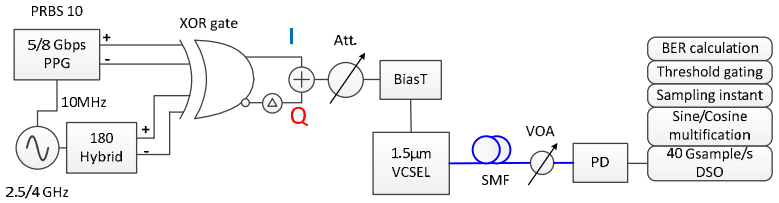

Fig. 7. Experimental setup: Pulse pattern generator (PPG), photodetector (PD), variable optical attenuator (VOA), single mode fiber (SMF), digital storage oscilloscope (DSO).

3.1. Half-cycle 4-QAM signal generation

To generate the electrical half-cycle 4-QAM signal, we used the method proposed in [12]. However, in our case, the subcarrier frequency was equal to half the symbol rate. 2.5/4-GHz subcarrier and synchronized 5/8-Gbps data with PRBS length of 2^{10}-1 were fed to a 13-GHz bandwidth XOR gate (Inphi 13610XR) to create two BPSK signals in the two outputs of the XOR gate. Due to the slow response of the XOR gate, the data bit stream was delayed approximately $\pi/4$ to force the XOR outputs always cross the zero level regardless the input bits. One output of the XOR gate was delayed and then combined with the other one using a power combiner to form a 4-QAM signal. The delay time was optimized in order to secure that the two signals from the XOR outputs are uncorrelated and 90 degrees out of phase. Utilizing a XOR gate to generate half-cycle QAM signals means transmitters of half-cycle QAM signals can be integrated using existing semiconductor process technologies. Compact, low-power transmitters can be produced.

The half-cycle QAM signal has some special features. Firstly, the first null in the spectrum of the signal is at 1.5 times the symbol rate while the first null point of single cycle QAM modulation is at twice the symbol rate. This means that the spectral efficiency of half-cycle QAM modulation is improved by 25% compared to single cycle modulation. The spectra of the generated half-cycle and single-cycle 5-Gbaud 4-QAM signals are illustrated in Fig. 5. It is observed that the width of the first lobe of the half-cycle modulation and the single-cycle modulation is 7.5 and 10 GHz, respectively. In comparison with a OOK signal at the same bit rate, the spectrum of the half-cycle signal has a similar shape to that of the OOK signal but the width of slopes is smaller. For instance, in the case of the 4-QAM signal, the first lobe is 25% less and higher order lobes are 50% less than that of the OOK signal. Secondly, unlike the single-cycle QAM signal, most of the power of the half-cycle QAM signal is concentrated in the low frequency region. This makes the signal more tolerant towards high-frequency roll-off of VCSELs and photodiodes.

3.2. Half-cycle QAM signal transmission

The generated 4-QAM signal was fed to an un-cooled 1.5-μm VCSEL using a BiasT. The threshold current of the VCSEL was 17 mA and it was biased at 22.5 mA for the best performance. With 5-Gbaud data, the optical signal from the VCSEL was transmitted over

#176871 - $15.00 USD Received 2 Oct 2012; revised 11 Nov 2012; accepted 12 Nov 2012; published 17 Jan 2013

20-km standard SMF. The 8-Gbaud signal was transmitted through 3-km SMF. A variable optical attenuator (VOA) was utilized to vary the optical power level into the photodetector (PD). The 3-dB bandwidth of the VCSEL, the evaluation board and the PD was approximately 10 GHz. The photodetected signal was digitized using a 40-GSamples/s digital storage oscilloscope (DSO) for offline digital signal processing (DSP). The DSP algorithm was kept simple without any equalization technique. It includes I/Q detection, optimal sampling, threshold gating and bit error rate (BER) calculation. It indicates that receivers for half-cycle QAM signals can be developed by using the current technologies for receivers of OOK and PAM signals without employing a high-speed ADC.

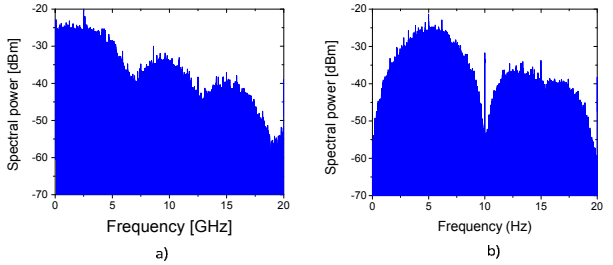

Fig. 8. Spectrum of (a) 5-Gbaud half-cycle 4-QAM signal and (b) 5-Gbaud single-cycle 4-QAM signal.

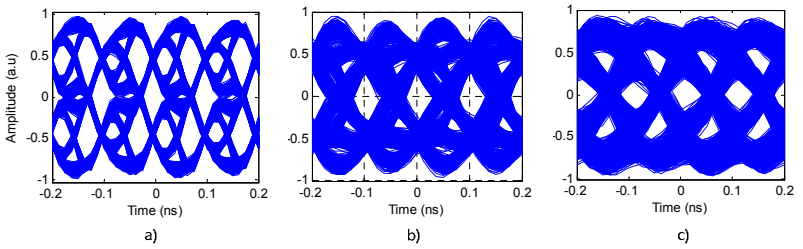

Fig. 9. Eye-diagram of electrical 10-Gbps 4-QAM signal: (a) after XOR gate and after photodetection (b) at B2B and (c) after 20-km SSMF transmission.

4. Experimental results

4.1. Performance of half-cycle QAM signals

The eye-diagrams of the 10-Gbps 4-QAM signals driving the VCSEL, detected signals at B2B and after fiber transmission is illustrated in Fig. 6. To assess the performance of the system, approximately 150k symbols (300k bits) were used to calculate the BER of the signals at both data rates. This number of symbols is limited by BER measurement using offline processing. The lowest detectable BER when there is error is approximately 3.3 10^{-6}. Figure 3 shows the BER of the signals B2B and after fiber transmission. For the 5-Gbaud signal, the optical power to achieve BER of 10^{-5} was about −12 dBm and −10 dBm for B2B and fiber transmission cases, respectively. Assuming that product code with shortened BCH (1023,992) (Bose-Chaudhuri-Hocqenghem) component codes is used and 7% payload is utilized for FEC header, the limit of pre-FEC BER aiming for after- FEC BER of 10^{-15} is 4.8×10^{-3} [14]. At this FEC limit, the receiver sensitivity B2B was approximately −15 dBm and the power penalty after 20-km SSMF transmission was only 2.5 dB.

#176871 - $15.00 USD Received 2 Oct 2012; revised 11 Nov 2012; accepted 12 Nov 2012; published 17 Jan 2013

For the 8-Gbaud signal B2B, as shown in Fig. 3(b), the receiver sensitivity at BER of 10^{-5} was about −6.7 dBm and at the FEC limit was −11.0 dBm. Due to the increased signal bandwidth and the strong effect of jitter after fiber transmission, the 8-Gbaud signal has higher transmission power penalty than the 5-Gbaud signal. After 3-km SMF, the power penalty was approximately 1.5 dB. In general, the receiver sensitivity was approximately 5 dB worse than for the 5-Gbaud signal. This performance limitation are attributed the imperfection of the generated QAM signal before modulation and limited bandwidth of the transceivers. The generated 8-Gbaud signal had lower signal-to-noise ratio (SNR) than the 5-Gbaud signal and the bandwidth of the 8-Gbaud signal was 12 GHz. Examples of the constellations of both 5-Gbaud and 8-Gbaud signals before modulating the VCSEL and at B2B are presented in Fig. 8 and Fig. 9.

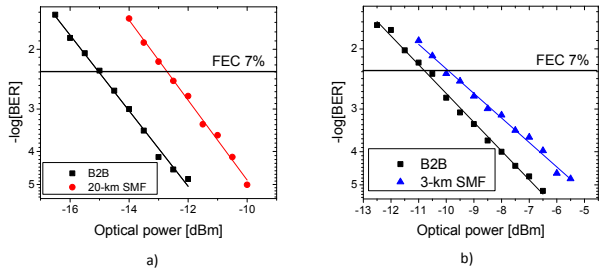

Fig. 10. Performance of 4-QAM signals at B2B and after fiber transmission: (a) 5 Gbaud (10Gbps) and (b) 8 Gbaud (16 Gbps).

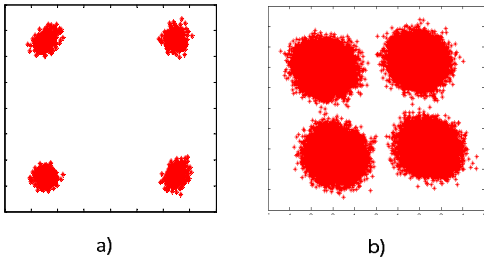

Fig. 11. Constellation of 5-Gbaud 4-QAM signal: (a) generated electrical signal and (b) at −12.0 dBm B2B.

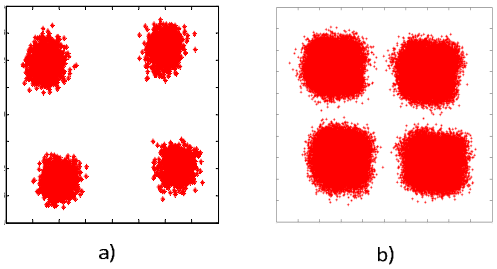

Fig. 12. Constellation of 8-Gbaud 4-QAM signal: (a) generated electrical signal and (b) at −6.5 dBm B2B.

#176871 - $15.00 USD Received 2 Oct 2012; revised 11 Nov 2012; accepted 12 Nov 2012; published 17 Jan 2013

4.2. Comparison with OOK signal

In this section, we compare the performance of our proposed half-cycle QAM signal with the conventional OOK signals. Two data rates of 5 Gbps and 10 Gbps with direct current (DC) removed were chosen for the comparison with 5-Gbaud 4-QAM signal. The 5-Gbps OOK signal has the same baudrate while the 10-Gbps signal has the same data rate to the half-cycle QAM signal. The peak-to-peak voltage (V_{p-p}) of OOK signal driving the VCSEL was chosen to be equal to the V_{p-p} of the half-cycle QAM signals at the optimal sampling points as shown in Fig. 2(a). No other conditions of the experiment were changed. The performance of OOK signals at B2B and after 20-km fiber transmission is illustrated in Fig. 4.

At the FEC limit, the sensitivity of the QAM signal was approximately 2 dB and 1.5 dB lower than that of 5-Gbps and 10-Gbps OOK signal because the QAM signal has lower signal-to-noise ratio (SNR). The power penalty after 20-km fiber transmission of 5-Gbps OOK signal was only 1 dB but power penalty of 10-Gbps signal was about 3-dB at FEC limit and increased up to 5-dB at BER of 10^{-5}. It means that the half-cycle QAM signal has improved the dispersion tolerance by only 0.5 dB at FEC limit but it increases dramatically at lower BER. At BER of 10^{-5}, 2.5-dB improvement has been observed.

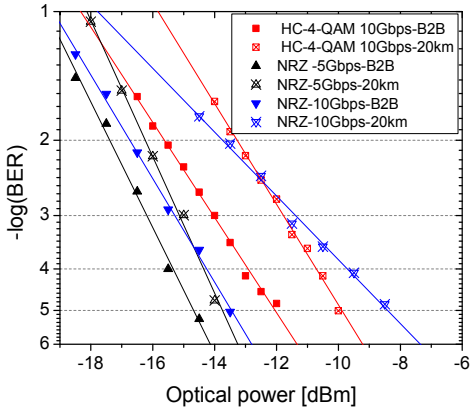

Fig. 13. Performance of 5-Gpbs and 10-Gbps NRZ signals at B2B and after fiber transmission in comparison with 10-Gbps half-cycle 4-QAM signal.

6. Conclusions

We have investigated QAM modulation utilizing sub-cycle subcarrier for VCSEL-based optical links to improve spectral efficiency. The transmission of 10-Gbps 4-QAM data in 7.5-GHz electrical bandwidth over 20-km single mode fiber was demonstrated with BER below the FEC limit and only 2.5-dB power penalty. Half-cycle signals have superior dispersion tolerance compared to OOK signals at the same data rate. Spectral efficiency can be improved by increasing the levels of the QAM signal. Both the transmitter and the receiver can be implemented using available electronics. Half-cycle subcarrier QAM modulation has potential for applications in high-speed PON networks as well as high-performance data centers.

#176871 - $15.00 USD Received 2 Oct 2012; revised 11 Nov 2012; accepted 12 Nov 2012; published 17 Jan 2013

Paper 10: Half-cycle modulation for VCSEL based 6-Gbaud 4-QAM transmission over 1 km multimode fibre link

T. T. Pham, R. Rodes, J. Estaran, J. Bevensee Jensen and I. Tafur Monroy "Half-cycle modulation for VCSEL based 6-Gbaud 4-QAM transmission over 1 km multimode fibre link," *IET Electronics Letters*, vol. 48, no. 17, pp. 1074–1076, 2012.

Half-cycle modulation for VCSEL based 6-Gbaud 4-QAM transmission over 1 km multimode fibre link

T.T. Pham, R. Rodes, J. Estaran, J. Bevensee Jensen and I. Tafur Monroy

A subcarrier multiplexing system with the subcarrier frequency at half the baud rate to improve the spectral efficiency is demonstrated. A 12 Gbit/s 4-QAM signal in 9GHz bandwidth was successfully transmitted over a 1 km OM4 MMF 850 nm VCSEL without any equalisation method. The 1.5 dB power penalty was improved compared to an OOK signal at the same data rate.

Introduction: The combination of short-wavelength vertical cavity surface-emitting lasers (VCSELs) and multimode fibre (MMF) is the most attractive solution for data communication in data centres, high performance computing (HPC) and enterprise local access networks (LANs). During recent years, there has been an ongoing burgeoning demand for high-speed interconnects in those networks. To meet that demand, it is expected that optical links need to be updated to higher data rates. For instance, 100 Gbit/s and beyond will be used for data centres in the near future [1]. High speed VCSELs operating at up to 40 Gbit/s on-off keying (OOK) have been developed recently [2, 3]. However, optical links using OOK modulation at such high speed suffer seriously from modal dispersion and chromatic dispersion that significantly reduces the transmission distance. It is desirable to maintain the transmission distance when the data rate increases. Implementation of equalisation is a possible solution to improve transmission reach [4]. Spectrally efficient modulation formats including pulse amplitude modulation (PAM) and subcarrier modulation have been proposed as attractive alternatives [5–7]. PAM is the simple format but it has only one degree of freedom. On the other hand, subcarrier modulation provides two dimensions where the phase as well as the amplitude of a subcarrier can be modulated. The concept of using half-cycle and single-cycle subcarrier frequency for modulation was introduced in the electronic domain in [8]. Transmission of a 10-Gbaud 16-QAM single-cycle signal in a 20 GHz bandwidth over 200 m MMF using 850 nm VCSELs has been reported [5]. Multi-tone modulation (DMT), using multiple orthogonal subcarriers also has been proposed and demonstrated recently [7]. While promising as a high spectral efficiency technique, DMT requires fast analogue-to-digital (ADC) and digital-to-analogue (DAC) converters to support high-speed transmission and linear transmitter circuitry to overcome peak-to-average-power ratio (PAPR) problems.

In this Letter, we present what we believe to be the first optical implementation and demonstration of half-cycle modulation employing a directly modulated VCSEL suitable for optical interconnects. By using a subcarrier frequency at half the baud rate, the spectrum of the QAM signal is reduced by 25% compared to conventional QAM modulation. Transmission of a 6-Gbaud 4-QAM signal over 1 km MMF using 9 GHz bandwidth was successfully achieved with a bit error rate (BER) below the limit of the forward error correction (FEC). The performance comparison with an OOK signal at the same data rate shows that the half-cycle QAM signal improves 1.5 dB power penalty after 1 km MMF transmission.

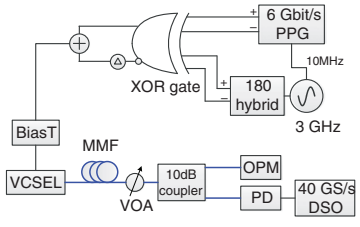

Fig. 1 *Experimental setup*

Pulse pattern generator (PPG), photodetector (PD), variable optical attenuator (VOA), multimode fibre (MMF), optical power meter (OPM), digital storage oscilloscope (DSO)

Experimental setup and results: The experimental setup of the system is presented in Fig. 1. To implement real-time generation of an electrical half-cycle 4-QAM signal we used the method proposed in [6]. However, in our case the subcarrier frequency is equal to half of the bit rate. A 6 Gbit/s $2^{10} - 1$ bit long pseudorandom binary sequence (PRBS) and a synchronised 3 GHz sinusoidal subcarrier were fed to a 13 GHz bandwidth XOR gate (Inphi 13610XR) to create two BPSK signals with opposite sign in the two outputs of the XOR gate. One output of the XOR gate was controlled by an electrical delay line to secure that it is uncorrelated and 90° out of phase with the other. Two BPSK signals were then combined together using a power combiner to form a 4-QAM signal. The eye-diagram of the 6 Gbaud 4-QAM signal is illustrated in Fig. 2*a*. The arrows point to the optimal sampling points for I and Q channels where the interference from Q and I channels is eliminated.

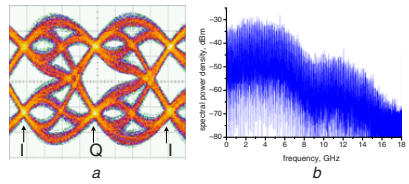

Fig. 2 *Eye-diagram of generated 4-QAM signal, 95 mV/div and 20 ps/div, and spectrum of generated 4-QAM signal*

a Eye-diagram
b Spectrum

The spectrum of the generated half-cycle 6-Gbaud 4-QAM signals are illustrated in Fig. 2*b*. Generally, in single-subcarrier multiplexing systems when the RF signal is generated by upconversion of a baseband signal to the RF frequency band, the bandwidth of the RF signal is twice the bandwidth of the baseband signal. For example, in [5], with single-cycle modulation where the frequency of the subcarrier is equal to the baud rate of 10 Gbaud, the width of the first lobe of the RF signal is 20 GHz. However, in the case of half-cycle QAM modulation, as presented in Fig. 2*a* the width of the first lobe in the spectrum of the signal is 9.0 GHz, 1.5 times the symbol rate. This means that the spectral efficiency of half-cycle QAM modulation is improved by 25% compared to single cycle modulation. Additionally, most of the power of the half-cycle QAM signal is concentrated in the low frequency region. This makes the signal more tolerant towards high-frequency roll-off of VCSELs and photodiodes.

The generated 4-QAM signal was fed to a commercially available 10 GHz 850 nm VCSEL using a BiasT. The threshold current of the VCSEL was about 1.0 mA and it was biased at 6.5 mA for best performance. The root-mean-square (RMS) spectral width of the VCSEL was 0.4 nm. The 6-Gbaud signal was transmitted through a OM4 MMF with effective modal bandwidth (EMB) of 4700 MHz-km. A variable optical attenuator (VOA) was utilised to vary the optical power level into a 10 GHz photodetector (PD). The photodetected signal was digitised using a 40-GSamples/s digital storage oscilloscope (DSO) for offline digital signal processing (DSP). The DSP algorithm was kept simple without implementation of any equalisation techniques. It includes I/Q detection, threshold gating and bit error rate (BER) calculation.

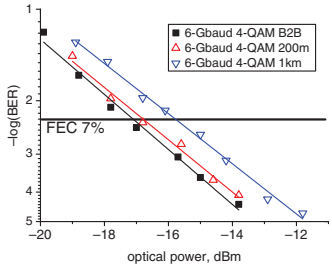

Fig. 3 *Performance of 6-Gbaud 4-QAM signals at B2B and after fibre transmission*

Approximately 50k symbols (100k bits) were used to calculate the BER of the signals for all cases of transmission. Fig. 3 presents the

performance of the half-cycle 6-Gbaud 4-QAM signals. Assuming that a 7% payload is used for the FEC header yielding 11.16 Gbit/s effective throughput of the link, the limit of pre-FEC BER aiming for an after-FEC BER of 10^{-15} is 4.8×10^{-3} [9]. The sensitivity at the FEC limit was approximately −17 dBm. After 200 m fibre transmission, a negligible power penalty was observed. 1 km fibre transmission, however, induced a 1.5 dB power penalty.

Comparison with OOK signal: In this Section, we compare the performance of our proposed half-cycle QAM signal with the conventional OOK signals. Two data rates of 9 and 12 Gbit/s were chosen for the comparison with the 6-Gbaud 4-QAM signal. The 9 Gbit/s OOK signal has the same bandwidth while the 12 Gbit/s signal has the same data rate as the half-cycle QAM signal. The peak-to-peak voltage $V_{p\text{-}p}$ of the OOK signal driving the VCSEL was chosen to be equal to the $V_{p\text{-}p}$ of the half-cycle QAM signals at the optimal sampling points as shown in Fig. 2*a*. No other conditions of the experiment were changed. The performance of OOK signals at B2B and after 1 km fibre transmission is illustrated in Fig. 4. At the FEC limit, the sensitivity of the QAM signal is lower than that of the 9 Gbit/s OOK signal because the QAM signal has lower signal-to-noise ratio (SNR). However, at the same data rate, the 12 Gbit/s OOK signal and the QAM signal have a similar sensitivity. It is because the performance of the 12 Gbit/s OOK signal is influenced by the bandwidth limitation of the transceiver. Similar to the half-cycle QAM signal, the power penalties of the 9 Gbit/s data for 1 km fibre transmission was approximately 1.5 dB. However, power penalty for the 12 Gbit/s OOK signal was about 3 dB. It indicates that the half-cycle QAM signal has improved the dispersion tolerance by 1.5 dB.

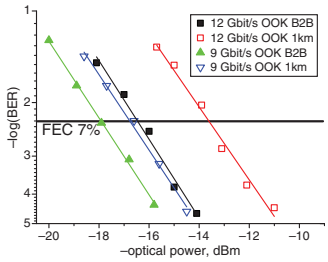

Fig. 4 *Performance of 6 and 9 Gbits OOK signals at B2B and after fibre transmission*

Conclusion: We have demonstrated a spectrally efficient subcarrier multiplexing system suitable for VCSEL based high-speed interconnects by using a subcarrier frequency at half the baud rate. Transmission of 10 Gbit/s 4-QAM data in 9 GHz bandwidth after 1 km MMF with BER below the FEC limit was successfully achieved. The spectral efficiency can be improved further by increasing the level of the QAM signal.

26 June 2012
doi: 10.1049/el.2012.2256
One or more of the Figures in this Letter are available in colour online.

T.T. Pham, R. Rodes, J. Estaran, J. Bevensee Jensen and I. Tafur Monroy (*DTU Fotonik, Department of Photonics Engineering, Technical University of Denmark, Kgs.Lyngby, Denmark*)

E-mail: ptit@fotonik.dtu.dk

References

1 InfiniBand Trade Association. www.infinibandta.org/
2 Blokhin, S.A., Lott, J.A., Mutig, A., Fiol, G., Ledentsov, N.N., Maximov, M.V., Nadtochiy, A.M., Shchukin, V.A., and Bimberg, D.: 'Oxide-confined 850 nm VCSELs operating at bitrates up to 40 Gbit/s', *Electron. Lett.*, 2009, **45**, pp. 501–503
3 Westbergh, P., Gustavsson, J.S., Kogel, B., Haglund, A., Larsson, A., Mutig, A., Nadtochiy, A., Bimberg, D., and Joel, A.: '40 Gbit/s error-free operation of oxide-confined 850 nm VCSEL', *Electron. Lett.*, 2010, **46**, pp. 1014–1016
4 Ingham, J.D., Penty, R.V., and White, I.H.: '10 Gb/s transmitter-based equalization for extended-reach multimode-fiber datacommunication links'. Proc. OFC, Anaheim, CA, USA, 2007, Paper OTuL4
5 Szczerba, K., Olsson, B.-E., Westbergh, P., Rhodin, A., Gustavsson, J.S., Haglund, A., Karlsson, M., Larsson, A., and Andrekson, P.A.: '37 Gbps tansmission over 200 m of MMF using single cycle subcarrier modulation and a VCSEL with 20 GHz modulation bandwidth'. Proc. ECOC, Torino, Italy, 2010, Paper We.7.B.2
6 Szczerba, K., Westbergh, P., Karout, J., Gustavsson, J., Haglund, A., Karlsson, M., Andrekson, P., Agrell, E., and Larsson, A.: '30 Gbps 4-PAM transmission over 200 m of MMF using an 850 nm VCSEL', *Opt. Express*, 2011, **19**, pp. B203–B208
7 Lee, S.C.J., Breyer, F., Randel, S., Cardenas, D., van den Boom, H.P.A., and Koonen, A.M.J.: 'Discrete multi-tone modulation for high-speed data transmission over multimode fibers using 850-nmVCSEL'. Proc. OFC, San Diego, CA, USA, 2009, Paper OWM2
8 Yeo, H., Chen, J., Bashirullah, R., Eisenstadt, W.R., and Lin, J.: 'Design of multigigabit-per-second transceiver for band-limited high-speed data communication using DC-free signaling', *IEEE Trans. Microw. Theory Tech.*, 2008, 56, pp. 1555–1564
9 Justesen, J.: 'Performance of product codes and related structures with iterated decoding', *IEEE Trans. Commun.*, 2011, **59**, pp. 407–415

Paper 11: Quad 14 Gbps L-band VCSEL-based System for WDM migration of 4-lanes 56 Gbps optical data links

J. Estaran, R. Rodes, **T. T. Pham**, M. Ortsiefer, C. Neumeyr,J. Rosskopf and I. Tafur Monroy "Quad 14 Gbps L-band VCSEL-based system for WDM migration of 4-lanes 56 Gbps optical data links," *OSA Optics Express*, accepted for publication, 2012.

Quad 14 Gbps L-band VCSEL-based system for WDM migration of 4-lanes 56 Gbps optical data links

Jose Estaran,[1,*] Roberto Rodes,[1] Tien Thang Pham,[1] Markus Ortsiefer,[2] Christian Neumeyr,[2] Jürgen Rosskopf,[2] and Idelfonso Tafur Monroy[1]

[1]*DTU Fotonik, Department of Photonics Engineering, Technical University of Denmark, DK2800 Kgs. Lyngby, Denmark*

[2]*VERTILAS GmbH, Lichtenbergstr. 8, D-85748 Garching, Germany*

[*]*jome@fotonik.dtu.dk*

Abstract: We report on migrating multiple-lane link into an L-band VCSEL-based WDM system. Experimental validation achieves successful transmission over 10 km of SMF at 4x14Gbps. Inter-channel crosstalk penalty is observed to be less than 0.5 dB and a transmission penalty around 1 dB. The power budget margin ranges within 6 dB and 7 dB.

OCIS codes: (060.0060) Fiber optics and optical communications; (200.4650) Optical interconnects.

References and links

1. H. Liu, C. F. Lam, and C. Johnson, "Scaling optical interconnects in datacenter networks opportunities and challenges for WDM," in *Proceedings of the 18th Annual Symposium on High Performance Interconnects*, 2010, 113 – 116.
2. A. Vahdat, H. Liu, X. Zhao, and C. Johnson, "The emerging optical data center" in *Proceedings of OFC/NOEFC '11*, Los Angeles Convention Center, Los Angeles, CA, 2011, OTuH2.
3. C. Kachris and I. Tomkos, "Power consumption evaluation of hybrid WDM PON networks for data centers," in *Proceedings of the 16th European Conference on Networks and Optical Communication (NOC)*, 2011, 118 – 121.
4. DatacenterDynamics (DCD) white paper, "The 2011 census," (DCD Industry CENSUS, 2011).
5. InfiniBand Trade Association, 2012. *http://www.infinibandta.org/index.php*.
6. Fiber Channel Industry Association, 2012.*http://www.fibrechannel.org/roadmaps*.
7. H. S. Hamza and J. S. Deogun, "WDM optical interconnects: a balanced design approach," IEEE/ACM Trans. Netw. **15**(6), 1565–1578 (2007).
8. J. Cheng, "Topics in VCSEL-based high-speed WDM optical interconnects," in *IEEE Avionics, Fiber-Optics and Photonics Technology Conference*, 2008, 65–66.
9. M. Haurylau, G. Chen, H. Chen, J. Zhang, N. A. Nelson, D. H. Albonesi, E. G. Friedman, and P. M. Fauchet, "On-chip optical interconnect roadmap: challenges and critical directions," IEEE J. Sel. Top. Quantum Electron. **12**(6), 1699–1705 (2006).
10. R. Rodes, J. Estaran, B. Li, M. Mueller, J. B. Jensen, T. Gründl, M. Ortsiefer, C. Neumeyr, J. Rosskopf, K. J. Larsen, M. Amann, and I. Tafur Monroy, "100 Gb/s single VCSEL data transmission link," in *OFC/NOEFC'12*, OSA Technical Digest (Optical Society of America, 2012), paper PDP5D.10.
11. L. Chrostowski, C.-H. Chang, R. Stone, and C. J. Chang-Hasnain, "Demonstration of long-wavelength directly modulated VCSEL transmission using SOAs," IEEE Photon. Technol. Lett. **14**(9), 1369–1371 (2002).
12. R. J. Stone, R. F. Nabiev, J. Boucart, W. Yuen, P. Kner, G. S. Li, R. Carico, L. Scheffel, M. Jansen, D. P. Worland, and C. J. Chang-Hasnain, "50 km error-free 10 Gbit/s WDM transmission using directly modulated long-wavelength VCSELs," Electron. Lett. **36**(21), 1793–1794 (2000).
13. FP7 European project GigaWam, "Next-generation WDM-PON enabling gigabit per-user data bandwidth". *http://www.gigawam.org/*.
14. J. C. Charlier and S. Krüger, "Long-wavelength VCSELs ready to benefit 40/100-GbE modules," Lightwave®, 2012.*http://www.lightwaveonline.com/articles/print/volume-28/issue-6/technology/long-wavelength-vcsel-technology-improves.html*.
15. A. Ran, IEEE P802.3bj 100 Gb/s Backplane and Copper Cable TaskForce 14 January 2012.
16. F. Chang, K. Onohara, and T. Mizuochi, "Forward error correction for 100 G transport networks," IEEE Commun. Mag. **48**(3), S48–S55 (2010).

#177306 - $15.00 USD Received 1 Oct 2012; revised 17 Nov 2012; accepted 19 Nov 2012; published 10 Dec 2012

1. Introduction

Over the past few years, the quick proliferation of Internet use and cloud computing applications has substantially increased the bandwidth needs not only in backbones but prominently in data processing centers (DPCs) [1]. Albeit great part of the traffic will continue to flow between end-users and such computer centers, an increasing fraction is flowing within the DPCs themselves [2, 3]. This situation has triggered a worldwide investment to upgrade the existing facilities or building new ones in order to cope with the growing bandwidth demand that has been estimated to reach $35BN in 2012 [4]. Accordingly, the major networking technologies for the interconnection of peripherals and data storage keep on releasing roadmaps and future milestones that clearly exceed the 10Gbps barrier, and therefore recently solutions such as fourteen data rate (FDR) of InfiniBand technology [5] or 16GFC of Fiber Channel [6] have been proposed. However, the need to scale to higher and bidirectional transmission capacities (bandwidth milestones reaching 300Gbps by 2013) [5] is also accompanied by the demand to secure high density, low cost, efficiency and reliability.

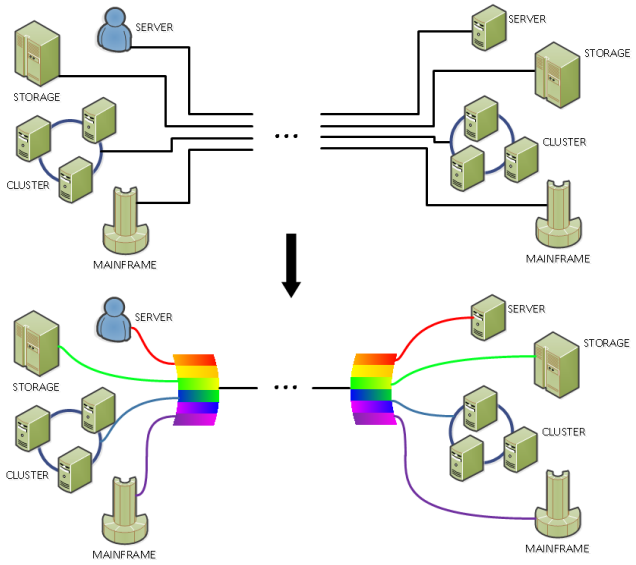

Fig. 1. Datacenter & Storage network topology migration. Multilane/multilink physical point-to-point (P2P) connections (top). L-band VCSEL-based WDM system (bottom).

In this context, wavelength division multiplexing (WDM) techniques in combination with compact integration of light sources and detectors, is an interesting technology candidate for delivering scalable and flexible optical data links with low power consumption, high data throughput, longer transmission distance, and the cost effectiveness needed to efficiently cope with present and future stringent bandwidth requirements in data centers [1, 7–9] See Fig. 1.

In concordance, regarding light sources, VCSELs offer an attractive combination of high bit rates, low power consumption and array integration that along with their tuning capabilities make them perfectly suitable for compact and wideband optical interconnects [8,10].

Long-wavelength technology is relatively new in vertical-cavity surface-emitting lasers (VCSELs). Some investigations [11, 12] have demonstrated the feasibility of long-reach

#177306 - $15.00 USD Received 1 Oct 2012; revised 17 Nov 2012; accepted 19 Nov 2012; published 10 Dec 2012

WDM transmissions at 2.5 Gbps, where L-band is especially suitable due to the lower impact of four-wave mixing (FWM) and the possibility of seizing upon distributed Raman amplification. Some other ongoing investigations are using L-band VCSELs as downstream (OLT to ONU) in a WDM-PON system as the new future proof FTTH technology [13].

In this paper we look into high-speed, cost-efficient and power-efficient VCSEL-based WDM system oriented towards short-range optical fiber connectivity. Four L-band VCSELs are directly modulated with quaternary pulse amplitude modulation (4-PAM) signal at 7 Gbauds to generate a total data nominal rate of 56 Gbps. The multilevel signal has been chosen because of its spectral efficiency,. The 4 lanes are launched into a 50 GHz spaced WDM system. Bit-error rate (BER), crosstalk penalty, transmission penalty and power margin are measured for one of the middle carriers.

The paper is organized as follows. In section 2, a description of the VCSEL used for signal modulation is presented. In section 3, the experimental setup is shown and described. In section 4, details about the digital signal processing (DSP) are provided. Finally, in section 5 the main results and findings are presented.

2. Long-wavelength VCSELs

Historically, VCSELs for longer wavelengths of 1300 to 1700 nm have been difficult to produce because of the refractive index of InGaAsP. But in the early 2000s, development of different combinations of III-V elements led to more practical long-wavelength VCSELs [14]. In general, VCSELs are rapidly becoming the preferable light source for interconnect applications owed to an interesting combination of high modulation bandwidth, low power consumption and reduced manufacturing cost [10]. Besides, their 2-D array integrability, their tuning capabilities and the light coupling ease due to its circular beam, make them perfectly suitable for WDM systems. The following section provides the reader with relevant data about the main characteristics of the device focusing on tunability and temperature considerations.

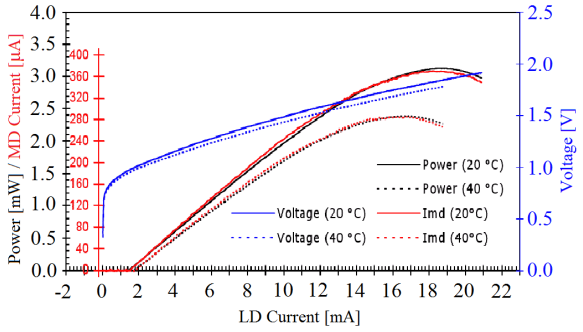

Fig. 2. L-I-V curve of VCSEL#3 and monitor diode (MD) current.

The L-band VCSELs used for the experiments performed in this paper range between 1577 nm and 1583 nm. Such devices exhibit the following measured characteristics: maximum output power around 3 mW and a 3-dB modulation bandwidth of 10 GHz at 20°C. The lasers show fast rise and fall times, low threshold voltage (1.5 mA – 2 mA) with a maximum operating rating around 19 mA, excellent side mode suppression ratio (SMSR) performance and extremely low power dissipation. Figure 2 depicts the L-I-V curve of the VCSEL#3. For its part, VCSELs' tunability depends mainly on bias current and temperature. Table 1 presents concrete measured values about the lasers' tuning ranges at 20°C and 40°C. Figure 3 shows the graphical trend of the emitted wavelength variation with respect to the bias current and temperature for VCSEL#2 (1580.66 nm).

#177306 - $15.00 USD Received 1 Oct 2012; revised 17 Nov 2012; accepted 19 Nov 2012; published 10 Dec 2012

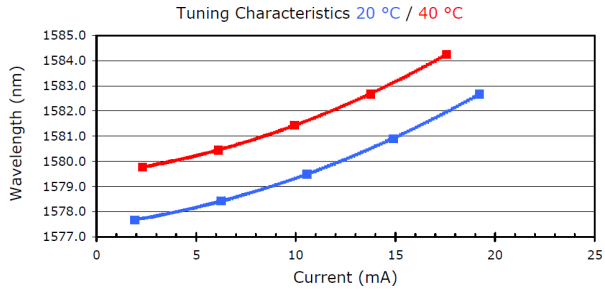

Fig. 3. Tuning characteristics with respect to bias current and temperature of VCSEL#2.

VCSELs are much more sensitive to bias currents concerning wavelength tunability than to temperature. Besides, changing temperature is a slow process, more complicated to control and considerably more power consuming. Thereby, the experiment was conducted inside an isolated room at ambience temperature and the measurements were taken after some stabilization minutes. The impact of the little temperature drifts were corrected through slight variations of the bias currents that never exceeded ± 0.5 mA max. An example of eye diagram correction through bias current is shown in Fig. 4.

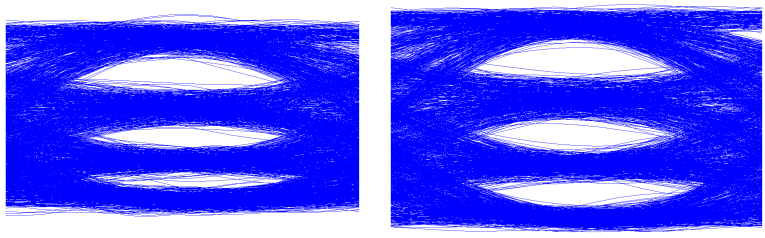

(a) **(b)**

Fig. 4. Illustration of a normalized digital eye diagram before bias current correction (a) and after bias current correction (b).

Table 1. Bias current and their corresponding wavelength interval delimiters for each VCSEL.

	20°C		40°C	
	Bias Current (mA)	Wavelength (nm)	Bias Current (mA)	Wavelength (nm)
VCSEL#1	6.82 / 15.51	1577.87 / 1580.37	6.75 / 14.32	1579.91 / 1582.13
VCSEL#2	6.25 / 14.89	1578.44 / 1580.90	6.12 / 13.75	1580.45 / 1581.44
VCSEL#3	6.23 / 14.48	1579.24 / 1581.90	6.08 / 13.10	1581.24 / 1583.50
VCSEL#4	6.86 / 14.53	1579.97 / 1582.57	6.98 / 13.40	1582.09 / 1584.31

3. Experimental setup

The experimental set-up is presented in Fig. 5. The pulse pattern generator (PPG) is used to generate two pseudorandom binary sequences (PRBS) NRZ streams of length 2^{15}-1 at 7 Gbps. The 4-PAM electrical signal is generated in the following way: Firstly, the two NRZ streams are passed through 10 dB and 3 dB attenuators respectively in order to reduce reflections and allow us to track the amplitudes while still keeping the convenient proportion for creating the multilevel signal. Time decorrelation matching is adjusted with a mechanical delay-line inserted into the higher power branch. Subsequently, the binary sequences are added up through a 6dB power combiner to make the 14 Gbps 4-PAM signal shown in Fig. 6. The 4-

#177306 - $15.00 USD Received 1 Oct 2012; revised 17 Nov 2012; accepted 19 Nov 2012; published 10 Dec 2012

PAM signal is replicated by four with a 10 GHz active RF splitter. The peak-to-peak voltage after amplification is set to 0.6 V for all the outputs and the time decorrelation between each of them is perform with internal and pre-configured delay lines. The offset of the input signal is tuned to locate the dynamic range well within the most linear range of the internal amplifier.

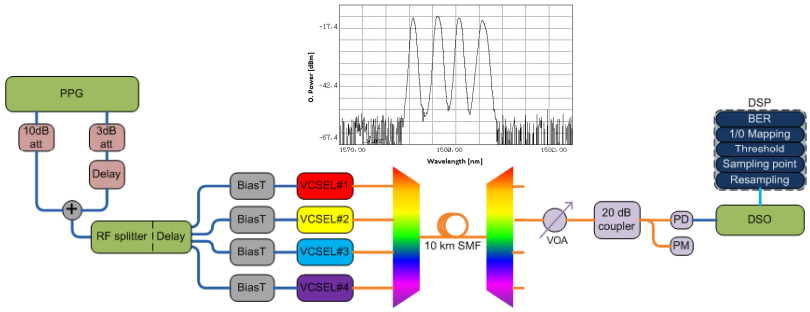

Fig. 5. Experimental setup. Pulse pattern generator (PPG), array waveguide grating (AWG), single mode fiber (SMF), digital storage oscilloscope (DSO), digital signal processing (DSP).

The four outputs of the splitter are driven into the L-band VCSELs. Bias-Ts and evaluation boards are used with an initial bias current of 10.5 mA. The cathode, anode and reference pin of the VCSELs were trimmed off to avoid interferences. Later on, they were appropriately welded to flexible flaps that were connected to the evaluation boards. In order to improve light coupling, four high-precision alignment stations were utilized to approach four independent cleaved fibers to the lasers' aperture. Backwards reflections were drastically reduced by adding index-matching oil to the fibers' end tips. The approaching process was controlled with one microscope and one optical power meter.

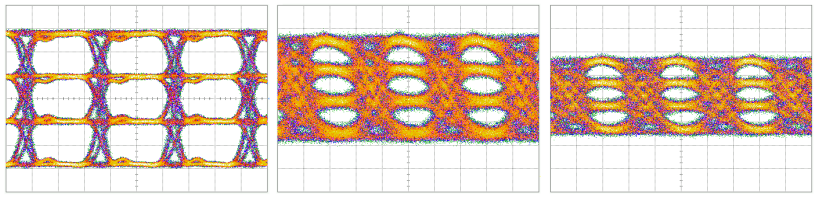

Fig. 6. Electrical 4-PAM signal (a). Optical 4-PAM signal after the VCSEL (b). Electrical 4-PAM after the photodiode (c).

At the optimum light coupling, the lasers showed ~2.5dBm output power for the initial bias current. In this stage the 4-PAM signals were injected (see Fig. 6.). The combined optical spectrum after the first AWG was analyzed. The pre-established 10.5 mA bias currents were tuned independently for each laser to make their output wavelengths match the 50 GHz-spaced AWG's channels. The center wavelengths are 1580.24 nm, 1580.66 nm, 1581.03 nm and 1581.43 nm. Z-axis alignment was modified to create the flat optical spectrum shown in Fig. 5. Minor changes in the bias currents and modulation amplitudes are performed at this stage in order to optimize the individual eye diagrams.

The WDM signal is propagated over a 10 km-long pool of SSMF and demultiplexed with another AWG. At the receiver side, the channel 1580.66 nm is measured. A variable attenuator, a 20dB coupler and an optical power meter are used to control and monitor the incoming optical power. One high-sensitivity PIN photodiode with integrated GaAs

#177306 - $15.00 USD Received 1 Oct 2012; revised 17 Nov 2012; accepted 19 Nov 2012; published 10 Dec 2012

preamplifier and 10GHz of 3-dB bandwidth is used to detect the signal. Finally, a 13 GHz digital storage oscilloscope (DSO) at 40 GS/s is used to store the signal for offline processing.

4. Digital signal processing (DSP)

Quaternary pulse amplitude modulation (4-PAM) is used to achieve 14 Gbps (7 Gbauds) due to the spectral efficiency of 2 bit/s/Hz.. Besides, doubling the modulation frequency in OOK requires more than double power consumption [15]. This section shortly develops on the offline demodulation stages of the 4-PAM signal and the enhancement features of the code to attain improved BER results.

4.1 General BER calculation

For each power level, 10 frames in chunks of 2^{15}-1 symbols (327670 symbols) are evaluated. Two samples were stored for each power level so that the final BER results are averaged. After storing the signal with the DSO, a ~3-fold up-sampling is performed. This makes around 20 samples per symbol hence allowing the correction of the eye diagram's tilt and facilitating the optimum sampling point calculation. After resampling, reshaping is performed for each of the chunks in order to create a matrix of dimensions 20x327670. This allows us to overlap all the symbols (see Fig. 4.) to calculate the 2-D variance and thereby the optimum sampling point of the combined shapeform.

The histograms for all of the chunks are calculated at the optimum sampling point with 60 bins each. By detecting the bin numbers with the lowest number of observations between peaks, the amplitude thresholds are located. The noise distribution is not taken into account. Once the optimum sampling points are determined, the 1/0 mapping is performed, giving 2 bits for every symbol analyzed (4-PAM). Finally, the BER is calculated by comparing the binary sequences obtained for the least significant bit (LSB) and most significant bit (MSB) with the circularly shifted PRBS used in the signal generation. The exact offset for each bit is calculated by performing x-correlation. When error counting yielded error free transmission, Gaussian fitting and estimated BER was applied. However, its utilization was exclusively necessary to confirm the absence of error floors when the 4 channels were transmitting.

4.2 Enhanced features

Some further advanced signal processing was implemented to improve the BER results. Here we briefly describe three of them. Desynchronization between DSO and our signal, eye diagram tilt correction and Gray coding emulation.

The effect of the desynchronization between the DSO and the signal is a relative displacement of the optimum sampling point with respect to the observation window. If this effect was not taken into consideration, a symbol was counted twice every certain amount of samples. This changes the PRBS offset and consequently increases the BER given that the displacement is only calculated in the very first iteration to reduce the computation time. In order to correct for this, the chunks were in turn subdivided into smaller pieces of around 5000 symbols and the displacement of the sampling point could be tracked with enough precision. When the error occurred, the repeated symbol was automatically deleted and the process continued.

The correction of the eye diagram's tilt literally straightens the eye diagram so that those points with higher variance in every level are put in a common sampling point for the four levels instead of calculating the optimum compromise. An example of this can be observed in Fig. 6 by comparing signal out of the VCSEL and the digitalized one.

Gray coding emulation can be performed when the PRBS is known as well as the relative sequence offset of the LSB with respect to the MSB. In such case, by performing a logical XOR between the original PRBS and itself displaced, a new PRBS is created for the LSB. This reduces the number of errors in the LSB since the mapping for the MSB remains the same.

#177306 - $15.00 USD Received 1 Oct 2012; revised 17 Nov 2012; accepted 19 Nov 2012; published 10 Dec 2012

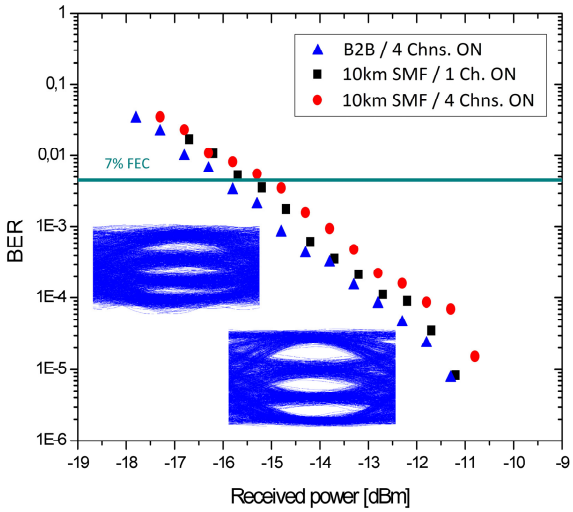

Fig. 7. Averaged BER versus received optical power.

5. Results

The experimental results for each of the three measurements conducted are shown in Fig. 7. Bit error rates are obtained for one of the center channels (1580.66 nm) in back-to-back configuration (blue triangles), after 10 km SMF when only that specific channel is transmitted (black squares) and after 10 km SMF when the four lanes are transmitted in parallel (red circles). Targeting post-FEC bit error rate of 10^{-15}, the green line in Fig. 7 indicates the threshold (4.5·10-3) [16] of a 7% overhead FEC code.

The BER performance difference between single-channel and four-channel transmission is negligible below ~16dBm received power. For higher power levels, an average crosstalk penalty of less than 0.5dB is observed. The comparison with back-to-back performance shows a transmission penalty of ~0.5dB with respect to single-lane configuration. Around 1dB penalty is observed as compared to the four-lane case with a local maximum of 1.3dB.

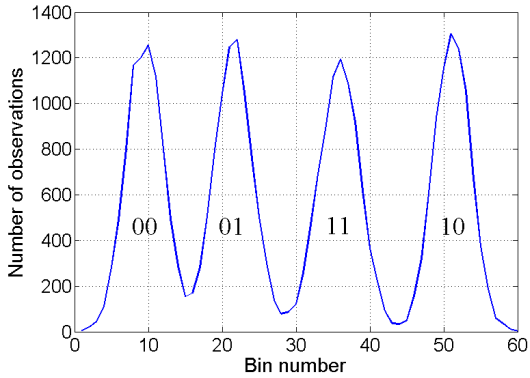

Fig. 8. Histogram of four-channel transmission frame (32767 bits) at –15dBm.

#177306 - $15.00 USD Received 1 Oct 2012; revised 17 Nov 2012; accepted 19 Nov 2012; published 10 Dec 2012

No error floors are observed within the tested received power interval and the WDM signal clearly exceeds the 7%-FEC threshold for received power levels higher than −15dBm. This grants error free transmission (BER~10^{-15}) under considerably relaxed power budget conditions allowing hence the allocation of ~6-7 dB extra loss along the link.

Figure 8 shows the received histogram at the optimum sampling point for a frame of BER~$2.5 \cdot 10^{-3}$ under full WDM operation at the 7%-FEC threshold, which corresponds to −15dBm. Gray mapping is superimposed. The slightly higher accumulation of observations between the 00-01 dip is due to slight instabilities that displace the optimum working point (effect illustrated in Fig. 4.)

6. Conclusions

4x14Gbps L-band VCSEL-based WDM transmission over 10 km of SSMF was investigated. Successful transmission of four channels with quaternary pulse amplitude modulation at 7Gbauds with post-FEC (7% overhead) error free operation has been proven. The crosstalk power penalty was measured to be ~0.5 dB and the power budget margin ranges between 6dB and 7dB. Our results show the potential of the reported system to migrate 4-lanes 56Gbps data links into a compact WDM link.

Acknowledgments

We would like to acknowledge VERTILAS GmbH and Ignis for providing VCSELs and AWGs respectively and the FP7 European project GigaWaM for partly funding this research.

#177306 - $15.00 USD Received 1 Oct 2012; revised 17 Nov 2012; accepted 19 Nov 2012; published 10 Dec 2012

List of Acronyms

ADC	analog-to-digital converter
ASIC	application-specific integrated circuit
AWG	arrayed waveguide grating
BER	bit error rate
BPSK	binary phase shift keying
BS	base station
CAP	carrierless amplitude phase modulation
CAPEX	capital expenditure
CATV	cable television
CD	chromatic dispersion
CS	central station
CW	continuous wave
DAC	digital-to-analog converter
DD	direct detection
DFB	distributed feedback laser
DGD	differential group delay
DML	directly modulated laser
DMT	discrete multi-tone

DP dual-polarization

DSP digital signal processing

EAM electro-absorption modulator

EIRP equivalent isotropically radiated power

EML electro-absorption modulated laser

EPON Ethernet passive optical network

FBG fiber Bragg grating

FCC Federal Communications Commission

FDM frequency-division multiplexing

FEC forward error correction

FFT fast Fourier Transform

FTTH Fiber-to-the-home

GPON gigabit passive optical network

GSM Global System for Mobile Communications

GVD group-velocity dispersion

HDTV high-definition television

IM intensity modulation

IC integrated-circuit

IR impulse radio

ISI inter-symbol interference

LAN local area network

LTE Long Term Evolution

MAC media access control

MMF multimode fiber

mmW	millimeter-wave
MZM	Mach-Zehnder modulator
NLOS	non light-of-sight
NRZ	non return-to-zero
OFDM	orthogonal frequency-division multiplexing
OLT	optical line termination
ONU	optical network unit
OOK	on-off keying
OPEX	operating expense
PAM	pulse amplitude modulation
PCB	printed circuit board
PD	photodiode
PMD	polarization-mode dispersion
PON	passive optical network
PSK	phase shift keying
PSNR	peak signal-to-noise ratio
QAM	quadrature amplitude modulation
QPSK	quadrature phase shift keying
RoF	radio-over-fiber
RSOA	reflective semiconductor optical amplifier
SAN	storage area network
SE	spectral efficiency
SCM	subcarrier multiplexing
SMF	single-mode fiber

SNR signal-to-noise ratio

SOA semiconductor optical amplifier

TDM time-division multiplexing

UWB ultra-wide band

UWBoF UWB-over-fiber

VCSEL vertical-cavity surface-emitting laser

VoD video-on-demand

VoIP voice-over-IP

WDM wavelength division multiplexing

WLAN wireless local area network

WiMAX Worldwide Interoperability for Microwave Access

WPAN wireless personal area network

WWAN wireless wide area network

Bibliography

[1] International Data Corporation (IDC), *http://www.idc.com*.

[2] K. Sato and H. Hasegawa, "Optical networking technologies that will create future bandwidth-abundant networks [Invited]," *Journal of Optical Communications and Networking*, vol. 1, pp. A81–A93, July 2009.

[3] H. Rohde, S. Smolorz, E. Gottwald, and K. Kloppe, "Next generation optical access: 1 gbit/s for everyone," in *35th European Conference on Optical Communication, ECOC '09*, Sept. 2009.

[4] C. Lin, *Broadband optical access networks and fiber-to-the-home: systems technologies and deployment strategies*, John Wiley & Sons, Inc., 2006.

[5] J. Prat, *Next-generation FTTH passive optical networks*, Springer, 2008.

[6] A. Banerjee, Y. Park, F. Clarke, H. Song, S. Yang, G. Kramer, K. Kim, and B. Mukherjee, "Wavelength-division-multiplexed passive optical network WDM-PON technologies for broadband access: a review," *Journal of Optical Networking*, vol. 4, no. 11, pp.737–758, 2005.

[7] P. Vetter "Next Generation Optical Access Technologies," in *38th European Conference on Optical Communication, ECOC 2012*, Sept. 2012.

[8] GigaWaM website, *http://www.gigawam.com/*

[9] P. K. Bondyopadhyay, "Guglielmo Marconi – The father of long distance radio communication – An engineer's tribute". In *Proceedings of 25th European Microwave Conference*, p. 879, 1995.

[10] C. Park and T. S. Rappaport, "Short-Range Wireless Communications for Next-Generation Networks: UWB, 60 GHz Millimeter-Wave

WPAN, And ZigBee," *IEEE Wireless Communications*, vol. 14, no. 4, pp. 70–78, 2007.

[11] FCC, "Revision of part 15 of the commission rules regarding ultra-wideband transmission systems," Feb. 2002.

[12] D. Porcine, P. Research, and W. Hirt, "Ultra-wideband radio technology: potential and challenges ahead," *IEEE Communication Magazine*, vol. 41, no. 7, pp. 66-74, Jul. 2003.

[13] S. K. Yong, C.-C. Chong, "An overview of multigigabit wireless through millimeter wave technology: potentials and technical challenges," *EURASIP J. Wireless Commun. Netw*, 2007.

[14] K.-C. Huang and D. J. Edwards, *Millimetre Wave Antennas for Gigabit Wireless Communications: A Practical Guide to Design and Analysis in a System Context*, Wiley, 2008.

[15] S. K. Yong, P. Xia, and A. Valdes-Garci, *60GHz Technology for Gbps WLAN and WPAN: From Theory to Practice*, Wiley, 2008.

[16] FCC, "Millimeter Wave Propagation: Spectrum Management Implications," available at *http://fcc.gov/*

[17] B. Langen, G. Lober, and W. Herzig, "Reflection and transmission behavior of building materials at 60ghz," In *Proceedings of IEEE PIMRC 1994*, pp. 505-–509, 1994.

[18] ECMA. International., "TC48 High rate wireless communications,", *www.ecma-international.org*

[19] WirelessHD consortium, *www.wirelesshd.org/*

[20] IEEE 802.15 Task Group 3c, *www.ieee802.org/15/pub/TG3c.html*

[21] C2G website *http://www.cablestogo.com.*

[22] G. Shen, R. S. Tucker, and C. J. Chae, "Fixed mobile convergence architectures for broadband access: integration of EPON and WiMAX," *IEEE Communications Magazine*, vol. 45, no. 8, pp. 44 –50, Aug. 2007.

[23] T. Koonen, "Trends in optical access and in-building networks," in *34th European Conference on Optical Communication, 2008. ECOC 2008*, pp. 1–31, Sept. 2008.

[24] M. Popov, "The convergence of wired and wireless services delivery in access and home networks," in *Conference on Optical Fiber Communication, National Fiber Optic Engineers Conference, (OFC/NFOEC 2010)*, Mar. 2010.

[25] M. Ali, G. Ellinas, H. Erkan, A. Hadjiantonis, and R. Dorsinville, "On the vision of complete fixed-mobile convergence," *IEEE/OSA Journal of Lightwave Technology*, vol. 28, pp. 2343 –2357, Aug. 2010.

[26] G. K. Chang, A. Chowdhury, Z. Jia, H. C. Chien, M. F. Huang, J. Yu, and G. Ellinas, "Key technologies of WDM-PON for future converged optical broadband access networks," *IEEE/OSA Journal of Optical Communications and Networking*, vol. 1, pp. C35 –C50, Sept. 2009.

[27] N. Ghazisaidi, M. Maier, and C. Assi, "Fiber-wireless (FiWi) access networks: A survey," *IEEE Communications Magazine*, vol. 47, pp. 160 –167, Feb. 2009.

[28] X. Yu, J. B. Jensen, D. Zibar, C. Peucheret, and I. T. Monroy, "Converged wireless and wireline access system based on optical phase modulation for both radio-over-fiber and baseband signals," *IEEE Photonics Technology Letters*, vol. 20, pp. 1814 –1816, Nov. 2008.

[29] G. P. Agrawal, *Nonlinear Fiber Optics. Academic Press*, Fourth edition, 2006.

[30] L. García Larrodé, "Radio over fiber distributed antenna systems for in-building broadband wireless services," *PhD thesis*, 2010.

[31] T. Yamamoto, "High-speed directly modulated lasers," in *Conference on Optical Fiber Communication, National Fiber Optic Engineers Conference, (OFC/NFOEC 2012)*, Paper OTh3F.5, Mar. 2012.

[32] G. P. Agrawal, N. K. Dutta, *Long-wavelength semiconductor lasers*, Van Nostrand Reinhold, 1986.

[33] J.C. Cartledge and G.S. Burley, "The Effect of Laser Chirping on Lightwave System Performance" *IEEE/OSA Journal of Lightwave Technology*, vol. 7, no. 3, pp. 568–573, 1989.

[34] L. A. Coldren, S. W. Corzine, *Diode Lasers and Photonic Integrated Circuits*," Wiley Series in Microwave and Optical Engineering, 1995.

[35] The Optical Internetworking Forum, *www.oiforum.com*

[36] E.Lach, W. Idler, “Modulation formats for 100G and beyond,” *Optical Fiber Technology*, vol. 17, pp. 377—386, 2011.

[37] J. Proakis and M. Salehi, *Digital communications*, McGraw-Hill, 2007.

[38] H. Rohling, *Signals and Communication Technology: Ofdm: Concepts for Future Communication Systems*, Springer, 2011.

[39] M. Gagnaire, *Broadband Local Loops for High-Speed Internet Access*, Artech House Telecommunications Library, 2003.

[40] M. R. Mahfouz, Z. Cemin, M.J. Kuhn, B.C. Merkl, A.E. Fathy, and M.R. Mahfouz, "Investigation of high-accuracy indoor 3-D positioning using UWB technology," *IEEE Transactions on Microwave Theory and Techniques*, vol. 58, no. 1, 2010.

[41] J. Han and C. Nguyen, “Development of a tunable multi-band UWB radar sensor and its applications to subsurface sensing,” *IEEE Sensors Journal*, vol. 7, no. 1, pp. 51-58, Jan. 2007.

[42] P. Withington, H. Fluhler, and S. Nag, "Enhancing homeland security with advanced UWB sensors," *IEEE Microwave Magazine*, vol. 4, no. 3, pp. 51-58, 2003.

[43] The IEEE 802.15 Working Group for Wireless Personal Area Networks, *www.ieee802.org/15/*

[44] M. Wah, C. Yee, and M. L. Yee, “Wireless ultra wideband communications using radio over fiber,” in *2003 IEEE Conference on Ultra Wideband Systems and Technologies*, pp. 265–269, Nov. 2003.

[45] C. M. Tan, L. C. Ong, M. L. Yee, B. Luo and P. K. Tang, “Transmission of ultra wide band radio using multimode radio-over-fiber system,” in *Proc. of Asia-Pacific Microwave Conference Proceedings, 2005. APMC 2005*, Dec. 2005.

[46] R. Llorente, T. Alves, M. Morant, M. Beltran, J. Perez, A. Cartaxo, and J. Marti, “Ultra-wideband radio signals distribution in FTTH networks,” *IEEE Photonics Technology Letters*, vol. 20, pp. 945 –947, June 2008.

[47] J. Yao, F. Zeng, and Q. Wang, “Photonic generation of ultrawideband signals,” *IEEE/OSA Journal of Lightwave Technology*, vol. 25, pp. 3219–3235, 2007.

[48] Q. Wang and J. Yao, "An electrically switchable optical ultrawideband pulse generator", *IEEE/OSA Journal of Lightwave Technology* vol. 25, no. 11, pp. 3626–3633, 2007.

[49] Q. Wang, F. Zeng, S. Blais, and J. Yao, "Optical ultrawideband monocycle pulse generation based on cross-gain modulation in a semiconductor optical amplifier", *OSA Optics Letters*, vol. 31, pp. 3083–3085, 2006.

[50] C. Wang, F. Zeng, and J. P. Yao, "All-fiber ultra wideband pulse generation based on spectral shaping and dispersion-induced frequency-to-time conversion," *IEEE Photonics Technology Letters*, vol. 19, no. 3, pp. 137—139, Feb. 2007.

[51] H. Chen, M. Chen, C. Qiu, S. Xie, "A novel composite method for ultra-wideband doublet pulses generation", *IEEE Photonics Technology Letters*, vol. 19, no. 24, pp. 2021–2023, 2007.

[52] J. Li, S. Fu, K. Xu, J. Wu, J. Lin, M. Tang, and P. Shum, "Photonic ultrawideband monocycle pulse generation using a single electro-optic modulator," *OSA Optics Letters*, vol. 33, pp. 288–290, 2008.

[53] J. Dong, X. Zhang, J. Xu, D. Huang, S. Fu, and P. Shum, "Ultrawideband monocycle generation using cross-phase modulation in a semiconductor optical amplifier", *OSA Optics Letters*, vol. 32, pp. 1223–1225, 2007.

[54] E. Zhou, X. Yu, X. Zhang, W. Xue, Y. Yu, J. Mørk, and I. T. Monroy, "Photonic generation of ultrawideband monocycle and doublet pulses by using a semiconductor-optical-amplifier-based wavelength converter," *OSA Optics Letters*, vol. 34, pp. 1336-–1338, 2009.

[55] A. Kaszubowska-Anandarajah, P. Perry, L. Barry, and H. Shams, "An IR-UWB photonic distribution system," *IEEE Photonics Technology Letters*, vol. 20, pp. 1884 –1886, Nov. 2008.

[56] W. P. Lin and J. Y. Chen, "Implementation of a new ultrawide-band impulse system", *IEEE Photonics Technology Letters*, vol. 17, no. 11, pp. 2418–2420, 2005.

[57] F. Zeng and J. Yao, "Ultrawideband impulse radio signal generation using a high-speed electrooptic phase modulator and a fiber-bragg-grating-based frequency discriminator," *IEEE Photonics Technology Letters*, vol. 18, pp. 2062 –2064, Oct. 2006.

[58] M. Abtahi, M. Mirshafiei, S. LaRochelle, and L. Rusch, "All-optical 500-mb/s UWB transceiver: An experimental demonstration," *IEEE/OSA Journal of Lightwave Technology*, vol. 26, pp. 2795–2802, Aug. 2008.

[59] Q. Wang, J. Yao, "UWB doublet generation using nonlinearly biased electro-optic intensity modulator", *Electronics Letters.*, vol. 42, no. 22, pp. 1304–1305, 2006.

[60] T. Kawanishi, T. Sakamoto, and M. Izutsu, "Ultra-wide-band radio signal generation using optical frequency-shift-keying technique," *IEEE Microwave Wireless Component Letters*, vol. 15, no. 3, pp. 153-–155, 2005.

[61] X. Yu and I. T. Monroy, "Distribution of photonically generated 5 Gbits/s impulse radio ultrawideband signals over fiber," *OSA Optics Letters*, vol. 36, no. 6, pp. 810—812, 2011.

[62] V. Torres-Company, K. Prince, and I. T. Monroy, "Fiber transmission and generation of ultrawideband pulses by direct current modulation of semiconductor lasers and chirp-to-intensity conversion", *OSA Optics Letters*, vol. 33, pp. 222–224, 2008.

[63] X. Yu, T. Braidwood Gibbon, M. Pawlik, S. Blaaberg, and I. Tafur Monroy, "A photonic ultra-wideband pulse generatorbased on relaxation oscillations of asemiconductor laser," *OSA Optics Express*, vol. 17, pp. 9680–9687, 2009.

[64] S. Pan and J. Yao, "Simultaneous provision of UWB and wired services in a WDM-PON network using a centralized light source," *IEEE Photonics Journal*, vol. 2, pp. 712–718, Oct. 2010.

[65] J. Jensen, R. Rodes, M. Beltran, and I. Monroy, "Shared medium 2 gbps baseband amp; 2 gbps UWB in-building converged optical/wireless network with multimode fiber and wireless transmission," in *Proc. 36th European Conference and Exhibition on Optical Communication (ECOC 2010)*, Sept. 2010.

[66] K. Prince, J. Jensen, A. Caballero, X. Yu, T. Gibbon, D. Zibar, N. Guerrero, A. Osadchiy, and I. Monroy, "Converged wireline and wireless access over a 78-km deployed fiber long-reach WDM PON," *IEEE Photonics Technology Letters*, vol. 21, pp. 1274 –1276, Sept. 2009.

[67] S. Pan, J. Yao, "IR-UWB-over-fiber systems compatible with WDM-PON networks," *IEEE/OSA Journal of Lightwave Technology*, vol. 29, no. 20, pp.3025-3034, 2011.

[68] A. Ngoma, M. Sauer, F. Annunziata, W. J. Jiang, C. T. Lin, J. Chen, P. T. Shih, and S. Chi, "Simple multi-gbps 60 GHz radio-over-fiber links employing optical and electrical data up-conversion and feed-forward equalization," in *Optical Fiber Communication Conference and Exposition and the National Fiber Optic Engineers Conference (OFC/NFOEC), 2009*, Paper. OWF2, 2009.

[69] Z. Jia, J. Yu, G. Ellinas, and G.-K. Chang, "Key enabling technologies for optical-wireless networks: Optical millimeter-wave generation, wavelength reuse, and architecture," *IEEE/OSA Journal of Lightwave Technology*, vol. 25, pp. 3452–3471, Nov. 2007.

[70] C. T. Lin, J. Chen, W. J. Jiang, L. Y. Wang He, p. T. Shih, C. H. Ho, and S. Chi "Ultra-high data-rate 60 GHz radio-over-fiber systems employing optical frequency multiplication and adaptive OFDM formats," in *Optical Fiber Communication Conference and Exposition and the National Fiber Optic Engineers Conference (OFC/NFOEC), 2011*, Paper. ThJ6, Mar. 2011.

[71] A. Caballero, D. Zibar, R. Sambaraju, J. Marti and I. Tafur Monroy, "High-capacity 60 GHz and 75-110 GHz band links employing all-optical OFDM generation and digital coherent detection," *IEEE/OSA Journal of Lightwave Technology.* vol. 30, no. 1, pp. 147–155, 2011.

[72] X. Pang, A. Caballero, A. Dogadaev, V. Arlunno, R. Borkowski, J. S. Pedersen, L. Deng, F. Karinou, F. Roubeau, D. Zibar, X. Yu, and I. Tafur Monroy, "100 Gbit/s hybrid optical fiber-wireless link in the W-band (75–110 GHz)," *OSA Optics Express*, vol. 19, pp. 24944–24949, 2011.

[73] A. Caballero Jambrina, "High capacity radio over fiber transmission links," *PhD thesis*, 2011.

[74] A. Flatman, In-premises optical fiber installed base analysis to 2007, in *IEEE 802.3 10 GBE over FDDI Grade Fiber Study*, 2004.

[75] N. Gomes, A. Nkansah, and D. Wake, "Radio over MMF techniques, Part I: RF to microwave frequency systems," *IEEE/OSA Journal of Lightwave Technology*, vol. 26, no. 15, pp. 2388—2395, Aug. 1, 2008.

[76] A. Koonen and L. García Larrodé, "Radio-over-MMF techniques. part II: microwave to millimeter-wave systems," *IEEE/OSA Journal of Lightwave Technology*, vol. 26, pp. 2396 –2408, Aug. 2008.

[77] L. García Larrodé and A. Koonen, "All-fiber full-duplex multimode wavelength-division-multiplexing network for radio-over-multimode-fiber distribution of broadband wireless services ,"*IEEE Transactions on Microwave Theory and Techniques*, vol. 56, no. 1, pp. 248–255, 2008.

[78] B. A. Khawaja and M. J. Cryan, "Millimetre-wave radio-over-fibre data transmission over multimode fibre," *Microwave and Optical Technology Letters*, vol. 53, no. 2, p. 254–256, 2011.

[79] A. Nkansah, A. Das, N. Gomes, and P. Shen, "Multilevel modulated signal transmission over serial single-mode and multimode fiber links using vertical-cavity surface-emitting lasers for millimeter-wave wireless communications," *IEEE Transactions on Microwave Theory and Techniques*, vol. 55, pp. 1219–1228, 2007.

[80] H. Singh, J. Oh, C. Kweon, X. Qin, H. R. Shao, and C. Ngo, "A 60 GHz wireless network for enabling uncompressed video communication," *IEEE Communications Magazine*, vol. 46, no. 12, pp.71–78, 2008.

[81] Z. Jia, H.-C. Chien, Y.-T. Hsueh, A. Chowdhury, J. Yu, and G.-K. Chang, "Wireless HD services over optical access systems: Transmission, networking, and demonstration," in *Optical Fiber Communication Conference and Exposition and the National Fiber Optic Engineers Conference (OFC/NFOEC), 2009*, pp. 1–3, 2009.

[82] M. Weiβ, "60 GHz photonic millimeter-wave communication systems," *PhD thesis*, 2010.

[83] M. Huang, K. B. Cheng, Y. Zhou, A. Pisano, and C. Chang-Hasnain, "Monolithic integrated piezoelectric MEMS-Tunable VCSEL," *IEEE Journal of Selected Topics in Quantum Electronics*, vol. 13, pp. 374–380, 2007.

[84] W. Hofmann, M. Gorblich, G. Bohm, M. Ortsiefer, L. Xie, and M.-C. Amann, "Long-wavelength 2-d VCSEL arrays for optical interconnects," in *Conference on Lasers and Electro-Optics, 2008 and 2008 Conference on Quantum Electronics and Laser Science. CLEO/QELS 2008*, May 2008.

[85] S. Blokhin, J. Lott, A. Mutig, G. Fiol, N. Ledentsov, M. Maximov, A. Nadtochiy, V. Shchukin, and D. Bimberg, "Oxide-confined 850 nm VCSELs operating at bit rates up to 40 gbit/s," *Electronics Letters*, vol. 45, no. 10, pp. 501–503, 2009.

[86] P. Westbergh, J. Gustavsson, B. Kogel, A. Haglund, A. Larsson, A. Mutig, A. Nadtochiy, D. Bimberg, and A. Joel, "40 gbit/s error-free operation of oxide-confined 850 nm VCSEL," *Electronics Letters*, vol. 46, pp. 1014–1016, 2010.

[87] K. Choquette, "The race toward long wavelength VCSELs," in *The 14th Annual Meeting of the IEEE Lasers and Electro-Optics Society, 2001. LEOS 2001*, vol. 2, pp. 594–595, 2001.

[88] V. Gambin, W. Ha, M. Wistey, H. Yuen, S. R. Bank, S. M. Kim, and J. S. Harris, " GaInNAsSb for 1.3–1.6-μm-long wavelength lasers grown by molecular beam epitaxy," *IEEE Journal of Selected Topics in Quantum Electronics*, vol. 8, no. 4, 2002.

[89] M. V. R. Murty, X. D. Huang, G. L. Liu, C. C. Lin, D. Xu, C. L. Shieh, H. C. Lee, and J. Cheng, "Long-wavelength VCSEL-based CWDM scheme for 10-GbE links," *IEEE Photonics Technology Letters*, vol. 17, pp. 1286–1288, 2005.

[90] M.-C. Amann and W. Hofmann, "InP-Based long-wavelength VCSELs and VCSEL arrays," *IEEE Journal of Selected Topics in Quantum Electronics*, vol. 15, pp. 861–868, 2009.

[91] W. Hofmann, M. Muller, P. Wolf, A. Mutig, T. Grundl, G. Bohm, D. Bimberg, and M.-C. Amann, "40 gbit/s modulation of 1550 nm VCSEL," *Electronics Letters*, vol. 47, no. 4, pp. 270–271, 2011.

[92] L. Xu, H. Tsang, W. Hofmann, and M.-C. Amann, "10-gb/s colorless re-modulation of signal from 1550nm vertical cavity surface emitting laser array in WDM PON," in *European Conference on Lasers and Electro-Optics 2009 and the European Quantum Electronics Conference. (CLEO Europe - EQEC 2009)*, June 2009.

[93] K. Prince, M. Ma, T. Gibbon, C. Neumeyr, E. Ronneberg, M. Ortsiefer, and I. Monroy, "Free-running 1550 nm VCSEL for 10.7 gb/s transmission in 99.7 km PON," *IEEE/OSA Journal of Optical Communications and Networking*, vol. 3, pp. 399–403, May 2011.

[94] B. Zhang, X. Zhao, L. Christen, D. Parekh, W. Hofmann, M. C. Wu, M. C. Amann, C. J. Chang-Hasnain, and A. E. Willner, "Adjustable chirp injection-locked 1.55-μm VCSELs for enhanced chromatic dispersion compensation at 10-Gbit/s," in *Optical Fiber Communication Conference (OFC 2008)*, paper OWT7, 2008.

[95] R. Rodes, J. Estaran, B. Li, M. Mueller, J. B. Jensen, T. Grundl, M. Ortsiefer, C. Neumeyr, J. Rosskopf, K. J. Larsen, M. C. Amann, and I. Tafur Monroy, "100 gb/s single VCSEL data transmission link," in *Conference on Optical Fiber Communication/ National Fiber Optic Engineers Conference OFC/NFOEC 2012*, Paper PDP5D.10, 20012.

[96] K. Szczerba, P. Westbergh, J. Karout, J.Gustavsson,A. Haglund, M. Karlsson, P. Andrekson, E. Agrell, and A. Larsson, "30 Gbps 4-PAM transmission over 200m of MMF using an 850 nm VCSEL," *OSA Optics Express*, vol. 19, pp. B203–B208, Mar. 2011.

[97] J. Lee, F. Breyer, S. Randel, J. Zeng, F. Huijskens, H. P. van den Boom, A. M. Koonen, and N. Hanik, "24-gb/s transmission over 730 m of multimode fiber by direct modulation of an 850-nm VCSEL using discrete multi-tone modulation," in *Optical Fiber Communication Conference (OFC 2007)*, paper PDP6, 2007.

[98] E. Hugues-Salas, R. Giddings, X. Jin, J. L. Wei, X. Zheng, Y. Hong, C. Shu, and J. Tang, "Real-time experimental demonstration of low-cost VCSEL intensity-modulated 11.25Gb/s optical OFDM signal transmission over 25km PON systems," *OSA Optics Express*, vol. 19, pp. 2979–2988, Feb. 2011.

[99] K. Szczerba, B.-E. Olsson, P. Westbergh, A. Rhodin, J.S. Gustavsson, A. Haglund, M. Karlsson, A. Larsson, P. A. Andrekson "37 Gbps Transmission Over 200 m of MMF Using Single Cycle Subcarrier Modulation and a VCSEL with 20 GHz Modulation Bandwidth," in *Proc. 36th European Conference and Exhibition on Optical Communication (ECOC 2010)*, paper We.7.B.2, Sept. 2010.

[100] J. D. Ingham, R. Penty, I. White, and D. Cunningham, "40 Gb/s carrierless amplitude and phase modulation for low-cost Optical datacommunication links," in *Optical Fiber Communication/National Fiber Optic Engineers Conference (OFC/NFOEC 2011)*, Paper OThZ3, 2011.

[101] M. B. Othman, X. Zhang, L. Deng, M. Wieckowski, J. Bevensee Jensen, and I. Tafur Monroy, "Experimental investigations demonstration of 3D/4D-CAP modulation with DM-VCSELs," *IEEE Photonic Technology Letters*, vol. 24, no. 22, pp. 2009–2012, 2012.

[102] C. Cole, "Beyond 100G client optics," *IEEE Communications Magazine*, vol. 50, no. 2, pp. s58–s66, 2012.

ISBN: 978-87-93089-17-4

Published by:
DTU Fotonik
Department of Photonic Engineering
Technical University of Denmark
Ørstyeds Plads, building 343
DK-2800 Kgs. Lyngby

Tien-Thang Pham was born in 24th May, 1982 in Hai Duong, Vietnam.

He received Master degree in Electrical and Electronic Engineering from Yonsei University, South Korea in August 2009 and Ph.D. degree in Photonics Engineering from Technical University of Denmark in January 2013. During Ph.D. study, Tien-Thang Pham was visiting scholar with Dept. of Electrical and Electronic Engineering, University of California, Berkeley in 2011 and a DSP intern at Finisar Corp in 2012. Since March 2013, he works as a DSP engineer at Finisar Corp in Sunnyvale, CA, USA and is involved in development of advanced transceivers for datacom and telecom applications.